Elastodynamic homogenization methods and imperfect interface models for composites

Weizhi Luo

UNIVERSITÉ PARIS-EST

MSME Laboratoire Modélisation et Simulation Multi Echelle

THÈSE DE DOCTORAT DE L'UNIVERSITÉ PARIS-EST

École doctorale Sciences, Ingénierie et Environnement

présentée par

Wei-Zhi LUO

pour obtenir le grade de

DOCTEUR DE L'UNIVERSITÉ PARIS-EST

Sujet de la thèse

Elastodynamic homogenization methods and imperfect interface models for composites

Soutenue le 29 janvier 2021 devant le jury composé de

Rapporteur	Stéphane BERBENNI	Directeur de recherche au CNRS Université de Lorraine
Rapporteur	Thomas MICHELITSCH	Directeur de recherche au CNRS Sorbonne Université
Examinateur	Géry DE SAXCE	Professeur Université de Lille
Examinatrice	Xiaojing GONG	Professeur Université Toulouse III
Directeur de thèse	Qi-Chang HE	Professeur Université Gustave Eiffel
Co-encadrant	Hung LE QUANG	Maître de conférences Université Gustave Eiffel

Abstract

This work, motivated by the recent development of metamaterials, has the double objective of contributing to the elaboration of elastodynamic homogenization methods for periodic composite materials and of contributing to the establishment of imperfect elastodynamic interface models for composite materials. The first part of this thesis is concerned with Willis' theory of elastodynamic homogenization and the two-scale elastodynamic homogenization method. In view of the difficulties in obtaining the effective constitutive laws in Willis' theory, an efficient iterative method is proposed to obtain precise dispersion relations and to build the effective constitutive laws in the cases of low frequency and long wavelength. At the same time, the two-scale homogenization method is developed with the help of an assumption which allows avoiding the tedious derivation of high-order asymptotic terms and obtaining a general high-order expression of the effective impedance. These results are applied and illustrated in the case of laminated composites.

In the second part of the work, imperfect elastodynamic interface models are established by replacing, in a composite, an interphase of thin uniform thickness with an imperfect interface of zero thickness satisfying equivalent jump conditions. These models are in fact an elastodynamic extension of the corresponding imperfect elastostatic ones. Finally, they are numerically implemented and illustrated by using the Finite Difference Time Domain (FDTD) and the Explicit Simplified Interface Method (ESIM).

Key words : Composite; Elastodynamics; Homogenization; Asymptotic analysis; Imperfect interface; Jump condition; Numerical method.

Résumé

Ce travail de thèse, motivé par le développement récent de métamatériaux, a pour double objectif de contribuer à l'élaboration de méthodes d'homogénéisation élastodynamique pour les matériaux composites périodiques et de contribuer à l'établissement de modèles d'interface imparfaite élastodynamique pour les matériaux composites. La première partie de ce travail de thèse s'intéresse à la théorie d'homogénéisation élastodynamique de Willis et à la méthode d'homogénéisation élastodynamique à deux échelles. Au vu des difficultés liées à l'obtention des lois constitutives effectives dans la théorie de Willis, une méthode itérative efficace est proposée pour obtenir des relations de dispersion précises et pour construire les lois constitutives effectives dans les cas à basse fréquence et à grande longueur d'onde. En même temps, la méthode d'homogénéisation à deux échelles est développée à l'aide d'une hypothèse permettant d'éviter la dérivation fastidieuse de termes asymptotiques d'ordre élevé et d'obtenir une expression générale d'ordre élevé de l'impédance effective. Ces résultats sont appliqués et illustrés dans le cas des composites stratifiés.

Dans la deuxième partie du travail, des modèles d'interface élastodynamique imparfaite sont établis en remplaçant, dans un composite, une interphase d'épaisseur uniforme mince par une interface imparfaite d'épaisseur nulle qui satisfont à des conditions de saut équivalentes. Ces modèles sont en fait une extension élastodynamique des modèles d'interface élastostatique imparfaite correspondants. Enfin, ils sont numériquement implantés et illustrés à l'aide du domaine temporel à différence finie (FDTD) et de la méthode d'interface simplifiée explicite (ESIM).

Mots clés : Composite ; Elastodynamique ; Homogénéisation ; Analyse asymptotique ; Interface imparfaite ; Condition de saut ; Méthode numérique.

Acknowledgement

Time flies, three years have passed in a twinkle. During my Ph.D., my teachers, colleagues, and friends all gave me great help, and I confess that I could not finish my thesis work without them.

First of all, I am very grateful to Mr. Stéphane BERBENNI and Mr. Thomas MICHELITSCH for being my thesis reporter and for their valuable advice and constructive comments. I also thank my jury members, Mr. Géry DE SAXCE and Ms. Xiaojing GONG, for agreeing to participate in my graduation defense and evaluating my work.

Secondly, I would like to send my sincere gratitude and respect to my thesis adviser Mr. Qi-Chang HE. During the last three years, he showed me his strong scientific research spirit and academic level and gave me great patience and rich enthusiasm. Similarly, I would also like to appreciate my co-supervisor Mr. Hung LE QUANG for his patient help and careful guidance in my work, which has helped me avoid many potential problems.

Thirdly, I would like to thank my colleagues who have been with me for three years, and their discussions have benefited me a lot, and their company and encouragement have provided me with the courage and motivation to persist. The laboratory MSME is a big family, the mutual help and perfect research environment among the members are the indispensable conditions for me to complete the thesis. This doctoral experience in the laboratory will be a wonderful memory in my life. I hope all laboratory members can accept my most sincere gratitude.

Finally, I would like to thank my family and friends. They may not have helped me in my study and work, but they can always be my spiritual support when I feel confused and helpless. I especially want to thank my parents for teaching me how to appreciate life, which is another great dedication after they gave me life.

Notations

• Tensor notations

$u, \boldsymbol{u}$	scalar and vector
$\boldsymbol{A}, \mathbb{A}$	second-order and fourth-order tensor
$\otimes$	tensor product : $(\boldsymbol{u} \otimes \boldsymbol{v})_{ij} = u_i v_j$
$\otimes^s$	symmetric tensor product : $(\boldsymbol{u} \otimes^s \boldsymbol{v})_{ij} = \frac{1}{2}(u_i v_j + u_j v_i)$
$\cdot$	scalar product : $\boldsymbol{u} \cdot \boldsymbol{v} = u_i v_i$
$:$	double-dot product : $\boldsymbol{A} : \boldsymbol{B} = A_{ij} B_{ij}$
$\odot^n$	n-th dot product : $\boldsymbol{A} \odot^2 \boldsymbol{B} = \boldsymbol{A} : \boldsymbol{B} = A_{ij} B_{ij}$

• Common mathematical notations for PART I

$\langle \cdot \rangle$	volume average operator
$\boldsymbol{u}, \boldsymbol{v}$	displacement vector and velocity vector
$\boldsymbol{\sigma}, \boldsymbol{\varepsilon}$	strain tensor and stress tensor
$\boldsymbol{k}, w$	wave number and angular frequency
$\boldsymbol{E}_0, \boldsymbol{f}$	eigenstrain and body force
$\boldsymbol{\rho}, \mathbb{C}$	second-orde rmass density tensor and fourth-order stiffness tensor
$\boldsymbol{\rho}^{eff}, \mathbb{C}^{eff}$	effective density tensor and effective elastic tensor
$\mathcal{Z}$	effective impedance
$\boldsymbol{S}^e, \boldsymbol{T}^e$	effective constitutive law components
$\boldsymbol{I}, \mathbb{I}$	second-order and fourth-order identity tensor
$\mathcal{L}, \mathcal{M}$	third-order tensor and second-order tensor to be determined
$\mathcal{X}, \eta$	local tensors (related to the micro variable $\boldsymbol{y}$)

• Common mathematical notations for PART II

$\boldsymbol{N}, \boldsymbol{T}$	normal and tangent projection operators
$\boldsymbol{u}, \boldsymbol{n}$	displacement vector and normal vector interfacial
$\boldsymbol{\sigma}, \boldsymbol{\tau}$	stress tensor and traction vector
G, ρ	shear modulus and mass density
$\mathcal{R}, \mathcal{T}$	reflection coefficient and projection coefficient
$\mathbb{P}^{\perp}, \mathbb{P}^{\parallel}$	fourth-order normal and tangent operators
$\mathbb{C}, \mathbb{S}$	fourth-order stiffness tensor and compliance tensor
$\mathbb{A}, \mathbb{B}$	fourth-order tensors to be determined
$\boldsymbol{\mathcal{P}}, \boldsymbol{\mathcal{Q}}$	coefficient matrices (related to Taylor expansion and jump conditions)

General introduction

Dynamic homogenization methods for periodic composites

Metamaterials and periodic composites

Metamaterials are defined as artificial materials with some physical properties that are not available in nature. These "abnormal" materials are artificial composites designed to achieve certain special physical phenomena and applications. The existence of metamaterials provides a medium for people to explore the connection between the micro-world and the macro-world, and also makes people realize that even the simple arrangement and combination of microstructure can greatly affect the macroscopic performance of composites.

In recent years, research on metamaterials has attracted great interest from researchers. For instance, the study of optical invisibility cloaks (Chen & Chan, 2010), metamaterials with negative physical properties (Pendry, 2000; Smith et al., 2000; Fang et al., 2006), and phononic crystals (Liu et al., 2000) with local resonance at specific frequencies band have attracted great attention. In fact, it has long been realized that the special microstructure of metamaterials (such as phononic crystals, photonic crystals) gives rise to unnatural macroscopic properties (Willis, 1985; Auriault & Bonnet, 1985).

In view of the microscopic periodic arrangement of metamaterials, perturbations with wavelengths greater than or much greater than the size of their periodic cells will exhibit frequency dependence. The reason is that under the influence of these fluctuations, the materials of the cells do not exist independently, but reflect the synergy between each other. Two intuitive examples are the "negative" effective density exhibited by the local resonance

of phononic crystals (Liu et al., 2005) and the frequency "band" in the homogenized dispersion curves of periodic elastic composites (Nemat-Nasser et al., 2011). For such a periodic structure with very different microscopic properties and macroscopic behaviors, a reasonable homogenization method can effectively reduce the complicated calculations at the microscopic scale, thereby reducing computational consumption.

Overview of dynamic homogenization methods

The purpose of the dynamic homogenization method is to predict the macroscopic properties of the composite material through its microstructure: by "packaging" the representative volume element (RVE) to study the dependence of the effective constitutive relationship on frequency and wavelength. In some homogenization theories, the description of the microscopic physical field is quite innovative. For example, in the dynamic elasticity problem, the representative result is the "average" description of the displacement field on the microscopic scale shown in Keller (1960, 1977). The result of this "smooth" description is the expected value of microscopic local disturbances. In the subsequent research and development, the definition of "volume average" (or called "ensemble average") has been widely used in the homogenization description. In this "average" mechanism, the local average of microscopic fluctuations is considered to be the homogenization result of the microstructure response. In addition, there is also some weighted description of "average" in the work of Milton & Willis (2007).

The establishment of effective constitutive laws can more effectively describe the homogenization behavior of microstructures. Regarding the research on the macroscopic effective constitutive law of composites, the dynamic homogenization theory proposed by Willis is more completed, and more details can be found in the original article Willis (1997). The initial development of Willis' theory was to describe the scattering of incident waves in inclusion problems, such as the introduction of momentum polarization "$\boldsymbol{\pi}$" and stress polarization "$\boldsymbol{\tau}$" to cope with variations in effective density and effective modulus (Willis, 1980a, 1980b). A complete part of Willis' theory is presented in Willis (1997), it presents a coupling relation, which is non-local in space and time, between the local displacement field and the stress polarization and momentum polarization fields. In some later examples (Willis, 2009; Willis, 2011; Willis, 2012), Willis' theory gradually got new

development.

In the periodic composites that we discussed, the wave response of the macrostructure is simpler. With the help of Floquet-Bloch wave expansion, the macro wave is treated separately from the local disturbance of the periodic microstructure. This idea was shown in Amirkhizi & Nemat-Nasser (2008) for electromagnetic waves and then developed by others for elastic waves, for instance, over layered elastic composites in Nemat-Nasser et al. (2011) and Shuvalov et al. (2011); over periodic elastic composites in Nemat-Nasser & Srivastava (2011, 2013) and Norris et al. (2012). In the research of homogenization theory in recent years, three application conditions are derived for the homogenization description of periodic media in Nassar et al. (2015), which present some limitations of frequencies and wavenumbers. And the application of the Hill-Mandel lemma is also discussed in Nemat-Nasser & Srivastava (2013) by comparison of the total *elastodynamic energy* and the total *complementary elastodynamic energy*.

Asymptotic methods of dynamic homogenization theory

With the development of the dynamic homogenization theory of composites, some asymptotic methods have gradually attracted researchers' attention, such as the asymptotic method based on the two-scale description. For the acoustic stage of the dispersion curves, that is the case of long-wavelength (LW) and low-frequency (LF), the description of the two-scale of macro and micro scale provides the possibility of analyzing macro behavior through microstructure. The development of the two-scale description can be traced back to the work of Bensoussan et al. (2011, reprinting of the 1978 version). The introduction of the small parameter ϵ effectively represents the asymptotic expression of the fluctuation of the macro wave on the microscale. At the same time, the definition of the small parameter ϵ also determines the ratio of the microscale to the macroscale, which defines the range of wavelengths (or wavenumbers) that can be homogenized. The micro-scale definition provided in the two-scale representation makes the hierarchical equations of the dynamic equation also satisfy the homogenization condition. A series of asymptotic elastodynamic homogenization methods were proposed for periodic media with some approximation as-

sumptions (*e.g.* frequencies and wavelengths), for example, some asymptotic analysis based on the two-scale method for long wavelengths (LW) and low frequencies (LF) cases were proposed (Boutin, 1996; Smyshlyaev & Cherednichenko, 2000). Subsequently, the two-scale homogenization description was widely applied (Fish et al., 2002a, 2002b; Wautier & Guzina, 2015). Higher-order series expressions are also used for asymptotic method (Andrianov et al., 2008; Kalamkarov et al., 2009; Andrianov et al., 2011; Andrianov et al., 2013). And an asymptotic method up to the 8-th order is applied (Hu & Oskay, 2017, 2018, 2019). As the asymptotic order increases, the effective modulus and effective density converge to the dynamic homogenization solution.

Thin homogeneous intermediate layer model and equivalent jump conditions

When studying the dynamics of composite materials, if we do not consider the special interface conditions, we can regard the tightly bonded interface of two materials as a perfect interface. In the context of mechanics, both the displacement field $\boldsymbol{u}$ and the traction vector $\boldsymbol{\tau} = \boldsymbol{\sigma} \cdot \boldsymbol{n}$ of the particles at the interface are continuous. In other words, on the perfect interface, both the tangential component of the strain field and the normal component of the stress field show continuity (Hadamard, 1903; Hill, 1961). In linear isotropic elastic materials, the normal and tangential components of the physical field were first introduced as the "interior" and "exterior" parts (Hill, 1972). This decomposition was later replaced by two orthogonal fourth-order interfacial operators and extended to general anisotropic elastic materials (Laws, 1975). This rigorous and elegant algebraic representation has been widely developed in Walpole (1981) and Hill (1983).

In addition, when dealing with interface problems, the interface is often not suitable for being considered as being perfect. In this case, it is necessary to introduce an imperfect interface model in which the physical field satisfies a certain jump relationship. Among the various imperfect interface models, two typical ones are worth noting: the spring-layer model and the interface stress model. These two interface models respectively correspond to the composite materials of two linear elastic materials with a very "soft" or "hard" thin interphase layer. The first spring-layer model allows the traction vector (the normal

component of the stress field) to be continuous at the interface, while the displacement field has a jump relationship that is linear with the traction vectors on both sides of the interface. The second interface stress model defines that the displacement field is continuous at the interface, but the traction vector has a discontinuous jump relationship (derived from the tangential component of the strain field) and satisfies the Young-Laplace equation. The aforementioned "soft" or "hard" thin interphases are relative to their adjacent materials. In particular, if there are no extreme properties in the interphase layer, the displacement field and traction vector of the imperfect interface exhibits a jumping relationship at the interface. An excellent paper that made a general discussion on this equivalent imperfect interface is Gu & He (2011). The same problem was also discussed in Benveniste (2006). The applications of this equivalent imperfect interface can be found, for example, in Gu et al. (2014), Gu et al. (2015) and Benveniste (2006).

Numerical modeling of interface jump conditions

Considering that the interface connecting different media is perfect, some effective numerical methods are applied to different domains, such as the finite element method in the solid-solid dynamic problem, the finite difference and finite volume schemes in the fluid-solid problem. In this thesis, we do not consider the solid or liquid properties of the medium, but use the finite difference numerical method to implement the jump conditions of the thin intermeddle layer model. The purpose is to test the equivalent effect of the jump conditions model and the effectiveness of the imperfect interface model.

In the development of finite difference schemes, some effective difference schemes such as the Lax-Wendroff scheme and ADER-K scheme of the first-order hyperbolic equation deserve attention (see for example Schwartzkopff et al., 2002; Schwartzkopff et al., 2004). In terms of numerical modeling, the Explicit Simplified Interface Method (ESIM) provides an effective solution that allows smooth interfaces not to rely on finite difference meshes, or called an "arbitrary-shaped" interface. (Piraux & Lombard, 2001; Lombard & Piraux, 2004, 2006; Chiavassa & Lombard, 2011). An excellent acoustic wave propagation case based on ESIM and ADER scheme was demonstrated in Lombard et al. (2017). The equivalent jump conditions refer to the homogenized middle layer model (David et al.,

2012; Marigo & Maurel, 2016, 2017; Marigo et al., 2017) or the resonance model of high-contrast inclusions (Pham et al., 2017).

In the application of the ESIM in this thesis, we identify several limitations. First, the radius of curvature of parallel smooth interfaces (boundaries of the thin interphase layer) needs to be greater than the thickness of the thin interlayer. This requirement is to ensure that the point on the interface is unique to the virtual point. Second, in order to ensure the stability of the numerical results, the number of Taylor points on both sides of the thin interphase layer should be greater than half of the difference-points in the central difference scheme, which has a similar meaning to the selection of the Taylor series radius d in Lombard et al. (2017).

Part I

Elastodynamic homogenization methods for periodic composites

Chapter 1

Preliminaries

In this chapter, we mainly introduce some preliminaries of the dynamic homogenization of periodic composites, such as the Bloch-wave representation, the definition of effective fields, and the analytical solution of the dispersion relationship of one-dimensional layered composites. Without loss of generality, all matrix operations and definitions are carried out in three-dimensional space $\mathbb{R}^3$, which will be specifically explained for some 1D and 2D applications.

1.1 Periodic microstructure

1.1.1 Periodic representative volume element

Consider a three-dimensional (3D) periodic medium which is symbolized by Ω and occupies a 3D vector space $\mathscr{E}$. Let us choose three vectors $\boldsymbol{e}_i (i = 1, 2, 3)$ such that they form a basis for the vector space $\mathscr{E}$. Then, the vector space $\mathscr{E}$ can be defined by

$$\mathscr{E} = \{\boldsymbol{x} \mid \boldsymbol{x} = a_1\boldsymbol{e}_1 + a_2\boldsymbol{e}_2 + a_3\boldsymbol{e}_3,\ a_i \in \mathbb{R}\},$$

where $\mathbb{R}$ represents the sets of real numbers. Next, a periodic lattice $\mathscr{L}$, which has the definition

$$\mathscr{L} = \{\boldsymbol{x} \in \mathscr{E} \mid \boldsymbol{x} = a_i\boldsymbol{e}_i, a_i \in \mathbb{Z}\},$$

where $\mathbb{Z}$ indicates the sets of integers. In this periodic lattice $\mathscr{L}$, a representative volume element (RVE) can be defined as the smallest area enclosed by a half distance of adjacent lattice points:

$$T = \{\boldsymbol{x} \in \mathscr{E} \mid \forall \boldsymbol{r} \in \mathscr{L} - \{\boldsymbol{0}\},\ \|\boldsymbol{x}\| \leqslant \|\boldsymbol{x} - \boldsymbol{r}\|\}.$$

Assuming that a function $\boldsymbol{\phi}(x)$ represents the material properties (such as elastic modulus and mass density, etc.) of the periodic medium Ω, then $\boldsymbol{\phi}(x)$ has to satisfy the following periodic relationship:

$$\boldsymbol{\phi}(\boldsymbol{x}) = \boldsymbol{\phi}(\boldsymbol{x} + \boldsymbol{r}),\ \boldsymbol{x} \in T,\ \boldsymbol{r} \in \mathscr{L}. \tag{1.1}$$

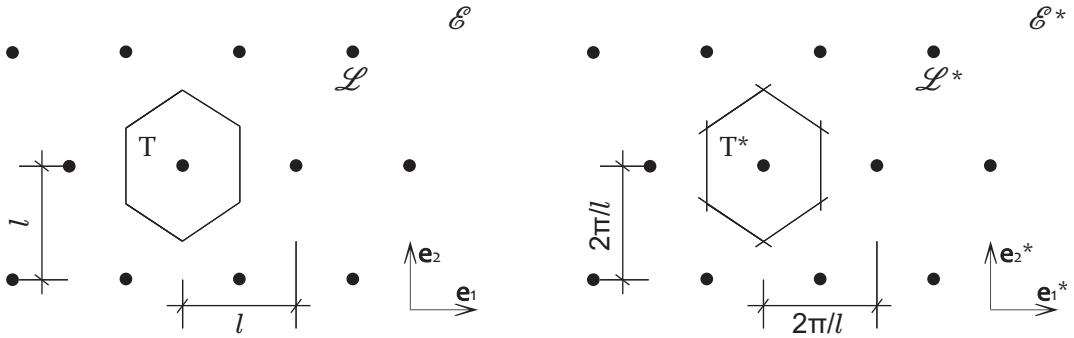

Figure 1.1: *(a) A 2D geometrical illustration of the periodic space $\mathscr{E}$ and the periodic lattice $\mathscr{L}$. The representative volume element (RVE) is defined as the smallest area enclosed by a half distance of adjacent lattice points. (b) The reciprocal model composed by the periodic space $\mathscr{E}^*$ and the periodic lattice $\mathscr{L}^*$, the unit cell T^* is defined as the first Brillouin zone of $\mathscr{L}^*$.*

The reciprocal space of $\mathscr{E}$ is denoted by $\mathscr{E}^*$, which has three base vectors $\boldsymbol{e}_i^*(i = 1, 2, 3)$. There exists a relation between the base vectors of $\mathscr{E}$ and $\mathscr{E}^*$: $\boldsymbol{e}_i \cdot \boldsymbol{e}_j^* = 2\pi\delta_{ij}$, where δ_{ij} is the Kronecker's delta symbol. Similar with the position vector $\boldsymbol{x}$, the wave number $\boldsymbol{k}$ plays the same role in reciprocal space $\mathscr{E}^*$, which can be defined as the combination of the reciprocal lattice $\mathscr{L}^*$ and the first Brillouin zone T^*: $\mathscr{E}^* = \mathscr{L}^* \cup T^*$. Fig.(1.1) illustrates an example of 2D hexagonal periodic RVE T and T^*.

1.1.2 Bloch-wave representation

The homogenized descriptions of periodic materials takes into account the different scale expression. The introduction of the Bloch-wave transformation is to express the definition of displacements in two scales (microscopic and macroscopic scales). In the same way, it also shows the result of "localization" and "homogenization" operations. The Fourier transform of a wave function $\boldsymbol{\phi}(\boldsymbol{x})$ gives

$$\boldsymbol{\phi}(\boldsymbol{x}) = \int_{\boldsymbol{k}\in\mathscr{E}^*} \tilde{\boldsymbol{\phi}}(\boldsymbol{k}) e^{i\boldsymbol{k}\cdot\boldsymbol{x}} d_{\boldsymbol{k}},$$

where $\boldsymbol{k}$ represents the wave number. Under the definition of the reciprocal lattice $\mathscr{L}^*$, the vector space $\mathscr{E}^*$ is the space combination of the lattice space $\mathscr{L}^*$ and the first Brillouin zone T^*. Considering the "local" scale for T^*, the integral of $\tilde{\boldsymbol{\phi}}(\boldsymbol{k})$ can be given as

$$\int_{\boldsymbol{k}\in\mathscr{E}^*} \tilde{\boldsymbol{\phi}}(\boldsymbol{k}) e^{i\boldsymbol{k}\cdot\boldsymbol{x}} d_{\boldsymbol{k}} = \int_{\boldsymbol{k}\in\mathscr{L}^*} \left(\int_{\boldsymbol{\xi}\in T^*} \tilde{\boldsymbol{\phi}}_{\boldsymbol{k}}(\boldsymbol{\xi}) e^{i\boldsymbol{\xi}\cdot\boldsymbol{x}} d_{\boldsymbol{\xi}} \right) e^{i\boldsymbol{k}\cdot\boldsymbol{x}} d_{\boldsymbol{k}}.$$

Then Bloch-wave expansion in the series form is shown as

$$\boldsymbol{\phi}(\boldsymbol{x}) = \sum_{\boldsymbol{k}\in\mathscr{E}^*} \tilde{\boldsymbol{\phi}}(\boldsymbol{k}) e^{i\boldsymbol{k}\cdot\boldsymbol{x}} = \sum_{\boldsymbol{k}\in\mathscr{L}^*} \tilde{\boldsymbol{\phi}}_{\boldsymbol{k}}(\boldsymbol{x}) e^{i\boldsymbol{k}\cdot\boldsymbol{x}} = \sum_{\boldsymbol{k}\in\mathscr{L}^*} \left(\sum_{\boldsymbol{\xi}\in T^*} \tilde{\boldsymbol{\phi}}_{\boldsymbol{k}}(\boldsymbol{\xi}) e^{i\boldsymbol{\xi}\cdot\boldsymbol{x}} \right) e^{i\boldsymbol{k}\cdot\boldsymbol{x}}.$$

This benefits from the Bloch-wave transform basis on the superposition for the periodic field $\tilde{\boldsymbol{\phi}}(\boldsymbol{k})$ over the periodic lattice space $\mathscr{L}^*$. In other words, this is due to the periodic property of the composite.

In the plane harmonic dynamics problem, we consider the Bloch-wave expansion as

$$\boldsymbol{\phi}(\boldsymbol{x}) = \tilde{\boldsymbol{\phi}}_{\boldsymbol{k}}(\boldsymbol{x}) e^{i(\boldsymbol{k}\cdot\boldsymbol{x} - wt)},$$

where $\tilde{\boldsymbol{\phi}}_{\boldsymbol{k}}(\boldsymbol{x})$ represents "local" amplitude and $\boldsymbol{k}$ stands for the "macro" wave number, the portion of e^{-iwt} represents the time dependence of the wave. In order to simplify the presentation, the time part e^{-iwt} is omitted in all the following contents.

1.2 Elastodynamics of periodic microstructure

1.2.1 Local dynamic equation

Let $\boldsymbol{u}$ be the displacement field over the periodic medium Ω. The linear constitutive relation between the stress field $\boldsymbol{\sigma}$ and the strain field $\boldsymbol{\varepsilon}$, and the linear momentum equation between the momentum field $\boldsymbol{p}$ and the velocity field $\boldsymbol{v}$ have the following form:

$$\boldsymbol{\sigma} = \mathbb{C} : \boldsymbol{\varepsilon} = \mathbb{C} : (\boldsymbol{\nabla} \otimes^s \boldsymbol{u}), \quad \boldsymbol{p} = \boldsymbol{\rho} \boldsymbol{v} = \boldsymbol{\rho} \dot{\boldsymbol{u}},$$

where $\otimes^s$ represents a symmetric gradient operator, the superscript point of $\dot{\boldsymbol{u}}$ stands for the time derivative of $\boldsymbol{u}$, and the tensor $\mathbb{C}$ and $\boldsymbol{\rho}$ are the fourth-order elastic stiffness tensor and the mass density tensor, respectively. Thanks to the local periodic condition, the property of tensors ($\mathbb{C}$, $\boldsymbol{\rho}$) satisfies the periodic condition (1.1).

Let us introduce the volume force $\boldsymbol{f}$. Using the Bloch-wave representation, we can write the displacement response of the harmonic volume force $\boldsymbol{f}(\boldsymbol{x}) = \tilde{\boldsymbol{f}}_{\boldsymbol{k}} e^{i\boldsymbol{k}\cdot\boldsymbol{x}}$ as $\boldsymbol{u}(\boldsymbol{x}) = \tilde{\boldsymbol{u}}_{\boldsymbol{k}}(\boldsymbol{x}) e^{i\boldsymbol{k}\cdot\boldsymbol{x}}$ over the periodic medium Ω. The gradient and divergence fields of $\boldsymbol{u}(\boldsymbol{x})$ are expressed as

$$\boldsymbol{\nabla} \boldsymbol{u}(\boldsymbol{x}) = (\boldsymbol{\nabla} + i\boldsymbol{k}) \otimes \tilde{\boldsymbol{u}}_{\boldsymbol{k}}(\boldsymbol{x}) e^{i\boldsymbol{k}\cdot\boldsymbol{x}}, \quad \boldsymbol{\nabla} \cdot \boldsymbol{u}(\boldsymbol{x}) = (\boldsymbol{\nabla} + i\boldsymbol{k}) \cdot \tilde{\boldsymbol{u}}_{\boldsymbol{k}}(\boldsymbol{x}) e^{i\boldsymbol{k}\cdot\boldsymbol{x}}.$$

Other local fields (like $\boldsymbol{v}$, $\boldsymbol{\varepsilon}$, $\boldsymbol{p}$, and $\boldsymbol{\sigma}$) also satisfy the Bloch-wave representation and local periodic condition (1.1). Ignoring the term $e^{i\boldsymbol{k}\cdot\boldsymbol{x}}$, the local dynamic equation can be simply written as

$$(\boldsymbol{\nabla} + i\boldsymbol{k}) \cdot [\mathbb{C} : (\boldsymbol{\nabla} + i\boldsymbol{k}) \otimes^s \tilde{\boldsymbol{u}}_{\boldsymbol{k}}] + \tilde{\boldsymbol{f}}_{\boldsymbol{k}} = -w^2 \boldsymbol{\rho} \tilde{\boldsymbol{u}}_{\boldsymbol{k}}. \tag{1.2}$$

1.2.2 Effective field description

In the homogenization step of dynamic equations, the effective field is defined as the volume average over the cell T:

$$\langle \boldsymbol{\phi}(\boldsymbol{x}) \rangle \equiv \langle \tilde{\boldsymbol{\phi}}_{\boldsymbol{k}}(\boldsymbol{x}) \rangle e^{i\boldsymbol{k}\cdot\boldsymbol{x}} = \left(\frac{1}{|T|} \int_T \tilde{\boldsymbol{\phi}}_{\boldsymbol{k}}(\boldsymbol{x}) d_T \right) e^{i\boldsymbol{k}\cdot\boldsymbol{x}}, \tag{1.3}$$

where $\langle\cdot\rangle$ stands for a local volume average operator. It provides an effective field definition to describe the local homogenization properties of microwaves. As the local stress field $\tilde{\boldsymbol{\sigma}}$ satisfies the periodic condition, the divergence of the stress field has a null mean ($\langle\boldsymbol{\nabla}\cdot\tilde{\boldsymbol{\sigma}}\rangle = \mathbf{0}$). Then, the homogenized dynamic equation can be expressed as

$$i\boldsymbol{k}\cdot\langle\tilde{\boldsymbol{\sigma}}\rangle + \langle\tilde{\boldsymbol{f}}\rangle = -iw\langle\tilde{\boldsymbol{p}}\rangle. \tag{1.4}$$

In this effective equation, the exploration of the relationship between the effective fields $\langle\tilde{\boldsymbol{\sigma}}\rangle$ and $\langle\tilde{\boldsymbol{p}}\rangle$, and the solution $\langle\tilde{\boldsymbol{u}}\rangle$ will become the core purpose. To this end, Willis' effective constitutive law perfectly solves this problem. With the introduction of a free-strain field $\tilde{\boldsymbol{E}}_0$ (Bloch-wave representation available), the effective constitutive law has the form:

$$\begin{bmatrix}\langle\tilde{\boldsymbol{\sigma}}\rangle\\ \langle\tilde{\boldsymbol{p}}\rangle\end{bmatrix} = \begin{bmatrix}\mathbb{C}^e & \boldsymbol{S}^e\\ \boldsymbol{T}^e & \boldsymbol{\rho}^e\end{bmatrix}_{(\boldsymbol{k},w)} \begin{bmatrix}\langle\tilde{\boldsymbol{\varepsilon}}\rangle - \tilde{\boldsymbol{E}}_0\\ \langle\tilde{\boldsymbol{v}}\rangle\end{bmatrix}, \tag{1.5}$$

where $\mathbb{C}^e$ and $\boldsymbol{\rho}^e$ represent the elastic stiffness and mass density components, $\boldsymbol{S}^e$ and $\boldsymbol{T}^e$ provide a non-local coupling interpretation between the effective fields $\langle\tilde{\boldsymbol{\sigma}}\rangle$, $\langle\tilde{\boldsymbol{v}}\rangle$ and $\langle\tilde{\boldsymbol{p}}\rangle$, $\langle\tilde{\boldsymbol{\varepsilon}}\rangle$, respectively. Here, the subscript $(\boldsymbol{k}, w)$ describes a frequency dependence for this effective constitutive law.

1.3 Dispersion relationship of layered materials

Considering a layered composite, the displacement response $\tilde{\boldsymbol{u}}$ is expressed as a solution to the following local dynamic equation (Bloch-wave representation available):

$$\boldsymbol{\nabla}\cdot\tilde{\boldsymbol{\sigma}} + \tilde{\boldsymbol{f}} = \boldsymbol{\rho}\ddot{\tilde{\boldsymbol{u}}}, \quad \tilde{\boldsymbol{\sigma}} = \mathbb{C} : \left((\boldsymbol{\nabla} + i\boldsymbol{k}) \otimes^s \tilde{\boldsymbol{u}}\right). \tag{1.6}$$

We take a three-phase layered composite as example, which has thickness ratios α_1, α_2 and α_3 (with $\alpha_1 + \alpha_2 + \alpha_3 = 1$) as shown in Fig.(1.3).

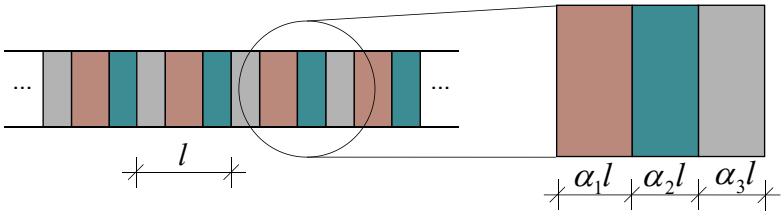

Figure 1.2: *Infinite three-phase periodic layered material model and the representative volume element (RVE) with the thickness ratio of* $\alpha_1 : \alpha_2 : \alpha_3$.

1.3.1 Analytical solution

In order to simplify the problem, we are interested in the case where the dispersion relationship of the layered composite can be reduced to a 1D case. The local dynamic equation is then expressed as

$$(\frac{\partial}{\partial x} + ik)\tilde{\sigma} + \tilde{f} = \rho\frac{\partial^2\tilde{u}}{\partial t^2}, \quad \tilde{\sigma} = E(\frac{\partial}{\partial x} + ik)\tilde{u}, \tag{1.7}$$

where E and ρ represent the elastic modulus and mass density, respectively. Considering the Fourier transform of the time derivative, in the frequency domain, the above dynamic equation can be written as a second-order non-homogeneous equation:

$$\frac{\partial^2\tilde{u}}{\partial x^2} + 2ik\frac{\partial\tilde{u}}{\partial x} + \left(\frac{\rho w^2}{E} - k^2\right)\tilde{u} = -\frac{\tilde{f}}{E},$$

and the corresponding equation for the case of $\tilde{f} = 0$ reads

$$\frac{\partial^2\tilde{u}}{\partial x^2} + 2ik\frac{\partial\tilde{u}}{\partial x} + \left(\frac{\rho w^2}{E} - k^2\right)\tilde{u} = 0.$$

The general solution $\tilde{u}_g(x)$ can be expressed as

$$\tilde{u}_g(x) = Ae^{zx} + Be^{z^*x},$$

where $z, z^* = -ik \pm iw\sqrt{\rho/E}$ are two solutions to the characteristic equation of Eq.(1.7), A and B are two coefficients to be determined.

We set the size of the periodic representative cell to be l (the thicknesses of the components are $\alpha_1 l$, $\alpha_2 l$ and $\alpha_3 l$), the continuity conditions of the displacement field $\tilde{u}$ and

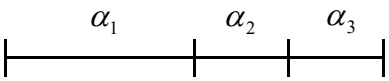

Figure 1.3: *The 1D equivalent diagrammatic sketch of the three-phase layered composite RVE with the thickness ratio of* $\alpha_1 : \alpha_2 : \alpha_3$.

traction vector $\tilde{\tau} = E\frac{\partial \tilde{u}}{\partial x}$ across the perfect interface can be expressed as

$$\tilde{u}_1(0) = \tilde{u}_2(l), \quad \tilde{u}_1(\alpha_1 l) = \tilde{u}_2(\alpha_1 l), \quad \tilde{u}_1\left((\alpha_1+\alpha_2)l\right) = \tilde{u}_2\left((\alpha_1+\alpha_2)l\right),$$
$$\tilde{\tau}_1(0) = \tilde{\tau}_2(l), \quad \tilde{\tau}_1(\alpha_1 l) = \tilde{\tau}_2(\alpha_1 l), \quad \tilde{\tau}_1\left((\alpha_1+\alpha_2)l\right) = \tilde{\tau}_2\left((\alpha_1+\alpha_2)l\right),$$

where $l_1 = \alpha_1 l$, $l_2 = (\alpha_1+\alpha_2)l$ and $l_3 = (\alpha_1+\alpha_2+\alpha_3)l = l$. With the help of general solution $\tilde{u}_g$, we can rewrite the above conditions into a matrix form:

$$\begin{bmatrix} 1 & 1 & 0 & 0 & -e^{z_3 l_3} & -e^{z_3^* l_3} \\ iw\eta_1 & -iw\eta_1 & 0 & 0 & -iw\eta_3 e^{z_3 l_3} & iw\eta_3 e^{z_3^* l_3} \\ e^{z_1 l_1} & e^{z_1^* l_1} & -e^{z_2 l_1} & -e^{z_2^* l_1} & 0 & 0 \\ iw\eta_1 e^{z_1 l_1} & -iw\eta_1 e^{z_1^* l_1} & -iw\eta_2 e^{z_2 l_1} & iw\eta_2 e^{z_2^* l_1} & 0 & 0 \\ 0 & 0 & e^{z_2 l_2} & e^{z_2^* l_2} & -e^{z_3 l_2} & -e^{z_3^* l_2} \\ 0 & 0 & iw\eta_2 e^{z_2 l_2} & -iw\eta_2 e^{z_2^* l_2} & -iw\eta_3 e^{z_3 l_2} & iw\eta_3 e^{z_3^* l_2} \end{bmatrix} \begin{bmatrix} A_1 \\ B_1 \\ A_2 \\ B_2 \\ A_3 \\ B_3 \end{bmatrix} = \begin{bmatrix} 0 \\ 0 \\ 0 \\ 0 \\ 0 \\ 0 \end{bmatrix},$$

where the impedance $\eta_i = \sqrt{\rho_i E_i}$, the velocity $c_i = \sqrt{E_i/\rho_i}$ and $z_i, z_i^* = -ik \pm iw/c_i$ for $i = (1, 2, 3)$.

The above matrix equation contains all the continuous conditions of different media across the interfaces and the periodic boundary conditions of the RVE. On the one hand, from a mathematical point of view, in order to ensure that coefficients A and B have non-zero solutions (or called non-trivial solutions), the coefficient matrix must have a zero determinant. This condition allows us to determine the dispersion relationship between the wave number k and the angular frequency w through the definition of the zero determinant of the coefficient matrix. On the other hand, from a physical point of view, when the solutions of A and B are both zero, it means that the material has no displacement response in all material layers. In theory, the result that both A and B are zero will only appear in the case of infinite stiffness of the material, and this kind of "infinity" stiffness material is not what we expect to have in this problem. Back to this three-phase layer

composite model, the zero determinant condition of the coefficient matrix can be simplified to the following expression:

$$\begin{aligned} 8\eta_1\eta_2\eta_3 cos(kl) = &(\eta_1+\eta_2)(\eta_2+\eta_3)(\eta_3+\eta_1)cos\left(wl(\frac{\alpha_1}{c_1}+\frac{\alpha_2}{c_2}+\frac{\alpha_3}{c_3})\right) \\ &-(\eta_1+\eta_2)(\eta_2-\eta_3)(-\eta_3+\eta_1)cos\left(wl(\frac{\alpha_1}{c_1}+\frac{\alpha_2}{c_2}-\frac{\alpha_3}{c_3})\right) \\ &-(\eta_1-\eta_2)(-\eta_2+\eta_3)(\eta_3+\eta_1)cos\left(wl(\frac{\alpha_1}{c_1}-\frac{\alpha_2}{c_2}+\frac{\alpha_3}{c_3})\right) \\ &-(-\eta_1+\eta_2)(\eta_2+\eta_3)(\eta_3-\eta_1)cos\left(wl(-\frac{\alpha_1}{c_1}+\frac{\alpha_2}{c_2}+\frac{\alpha_3}{c_3})\right) \end{aligned} . \tag{1.8}$$

Obviously, this relationship can be degraded into a two-phase layered composite case by setting two material properties to be the same. For example, in the two-phase layered composite model, we can get

$$4\eta_1\eta_2 cos(kl) = (\eta_1+\eta_2)^2 cos\left(wl(\frac{\alpha_1}{c_1}+\frac{\alpha_2}{c_2})\right) - (\eta_1-\eta_2)^2 cos\left(wl(\frac{\alpha_1}{c_1}-\frac{\alpha_2}{c_2})\right). \tag{1.9}$$

Multi-phase layered composite

Next, we consider a multi-layered periodic composite, we can also solve the analytical dispersion relation with the aid of the zero-determinant condition mentioned above. For example, in an n-layer ($n \geqslant 2$) infinitely periodic layered model, the size of the coefficient matrix formed by the interface continuity condition and the periodic boundary condition is $(2n*2n)$. Obviously, solving the zero-determinant relationship of the matrix is a tedious mathematical task. And in this subsection, we will directly give a simplified expression. The medium thickness ratio is set to α_i, and $\sum_{i=1}^{n}\alpha_i = 1$.

Before describing the dispersion relationship of multi-phase layered composites, we introduce two preliminary coefficients:

$$P_{(n)} = (\eta_1+\eta_2)(\eta_2+\eta_3)\ldots(\eta_{n-1}+\eta_n)(\eta_n+\eta_1), \quad Q_{(n)} = \frac{\alpha_1}{c_1}+\frac{\alpha_2}{c_2}+\ldots+\frac{\alpha_n}{c_n}.$$

In addition, we take m elements from a set of n elements and let the matrix $\mathcal{R}_{(n)}^{(m)}$ denote

the set of all combinations. Therefore, the total number of elements in $\mathcal{R}_{(n)}^{(m)}$ is C_n^m, where

$$C_n^m = \frac{n!}{m!(n-m)!}.$$

Let $\boldsymbol{r}_i$ be the i-th combination in the matrix $\mathcal{R}_{(n)}^{(m)}$. Next, we mark the η items and α items of $\boldsymbol{r}_i$ combination in $P_{(n)}^{(\boldsymbol{r}_i)}$ and $Q_{(n)}^{(\boldsymbol{r}_i)}$ as negative, and the rest as positive. For example, for $n = 4$ and $m = 2$, the combination $\boldsymbol{r}_i$ of $\mathcal{R}_{(n)}^{(m)}$ shows

$$\begin{aligned} &\boldsymbol{r}_1 = (1,2), \quad \boldsymbol{r}_2 = (1,3), \quad \boldsymbol{r}_3 = (1,4), \\ &\boldsymbol{r}_4 = (2,3), \quad \boldsymbol{r}_5 = (2,4), \quad \boldsymbol{r}_6 = (3,4). \end{aligned}$$

Take the combination $(\boldsymbol{r}_i) = (1,3)$ as an example, the parameters $P_{(n)}^{(\boldsymbol{r}_i)}$ and $Q_{(n)}^{(\boldsymbol{r}_i)}$ are given as

$$P_{(4)}^{(1,3)} = (-\eta_1 + \eta_2)(\eta_2 - \eta_3)(-\eta_3 + \eta_4)(\eta_4 - \eta_1), \quad Q_{(4)}^{(1,3)} = -\frac{\alpha_1}{c_1} + \frac{\alpha_2}{c_2} - \frac{\alpha_3}{c_3} + \frac{\alpha_4}{c_4}.$$

It is worth noting that when $m = 0$, the combination $\boldsymbol{r}_1$ is an empty set $\varnothing$, and the parameters $P_{(n)}^{(\varnothing)} = P_{(n)}$ and $Q_{(n)}^{(\varnothing)} = Q_{(n)}$ at this time. Finally, the dispersion relationship $(k - w)$ of n-phase layered composite can be given as

$$2^n \left(\prod_{m=0}^{n} \eta_m \right) cos(kl) = \frac{1}{2} \sum_{m=0}^{n} \left((-1)^m \sum_{i=1}^{C_n^m} P_{(n)}^{(\boldsymbol{r}_i)} cos\left(Q_{(n)}^{(\boldsymbol{r}_i)} wl \right) \right). \tag{1.10}$$

Obviously, the above expression satisfies the periodic condition, and the wave number can describe the $(k - w)$ dispersion relationship perfectly only in the stage $kl \leqslant \pi$, which is consistent with the wave number limitation proposed by Nassar et al. (2015). Similarly, this general expression can be degenerated to the case of three-layer composites (1.8) or two-layer composites (1.9) by defining the number of materials $n = 3$ or $n = 2$.

1.3.2 Finite Element solution

Using the same description as in the previous subsection, we consider a 1D model to replace this layered composite. In this problem, the finite element method is considered to

obtain the numerical results under the corresponding mesh (the accuracy of the numerical solution depends on the mesh size). Rewrite the local dynamic equation (3.2) in the frequency domain as

$$E\frac{\partial^2\tilde{u}}{\partial x^2} + 2ikE\frac{\partial\tilde{u}}{\partial x} + [E(ik)^2 - \rho(iw)^2]\tilde{u} + \tilde{f} = 0.$$

Integrating the above equation on the domain Ω and using a test function $\delta\tilde{u}$ (meeting the periodic conditions), we get

$$\int_\Omega E\frac{\partial^2\tilde{u}}{\partial x^2}\delta\tilde{u}d_x + \int_\Omega 2ikE\frac{\partial\tilde{u}}{\partial x}\delta\tilde{u}d_x + \int_\Omega [E(ik)^2 - \rho(iw)^2]\tilde{u}\delta\tilde{u}d_x + \int_\Omega \tilde{f}\delta\tilde{u}d_x = 0.$$

With the help of the divergence theorem and the periodic conditions, the local dynamic equation can be expressed as the following weak form equation:

$$-E\int_\Omega \frac{\partial\tilde{u}}{\partial x}\frac{\partial\delta\tilde{u}}{\partial x}d_x + 2ikE\int_\Omega \frac{\partial\tilde{u}}{\partial x}\delta\tilde{u}d_x + E\int_\Omega (ik)^2\tilde{u}\delta\tilde{u}d_x - \rho(iw)^2\int_\Omega \tilde{u}\delta\tilde{u}d_x + \int_\Omega \tilde{f}\delta\tilde{u}d_x = 0.$$

Try to rewrite the above equation as the form $k(\tilde{u},\delta\tilde{u}) - w^2 m(\tilde{u},\delta\tilde{u}) = f(\tilde{f},\delta\tilde{u})$, where the function $k(\cdot,\cdot)$, $m(\cdot,\cdot)$ and $f(\cdot,\cdot)$ are defined by

$$\begin{aligned}
k(\tilde{u},\delta\tilde{u}) &= E\int_\Omega \frac{\partial\tilde{u}}{\partial x}\frac{\partial\delta\tilde{u}}{\partial x}d_x - 2ikE\int_\Omega \frac{\partial\tilde{u}}{\partial x}\delta\tilde{u}d_x - E\int_\Omega (ik)^2\tilde{u}\delta\tilde{u}d_x,\\
m(\tilde{u},\delta\tilde{u}) &= \rho\int_\Omega \tilde{u}\delta\tilde{u}d_x,\\
f(\tilde{f},\delta\tilde{u}) &= \int_\Omega \tilde{f}\delta\tilde{u}d_x.
\end{aligned}$$

In the finite element method, the next work is some simple matrix description. With the help of Lagrangian polynomials (or Cramer's rule), the displacement interpolation function can be determined by the value of discrete points. Process all the elements in a loop, and assemble all the elementary systems to construct a global dynamic equation:

$$\left([K] - w^2[M]\right)[\tilde{U}] = [F].$$

At the same time, we introduce a matrix relationship $[P][\tilde{U}] = [0]$ to describe the interface continuous condition and the periodic boundary condition of the composite model, where

$[P]$ represents the coefficient matrix of discrete points corresponding to the continuity and periodic conditions. Using the method of Lagrange multipliers and introducing the Lagrange multiplier λ, we can construct a Lagrangian function

$$\left([K] - w^2[M]\right)[\tilde{U}] + \lambda[P][\tilde{U}] = [F].$$

The global matrices $[K]_{glob}$ and $[M]_{glob}$ can be constructed as

$$\left(\underbrace{\begin{bmatrix} [K] & [P]^{T^*} \\ [P] & [L] \end{bmatrix}}_{[K]_{glob}} - w^2 \underbrace{\begin{bmatrix} [M] & [0] \\ [0] & [L] \end{bmatrix}}_{[M]_{glob}} \right) \begin{bmatrix} [\tilde{U}] \\ [\tilde{\Lambda}] \end{bmatrix} = \begin{bmatrix} [F] \\ [0] \end{bmatrix},$$

where $[\tilde{\Lambda}]$ is an additional variable, the conjugate complex transpose superscript T^* makes the global matrix $[K]_{glob}$ satisfy Hermitian symmetry, and the matrix $[L]$ is constructed as a small parameter diagonal matrix. The matrix $[K]_{glob}$ and $[M]_{glob}$ are respectively composed of the elastic module E and the mass density ρ, and include all periodic and continuous conditions. Since the matrix $[K]_{glob}$ is related to the wave number k, the dispersion relationship will be determined by the generalized eigenvalues of the matrices $[K]_{glob}$ and $[M]_{glob}$:

$$[K]_{glob}[v] = \lambda[M]_{glob}[v],$$

where the generalized eigenvalues λ represent the square of the angular frequencies w^2, $[v]$ stand for the generalized eigenvectors.

1.3.3 Numerical example

Considering the quasi-static case, the homogeneous properties depend on the average material properties of the RVE. The effective elastic tensor $\mathbb{C}^{eff}$ and the mass density $\boldsymbol{\rho}^{eff}$ can be defined by the effective constitutive law and the effective momentum relation:

$$\langle \tilde{\boldsymbol{\sigma}} \rangle = \langle \mathbb{C} : \tilde{\boldsymbol{\varepsilon}} \rangle \equiv \mathbb{C}^{eff} : \langle \tilde{\boldsymbol{\varepsilon}} \rangle, \quad \langle \tilde{\boldsymbol{p}} \rangle = \langle -iw\boldsymbol{\rho} \cdot \tilde{\boldsymbol{u}} \rangle \equiv -iw\boldsymbol{\rho}^{eff} \cdot \langle \tilde{\boldsymbol{u}} \rangle.$$

Therefore, when we consider a multi-phase layered composite (n-phase) with thickness ratios α_i, in the equivalent 1D model, the average value of Young's modulus E^{eff} and mass density ρ^{eff} have

$$E^{eff} = (\sum_{i}^{n} \frac{\alpha_i}{E_i})^{-1}, \quad \rho^{eff} = \sum_{i}^{n} \alpha_i \rho_i.$$

The effective impedance of the quasi-static solution gives $\mathcal{Z} = iw\rho^{eff}iw - ikE^{eff}ik$. The dispersion relationship can be given by the zero determinant of the effective impedance $det\{\mathcal{Z}\} = 0$.

Next, we give an example of the three-phase layered model described earlier: the ratio of the media thickness α_1, α_2 and α_3 satisfies $\alpha_1 : \alpha_2 : \alpha_3 = 0.52 : 0.23 : 0.25$. And the cell size is set to $l = 0.01(m)$. In addition, the material properties of these three media are given as: the Young's modulus $E_1 = 3.0 \times 10^8(Pa)$, $E_2 = 2.0 \times 10^{11}(Pa)$, and $E_3 = 1.0 \times 10^{10}(Pa)$; the mass density $\rho_1 = 1000(kg/m^3)$, $\rho_2 = 3000(kg/m^3)$, and $\rho_3 = 900(kg/m^3)$. The two aforementioned methods (Analytical solution and numerical Finite Element solution) will be used to determine the $(k - w)$ dispersion relationship of this 1D equivalent model. Fig.(1.4a) shows the analytical solution (1.8) and the numerical solution (finite element solution) of the dispersion relationship between wave number k and angular frequency w. The comparison between the quasi-static dispersion relationship and the dynamic one is shown in Fig.(1.4b).

Obviously, in the dynamic problem (k is not zero), the dispersion relationship between k and w is not constant. This will also mean that there is a frequency dependence of the constitutive law, as shown in Eq.(1.5). It is worth mentioning that the finite element solution of the dispersion relationship can also be adapted to the general 2D situation, but its accuracy depends on the mesh size. However, the analytical solution is the limited. For more complex 2D models, the analytical solution expression does not seem to be easy to derive. For this reason, in the following two chapters, we will discuss two commonly used dynamic homogenization methods, namely Willis dynamic homogenization theory and two-scale asymptotic homogenization method, in the long-wavelength and low-frequency (LW-LF) cases.

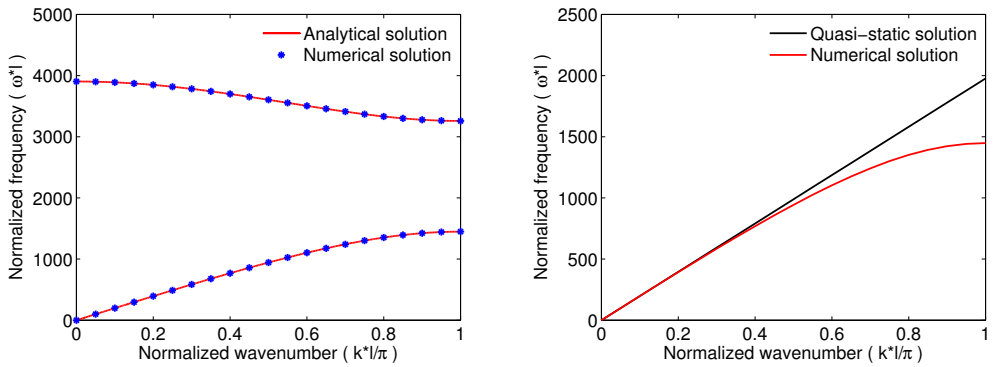

(a) (b)

Figure 1.4: *(a) Comparison of the acoustic (the curves on the bottom) and lowest optical (the curves on the top) dispersion curves for the numerical solution and the analytical solution, (b) Acoustic branch of dispersion curves for the Quasi-static solution and the analytical solution.*

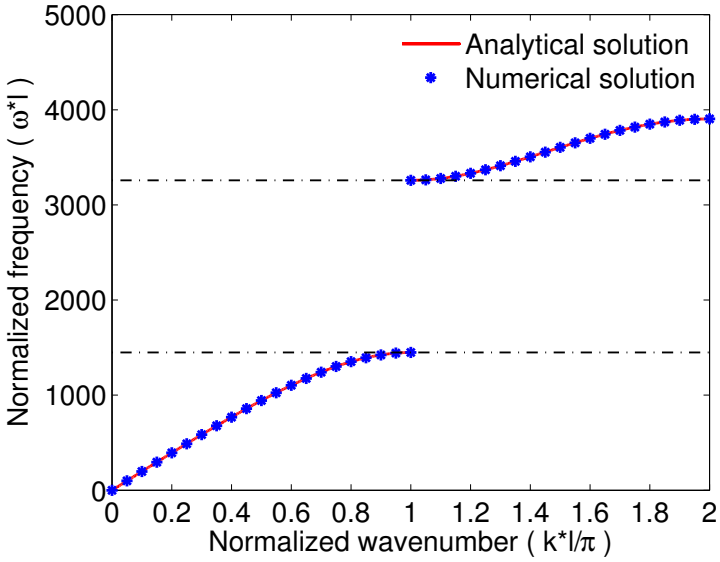

Figure 1.5: *Non-folding illustration of dispersion curves for the numerical solution and the analytical solution.*

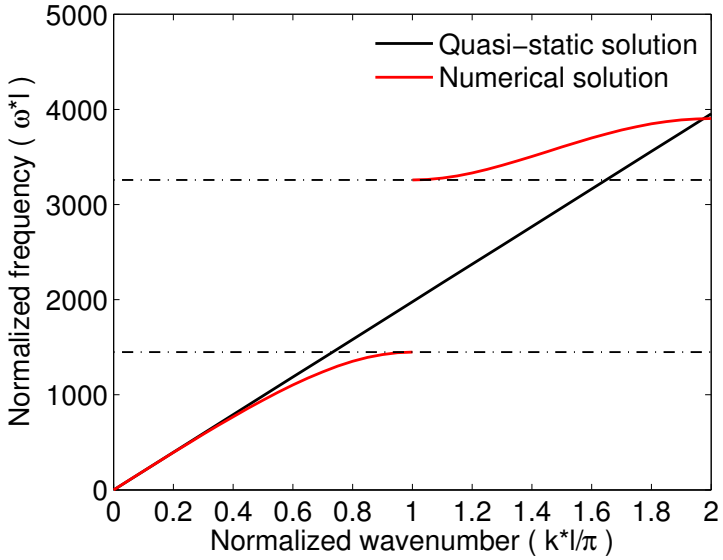

Figure 1.6: *Non-folding illustration of dispersion curves for the quasi-static solution and the analytical solution.*

Chapter 2

Willis' elastodynamic homogenization theory for periodic composites

This chapter will mainly introduce the Willis dynamic homogenization theory, and then introduce the numerical scheme to determine the effective constitutive law and the acoustic dispersion relationship. In dynamic elasticity problems, Willis' theory provides an effective constitutive law of the dynamic homogenization for the long-wavelength and low-frequency waves. In the optical dispersion stage, the numerical scheme shown in this chapter does not seem to be applicable, so the following main research content is based on the acoustic dispersion stage.

2.1 Willis' homogenization description

In this section, we mainly review the localization and homogenization description of Willis' theory and the resulting effective constitutive law.

2.1.1 Localization step

In Willis' elastodynamic homogenization theory presented in his work of 1997 (Willis, 1997), the solution of the local dynamic equation $\tilde{\boldsymbol{u}}$ can be expressed as a coupling of the homogenization solution to the effective strain field $\langle\tilde{\boldsymbol{\varepsilon}}\rangle$ and the effective velocity field $\langle\tilde{\boldsymbol{v}}\rangle$,

that can be expressed as

$$\tilde{\boldsymbol{u}} = \langle \tilde{\boldsymbol{u}} \rangle + \mathcal{A} : (\langle \tilde{\boldsymbol{\varepsilon}} \rangle - \tilde{\boldsymbol{E}}_0) + \boldsymbol{B} \cdot \langle \tilde{\boldsymbol{v}} \rangle, \tag{2.1}$$

where $\mathcal{A}$ and $\boldsymbol{B}$ are two localization tensors need to be determined, and the tensor $\tilde{\boldsymbol{E}}_0$ stands for a free-strain field. As definitions of the effective fields $\langle \tilde{\boldsymbol{\varepsilon}} \rangle$ and $\langle \tilde{\boldsymbol{v}} \rangle$, there exist a relationship between these two effective fields:

$$-iw\langle \tilde{\boldsymbol{\varepsilon}} \rangle = i\boldsymbol{k} \otimes^s \langle \tilde{\boldsymbol{v}} \rangle, \tag{2.2}$$

where wave number $\boldsymbol{k}$ and angular frequency w satisfy the dispersion relationship of the homogenized dynamic equation. These two effective fields are not independent of each other, which makes that the tensors $\mathcal{A}$ and $\boldsymbol{B}$ are interrelated.

One approach proposed in Willis' theory to obtain these two tensors is to introduce a free-strain field $\tilde{\boldsymbol{E}}_0$ (Bloch-wave representation available), which is independent of the effective velocity field. Correspondingly, the local dynamic equation takes the form

$$(\boldsymbol{\nabla} + i\boldsymbol{k}) \cdot \{\mathbb{C} : [(\boldsymbol{\nabla} + i\boldsymbol{k}) \otimes^s \tilde{\boldsymbol{u}} - \tilde{\boldsymbol{E}}_0]\} + \tilde{\boldsymbol{f}} = -w^2 \boldsymbol{\rho} \tilde{\boldsymbol{u}}, \tag{2.3}$$

where the local constitutive relationship has $\tilde{\boldsymbol{\sigma}} = \mathbb{C} : (\tilde{\boldsymbol{\varepsilon}} - \tilde{\boldsymbol{E}}_0)$. Importantly, the free-strain $\tilde{\boldsymbol{E}}_0$ and the volume force $\tilde{\boldsymbol{f}}$ have a dual effect in the equation. The Green's function $\boldsymbol{g}$ is introduced in order to make the homogenized dynamic equation solvable. It is defined as the solution of the following equation:

$$(\boldsymbol{\nabla} + i\boldsymbol{k}) \cdot \{\mathbb{C} : [(\boldsymbol{\nabla} + i\boldsymbol{k}) \otimes^s \boldsymbol{g}(\boldsymbol{x}, \boldsymbol{x}')]\} + |T|\boldsymbol{\delta}(\boldsymbol{x} - \boldsymbol{x}') = -w^2 \boldsymbol{\rho} \boldsymbol{g}(\boldsymbol{x}, \boldsymbol{x}'), \tag{2.4}$$

where the variables $\boldsymbol{x}$ and $\boldsymbol{x}'$ have the same meaning, $\boldsymbol{\delta}(\boldsymbol{x} - \boldsymbol{x}') \equiv \delta(\boldsymbol{x} - \boldsymbol{x}')\boldsymbol{I}$ represents the product of the Kronecker delta function $\delta(\boldsymbol{x} - \boldsymbol{x}')$ and the identity tensor $\boldsymbol{I}$.

According to the three necessary conditions for the Willis' homogenization theory derived in the work of Nassar et al. (2015), the Hill-Mandel lemma gives a virtual work

equation:

$$\langle |T|\boldsymbol{\delta}(\boldsymbol{x}-\boldsymbol{x}')\tilde{\boldsymbol{u}}(\boldsymbol{x}')\rangle = \langle ((\mathbb{C}:\tilde{\boldsymbol{E}}_0):[(\boldsymbol{\nabla}+i\boldsymbol{k})\otimes^s \boldsymbol{g}(\boldsymbol{x},\boldsymbol{x}')]^*\rangle + \langle \tilde{\boldsymbol{f}}\boldsymbol{g}^*(\boldsymbol{x},\boldsymbol{x}')\rangle,$$

where the superscript symbol $*$ indicates a complex conjugate field. With the help of the convolution definition, the left part of above equation can be rewritten as

$$\langle |T|\boldsymbol{\delta}(\boldsymbol{x}-\boldsymbol{x}')\tilde{\boldsymbol{u}}(\boldsymbol{x}')\rangle = \int_T \boldsymbol{\delta}(\boldsymbol{x}-\boldsymbol{x}')\tilde{\boldsymbol{u}}(\boldsymbol{x}')d_{\boldsymbol{x}'} \equiv |T|\tilde{\boldsymbol{u}}(\boldsymbol{x}).$$

According to the property of the Green's function: $\boldsymbol{g}^T(\boldsymbol{x},\boldsymbol{x}') = \boldsymbol{g}^*(\boldsymbol{x},\boldsymbol{x}')$, the local displacement field satisfies

$$\tilde{\boldsymbol{u}}(\boldsymbol{x}) = \langle [\boldsymbol{g}(\boldsymbol{x},\boldsymbol{x}')\otimes^s (\boldsymbol{\nabla}+i\boldsymbol{k})^*]:\mathbb{C}\rangle_{\boldsymbol{x}'}:\tilde{\boldsymbol{E}}_0 + \langle \boldsymbol{g}(\boldsymbol{x},\boldsymbol{x}')\rangle_{\boldsymbol{x}'}\cdot\tilde{\boldsymbol{f}}, \tag{2.5}$$

where the operator $\langle\cdot\rangle_{\boldsymbol{x}'}$ stands for a volume average of $\boldsymbol{x}'$ over the REV T.

Since the Green's function cannot be easily obtained, a feasible method is to set the solution of the dynamic equation as the following form:

$$\tilde{\boldsymbol{u}} = \mathcal{L}:\tilde{\boldsymbol{E}}_0 + \boldsymbol{M}\cdot\tilde{\boldsymbol{f}}, \tag{2.6}$$

which is equivalent to Eq.(2.5), the tensors $\mathcal{L}$ and $\boldsymbol{M}$ are the solutions in which the dynamic equation satisfies the combination of $(\tilde{\boldsymbol{E}}_0 = \boldsymbol{e}_i\otimes^s\boldsymbol{e}_j, \tilde{\boldsymbol{f}} = \boldsymbol{0})$ and $(\tilde{\boldsymbol{E}}_0 = \boldsymbol{0}, \tilde{\boldsymbol{f}} = \boldsymbol{e}_k)$, respectively. It is worth noting that the matrix $\mathcal{L}$ and $\boldsymbol{M}$ are also related to the Green's function $\boldsymbol{g}$ and a wave number-frequency combination $(\boldsymbol{k}, w)$. As such, comparing expressions (2.1) and (2.6), tensors $\mathcal{L}$ and $\boldsymbol{M}$ have similar effects with tensors $\mathcal{A}$ and $\boldsymbol{B}$. Similar to the tensors $\mathcal{A}$ and $\boldsymbol{B}$ in equation (2.1), the tensors $\mathcal{L}$ and $\boldsymbol{M}$ in (2.6) have similar roles.

2.1.2 Homogenization step

As mentioned earlier, the effective constitutive law can be expressed as Eq.(1.5). The component tensors $\mathbb{C}^e$, $\boldsymbol{S}^e$, $\boldsymbol{T}^e$, and $\boldsymbol{\rho}^e$ depend on the wave number-frequency combination $(\boldsymbol{k}, w)$, they can all be determined by the tensors $\mathcal{L}$ and $\boldsymbol{M}$. It is easy to give the expression

of the local fields $\tilde{\boldsymbol{\varepsilon}}$, $\tilde{\boldsymbol{v}}$ and the effective fields $\langle\tilde{\boldsymbol{\varepsilon}}\rangle$, $\langle\tilde{\boldsymbol{v}}\rangle$:

$$\begin{bmatrix}\tilde{\boldsymbol{\varepsilon}}\\ \tilde{\boldsymbol{v}}\end{bmatrix} = \begin{bmatrix}(\boldsymbol{\nabla}+i\boldsymbol{k})\otimes^s\mathcal{L} & (\boldsymbol{\nabla}+i\boldsymbol{k})\otimes^s\boldsymbol{M}\\ -iw\mathcal{L} & -iw\boldsymbol{M}\end{bmatrix}\begin{bmatrix}\tilde{\boldsymbol{E}}_0\\ \tilde{\boldsymbol{f}}\end{bmatrix}.$$

We notice that the effective field gives $\langle(\boldsymbol{\nabla}+i\boldsymbol{k})\otimes^s\mathcal{L}\rangle = \langle\boldsymbol{\nabla}\otimes^s\mathcal{L}\rangle + \langle i\boldsymbol{k}\otimes^s\mathcal{L}\rangle$, and the first part has a zero-average under the effective definition of periodic cell volume average (same property for $\boldsymbol{M}$). Then, the effective fields $\langle\tilde{\boldsymbol{\varepsilon}}\rangle$, $\langle\tilde{\boldsymbol{v}}\rangle$ satisfy

$$\begin{bmatrix}\langle\tilde{\boldsymbol{\varepsilon}}\rangle\\ \langle\tilde{\boldsymbol{v}}\rangle\end{bmatrix} = \begin{bmatrix}i\boldsymbol{k}\otimes^s\langle\mathcal{L}\rangle & i\boldsymbol{k}\otimes^s\langle\boldsymbol{M}\rangle\\ -iw\langle\mathcal{L}\rangle & -iw\langle\boldsymbol{M}\rangle\end{bmatrix}\begin{bmatrix}\tilde{\boldsymbol{E}}_0\\ \tilde{\boldsymbol{f}}\end{bmatrix}.$$

Thanks to the effective field definitions: $\langle\tilde{\boldsymbol{\sigma}}\rangle = \langle\mathbb{C}:(\tilde{\boldsymbol{\varepsilon}}-\tilde{\boldsymbol{E}}_0)\rangle$ and $\langle\tilde{\boldsymbol{p}}\rangle = \langle\boldsymbol{\rho}\cdot\tilde{\boldsymbol{v}}\rangle$, the effective constitutive law can be expressed as

$$\begin{bmatrix}\langle\tilde{\boldsymbol{\sigma}}\rangle\\ \langle\tilde{\boldsymbol{p}}\rangle\end{bmatrix} = \begin{bmatrix}\mathbb{C}^e & \boldsymbol{S}^e\\ \boldsymbol{T}^e & \boldsymbol{\rho}^e\end{bmatrix}\begin{bmatrix}\langle\tilde{\boldsymbol{\varepsilon}}\rangle-\tilde{\boldsymbol{E}}_0\\ \langle\tilde{\boldsymbol{v}}\rangle\end{bmatrix}.$$

Then it follows that the effective tensors $\mathbb{C}^e$, $\boldsymbol{S}^e$, $\boldsymbol{T}^e$ and $\boldsymbol{\rho}^e$ can be determined as

$$\mathbb{C}^e = \langle\mathbb{C}\rangle + \langle\mathbb{C}:[(\boldsymbol{\nabla}+i\boldsymbol{k})\otimes^s\boldsymbol{M}]\rangle\langle\boldsymbol{M}\rangle^{-1}\langle\mathcal{L}\rangle - \langle\mathbb{C}:[(\boldsymbol{\nabla}+i\boldsymbol{k})\otimes^s\mathcal{L}]\rangle \tag{2.7a}$$

$$\boldsymbol{S}^e = \frac{1}{iw}\left\{\langle\mathbb{C}:[\mathbb{I}-(\boldsymbol{\nabla}+i\boldsymbol{k})\otimes^s\mathcal{L}]\rangle\cdot i\boldsymbol{k} - \langle\mathbb{C}:[(\boldsymbol{\nabla}+i\boldsymbol{k})\otimes^s\boldsymbol{M}]\rangle\langle\boldsymbol{M}\rangle^{-1}(\boldsymbol{I}-\langle\mathcal{L}\rangle\cdot i\boldsymbol{k})\right\}, \tag{2.7b}$$

$$\boldsymbol{T}^e = iw(\langle\boldsymbol{\rho}\mathcal{L}\rangle - \langle\boldsymbol{\rho}\boldsymbol{M}\rangle\langle\boldsymbol{M}\rangle^{-1}\langle\mathcal{L}\rangle), \tag{2.7c}$$

$$\boldsymbol{\rho}^e = \langle\boldsymbol{\rho}\boldsymbol{M}\rangle\langle\boldsymbol{M}\rangle^{-1}(\boldsymbol{I}-\langle\mathcal{L}\rangle\cdot i\boldsymbol{k}) + \langle\boldsymbol{\rho}\mathcal{L}\rangle\cdot i\boldsymbol{k}. \tag{2.7d}$$

This result includes the shear wave example in Meng & Guzina (2018). Recalling the expression of the local displacement field $\tilde{\boldsymbol{u}}$ in Willis' theory, there exists a relationship between tensors $\mathcal{A}$ and $\boldsymbol{B}$ and tensors $\mathcal{L}$ and $\boldsymbol{M}$:

$$\mathcal{A} = \boldsymbol{M}\langle\boldsymbol{M}\rangle^{-1}\langle\mathcal{L}\rangle - \mathcal{L}, \tag{2.8a}$$

$$\boldsymbol{B} = \frac{1}{iw}\left[\boldsymbol{I}-\boldsymbol{M}\langle\boldsymbol{M}\rangle^{-1} + \left(\boldsymbol{M}\langle\boldsymbol{M}\rangle^{-1}\langle\mathcal{L}\rangle-\mathcal{L}\right)\cdot i\boldsymbol{k}\right]. \tag{2.8b}$$

Similarly, by using the expressions (2.8a) and (2.8b), the same result can be obtained by the related expression of Green's function in Nassar et al. (2015):

$$\begin{aligned}
\mathbb{C}^e &= \langle \mathbb{C} \rangle + \langle \mathbb{C} : [(\boldsymbol{\nabla} + i\boldsymbol{k}) \otimes^s \mathcal{A}] \rangle, \\
\boldsymbol{S}^e &= \langle \mathbb{C} : [(\boldsymbol{\nabla} + i\boldsymbol{k}) \otimes^s \boldsymbol{B}] \rangle, \\
\boldsymbol{T}^e &= -iw \langle \boldsymbol{\rho} \mathcal{A} \rangle, \\
\boldsymbol{\rho}^e &= \langle \boldsymbol{\rho} \rangle - iw \langle \boldsymbol{\rho} \boldsymbol{B} \rangle.
\end{aligned}$$

2.2 Effective constitutive law

2.2.1 Symmetry of component tensors

In the expression of the effective constitutive law of Willis homogenization theory, the effective constitutive tensors $\mathbb{C}^e$, $\boldsymbol{\rho}^e$ exhibit Hermitian symmetry, and the tensors $\boldsymbol{S}^e$, $\boldsymbol{T}^e$ show a negative conjugate equivalent relationship:

$$\mathbb{C}^e = (\mathbb{C}^e)^*, \quad \boldsymbol{\rho}^e = (\boldsymbol{\rho}^e)^*, \quad \boldsymbol{S}^e = -(\boldsymbol{T}^e)^*,$$

where $(\cdot)^*$ stands for the conjugate operator. These relationships can be proved by a simple transformation of the expressions (2.7a). Using the displacement expression (2.6), the effective dynamic equation (2.3) can be rewritten as

$$i\boldsymbol{k} \cdot \langle \mathbb{C} : [(\boldsymbol{\nabla} + i\boldsymbol{k}) \otimes^s (\mathcal{L} : \tilde{\boldsymbol{E}}_0 + \boldsymbol{M} \cdot \tilde{\boldsymbol{f}}) - \tilde{\boldsymbol{E}}_0] \rangle + \tilde{\boldsymbol{f}} = -w^2 \langle \boldsymbol{\rho} \cdot (\mathcal{L} : \tilde{\boldsymbol{E}}_0 + \boldsymbol{M} \cdot \tilde{\boldsymbol{f}}) \rangle. \quad (2.9)$$

Remark. *Set the free-strain $\tilde{\boldsymbol{\gamma}}$ and the volume force $\tilde{\boldsymbol{f}}$ to two eigen models ($\tilde{\boldsymbol{E}}_0 = \boldsymbol{e}_i \otimes^s \boldsymbol{e}_j, \tilde{\boldsymbol{f}} = \boldsymbol{0}$) and ($\tilde{\boldsymbol{E}}_0 = \boldsymbol{0}, \tilde{\boldsymbol{f}} = \boldsymbol{e}_k$), respectively, in combination with the virtual work theorem, the tensors $\mathcal{L}$ and $\boldsymbol{M}$ have the properties:*

$$(a) : \langle \boldsymbol{M} \rangle = \langle \boldsymbol{M}^* \rangle, \qquad (b) : \langle \mathbb{C} : [(\boldsymbol{\nabla} + i\boldsymbol{k}) \otimes^s \boldsymbol{M}] \rangle = \langle \mathcal{L}^* \rangle, \quad (2.10)$$

$$(c) : \langle \boldsymbol{\rho}\mathcal{L} \rangle \cdot i\boldsymbol{k} = -i\boldsymbol{k} \cdot \langle \boldsymbol{\rho}\mathcal{L} \rangle^*, \quad (d) : \langle \mathbb{C} : [(\boldsymbol{\nabla} + i\boldsymbol{k}) \otimes^s \mathcal{L}] \rangle = \langle \mathbb{C} : [(\boldsymbol{\nabla} + i\boldsymbol{k}) \otimes^s \mathcal{L}] \rangle^*, \quad (2.11)$$

where the asterisk symbol stands for the conjugate operator. At the same time, we have

$$-w^2\langle \boldsymbol{\rho}\cdot\boldsymbol{M}\rangle = \boldsymbol{I} + i\boldsymbol{k}\cdot\langle\mathcal{L}^*\rangle. \tag{2.12}$$

Proof. *The local effective dynamic equation (2.9) for two eigen models* ($\tilde{\boldsymbol{E}}_0 = \boldsymbol{e}_i\otimes^s\boldsymbol{e}_j, \tilde{\boldsymbol{f}} = \boldsymbol{0}$) *and* ($\tilde{\boldsymbol{E}}_0 = \boldsymbol{0}, \tilde{\boldsymbol{f}} = \boldsymbol{e}_k$) *can be simplified as*

$$i\boldsymbol{k}\cdot\langle\mathbb{C}:[(\boldsymbol{\nabla}+i\boldsymbol{k})\otimes^s\mathcal{L}-\boldsymbol{I}]\rangle = -w^2\langle\boldsymbol{\rho}\cdot\mathcal{L}\rangle, \tag{2.13a}$$

$$i\boldsymbol{k}\cdot\langle\mathbb{C}:(\boldsymbol{\nabla}+i\boldsymbol{k})\otimes^s\boldsymbol{M}\rangle + \boldsymbol{I} = -w^2\langle\boldsymbol{\rho}\cdot\boldsymbol{M}\rangle, \tag{2.13b}$$

where $\mathcal{L}$ and $\boldsymbol{M}$ are kinematically admissible solutions for equation (2.13a) and (2.13b). With the help of the virtual work principle, there are

$$\boldsymbol{0} = \langle\mathbb{C}:[(\boldsymbol{\nabla}+i\boldsymbol{k})\otimes^s\mathcal{L}]:[(\boldsymbol{\nabla}+i\boldsymbol{k})\otimes^s\boldsymbol{M}]^*\rangle - \langle\mathbb{C}:[(\boldsymbol{\nabla}+i\boldsymbol{k})\otimes^s\boldsymbol{M}]^*\rangle - w^2\langle\boldsymbol{\rho}\cdot\mathcal{L}:\boldsymbol{M}^*\rangle,$$
$$\langle\mathcal{L}^*\rangle = \langle\mathbb{C}:[(\boldsymbol{\nabla}+i\boldsymbol{k})\otimes^s\boldsymbol{M}]:[(\boldsymbol{\nabla}+i\boldsymbol{k})\otimes^s\mathcal{L}]^*\rangle - w^2\langle\boldsymbol{\rho}\cdot\boldsymbol{M}:\mathcal{L}^*\rangle.$$

Due to the Hermitian symmetry of tensor $\mathbb{C}$, it is easy to get $\langle\mathbb{C}:[(\boldsymbol{\nabla}+i\boldsymbol{k})\otimes^s\boldsymbol{M}]\rangle = \langle\mathcal{L}^*\rangle$. On the other hand, using the virtual work theorem for Eqs.(2.13a) and (2.13b), we have

$$\boldsymbol{0} = \langle\boldsymbol{C}:[(\boldsymbol{\nabla}+i\boldsymbol{k})\otimes^s\mathcal{L}]:[(\boldsymbol{\nabla}+i\boldsymbol{k})\otimes^s\mathcal{L}]^*\rangle - \langle\boldsymbol{C}:[(\boldsymbol{\nabla}+i\boldsymbol{k})\otimes^s\mathcal{L}]^*\rangle - w^2\langle\boldsymbol{\rho}\cdot\mathcal{L}:\mathcal{L}^*\rangle,$$
$$\langle\boldsymbol{M}\rangle = \langle\boldsymbol{C}:[(\boldsymbol{\nabla}+i\boldsymbol{k})\otimes^s\boldsymbol{M}]:[(\boldsymbol{\nabla}+i\boldsymbol{k})\otimes^s\boldsymbol{M}]^*\rangle - w^2\langle\boldsymbol{\rho}\cdot\boldsymbol{M}:\boldsymbol{M}^*\rangle.$$

Conjugating them and comparing them, there exist

$$\langle\boldsymbol{M}\rangle = \langle\boldsymbol{M}^*\rangle, \quad \langle\boldsymbol{C}:[(\boldsymbol{\nabla}+i\boldsymbol{k})\otimes^s\mathcal{L}]\rangle = \langle\boldsymbol{C}:[(\boldsymbol{\nabla}+i\boldsymbol{k})\otimes^s\mathcal{L}]^*\rangle.$$

Replacing these properties to Eqs.(2.13a) and (2.13b), we can also get

$$-w^2\langle\boldsymbol{\rho}\cdot\mathcal{L}\rangle = w^2\langle\boldsymbol{\rho}\cdot\mathcal{L}^*\rangle, \quad -w^2\langle\boldsymbol{\rho}\cdot\boldsymbol{M}\rangle = \boldsymbol{I} + i\boldsymbol{k}\langle\mathcal{L}^*\rangle.$$

According to the properties (2.10), (2.11) and (2.12), the Hermitian symmetry of all the component tensors $\mathbb{C}^e$, $\boldsymbol{S}^e$, $\boldsymbol{T}^e$ and $\boldsymbol{\rho}^e$ can be proved in the following way:

The component tensor $\mathbb{C}^e$: With the help of the properties (2.10) and the real tensor definition of $\mathbb{C}$, we have

$$\begin{aligned}
\mathbb{C}^e &= \langle\mathbb{C}\rangle + \langle\mathbb{C} : [(\boldsymbol{\nabla} + i\boldsymbol{k}) \otimes^s \boldsymbol{M}]\rangle\langle\boldsymbol{M}\rangle^{-1}\langle\mathcal{L}\rangle - \langle\mathbb{C} : [(\boldsymbol{\nabla} + i\boldsymbol{k}) \otimes^s \mathcal{L}]\rangle \\
&= \langle\mathbb{C}\rangle + \langle\mathcal{L}^*\rangle\langle\mathcal{M}\rangle^{-1}\langle\mathcal{L}\rangle - \langle\mathbb{C} : [(\boldsymbol{\nabla} + i\boldsymbol{k}) \otimes^s \mathcal{L}]\rangle \\
&= \langle\mathbb{C}\rangle^* + \left(\langle\mathcal{L}^*\rangle\langle\mathcal{M}\rangle^{-1}\langle\mathcal{L}\rangle\right)^* - \langle\mathbb{C} : [(\boldsymbol{\nabla} + i\boldsymbol{k}) \otimes^s \mathcal{L}]\rangle^* \\
&= (\mathbb{C}^e)^*,
\end{aligned}$$

The component tensor $\boldsymbol{S}^e$ and $\boldsymbol{T}^e$: With the help of the properties (2.10), (2.11) and (2.12), we have

$$\begin{aligned}
\boldsymbol{S}^e &= \frac{1}{iw}\left\{\langle\mathbb{C} : [\mathbb{I} - (\boldsymbol{\nabla} + i\boldsymbol{k}) \otimes^s \mathcal{L}]\rangle \cdot i\boldsymbol{k} - \langle\mathbb{C} : [(\boldsymbol{\nabla} + i\boldsymbol{k}) \otimes^s \boldsymbol{M}]\rangle\langle\boldsymbol{M}\rangle^{-1}(\boldsymbol{I} - \langle\mathcal{L}\rangle \cdot i\boldsymbol{k})\right\} \\
&= \frac{1}{iw}\left\{(i\boldsymbol{k} \cdot \langle\mathbb{C} : [(\boldsymbol{\nabla} + i\boldsymbol{k}) \otimes^s \mathcal{L} - \mathbb{I}]\rangle^*)^* - \langle\mathcal{L}^*\rangle\langle\boldsymbol{M}^{-1}\rangle(\boldsymbol{I} + i\boldsymbol{k} \cdot \langle\mathcal{L}^*\rangle)^*\right\} \\
&= \frac{1}{iw}\left\{-w^2\langle\boldsymbol{\rho}\mathcal{L}\rangle^* + w^2\langle\mathcal{L}^*\rangle\langle\boldsymbol{M}^{-1}\rangle\langle\boldsymbol{\rho}\boldsymbol{M}\rangle^*\right\} \\
&= -\left\{iw[\langle\boldsymbol{\rho}\mathcal{L}\rangle - \langle\boldsymbol{\rho}\boldsymbol{M}\rangle\langle\boldsymbol{M}^{-1}\rangle\langle\mathcal{L}\rangle]\right\}^* \\
&= -(\boldsymbol{T}^e)^*.
\end{aligned}$$

The component tensor $\boldsymbol{\rho}^e$: With the help of the properties (2.10) and (2.11), we have

$$\begin{aligned}
\boldsymbol{\rho}^e &= \langle\boldsymbol{\rho}\mathcal{M}\rangle\langle\mathcal{M}\rangle^{-1}(\boldsymbol{I} - \langle\mathcal{L}\rangle \cdot i\boldsymbol{k}) + \langle\boldsymbol{\rho}\mathcal{L}\rangle \cdot i\boldsymbol{k} \\
&= -w^2\langle\boldsymbol{\rho}\mathcal{M}\rangle\langle\mathcal{M}\rangle^{-1}\langle\boldsymbol{\rho}\mathcal{M}\rangle^* + \langle\boldsymbol{\rho}\mathcal{L}\rangle \cdot i\boldsymbol{k} \\
&= -w^2[\langle\boldsymbol{\rho}\mathcal{M}\rangle\langle\mathcal{M}\rangle^{-1}\langle\boldsymbol{\rho}\mathcal{M}\rangle^*]^* + (\langle\boldsymbol{\rho}\mathcal{L}\rangle \cdot i\boldsymbol{k})^* = (\boldsymbol{\rho}^e)^*,
\end{aligned}$$

It follows that the Willis effective constitutive law components $\mathbb{C}^e$ and $\boldsymbol{\rho}^e$ exhibit Hermitian symmetry, and the coupling components $\boldsymbol{S}^e$ and $\boldsymbol{T}^e$ exhibit negative Hermitian symmetry. In addition, the proof of these properties through an eigensystem of the dynamic equation is also presented in Meng & Guzina (2018).

2.2.2 Effective behavior

As shown in the previous sections, the effective constitutive law under a fixed wave number-frequency combination $(\boldsymbol{k}, w)$ has been determined. Now, we consider that the effective impedance $\mathcal{Z}$ represents the effective parameter of the system $\mathcal{Z}\langle\tilde{\boldsymbol{u}}\rangle = \tilde{\boldsymbol{f}}$. As the effective constitutive law shown in Eq.(2.7a), the effective impedance $\mathcal{Z}$ exhibits a correlation with tensor $\mathbb{C}^e$, $\boldsymbol{S}^e$, $\boldsymbol{T}^e$ and $\boldsymbol{\rho}^e$:

$$\mathcal{Z} = iw\boldsymbol{\rho}^e iw - i\boldsymbol{k}\cdot\boldsymbol{T}^e iw + i\boldsymbol{k}\cdot\boldsymbol{S}^e iw - i\boldsymbol{k}\cdot\mathbb{C}^e\cdot i\boldsymbol{k}. \tag{2.14}$$

To simplify the description, we try to use a simple linear relationship to represent the effective constitutive relationship with the effective tensors $\mathbb{C}^{eff}$ and $\boldsymbol{\rho}^{eff}$, rather than a coupling one:

$$\tilde{\boldsymbol{\Sigma}} = \mathbb{C}^{eff} : \tilde{\boldsymbol{E}}, \quad \tilde{\boldsymbol{P}} = \boldsymbol{\rho}^{eff}\cdot\tilde{\boldsymbol{V}},$$

where

$$\mathbb{C}^{eff} = \boldsymbol{S}^e(\boldsymbol{\rho}^{eff} - \boldsymbol{\rho}^e)^{-1}\boldsymbol{T}^e + \mathbb{C}^e, \quad \boldsymbol{\rho}^{eff} = \boldsymbol{T}^e : (\mathbb{C}^{eff} - \mathbb{C}^e)^{-1} : \boldsymbol{S}^e + \boldsymbol{\rho}^e. \tag{2.15}$$

Subsequently, these two effective tensors $\mathbb{C}^{eff}$ and $\boldsymbol{\rho}^{eff}$ associated with $(\boldsymbol{k}, w)$ are introduced to simplify the effective impedance expression, they also make the homogenized dynamic equation satisfy the form of $\mathcal{Z}\langle\tilde{\boldsymbol{u}}\rangle = \tilde{\boldsymbol{f}}$, there is

$$\mathcal{Z} = iw\boldsymbol{\rho}^{eff} iw - i\boldsymbol{k}\cdot\mathbb{C}^{eff}\cdot i\boldsymbol{k}. \tag{2.16}$$

Two feasible expressions of $\mathbb{C}^{eff}$ and $\boldsymbol{\rho}^{eff}$ can be determined according to Eq.(2.2). When we try to define the dispersion relationship as $\boldsymbol{\zeta} = iw/i\boldsymbol{k}$, there are

$$\mathbb{C}^{eff} = \mathbb{C}^e - \boldsymbol{S}^e \otimes^s \boldsymbol{\zeta}, \quad \boldsymbol{\rho}^{eff} = \boldsymbol{\rho}^e - \boldsymbol{\zeta}^{-1}\cdot\boldsymbol{T}^e.$$

In fact, the Eq.(2.2) also shows a dispersion relation between the wave number $\boldsymbol{k}$ and the frequency w, that is the actual dispersion relation $(\boldsymbol{k}, w)$ of the homogenized dynamic

Table 2.1: The iterative process of FEM method

Process.	
Step. 1	Chose the initial dispersion relation combination $(\boldsymbol{k} - w_{old})$;
Step. 2	Solve numerically the tensors $\boldsymbol{\mathcal{L}}$ and $\boldsymbol{M}$ by two combination of $\tilde{\boldsymbol{E}}_0$ and $\tilde{\boldsymbol{f}}$;
Step. 3	Determine the effective constitutive tensors $\boldsymbol{C}^e$, $\boldsymbol{S}^e$, $\boldsymbol{T}^e$ and $\boldsymbol{\rho}^e$;
Step. 4	Get the new version dispersion relation combination $(\boldsymbol{k} - w_{new})$ by the zero-determinant of effective impedance $\mathcal{Z}$;
Step. 5	Test the convergence condition: if the error $\frac{\lvert w_{new} - w_{old}\rvert}{\lvert w_{old}\rvert}$ is small enough, export the results; if not, return to the **Step. 2** by $w_{old} = mean\{w_{old}, w_{new}\}$.

equation.

After solving the effective tensors $\mathbb{C}^{eff}$ and $\boldsymbol{\rho}^{eff}$, a new dispersion relationship can be obtained from the zero-determinant of the effective impedance Eq.(2.16). In theory, the exact dispersion relationship can get matching results, that is, the dispersion relationship before and after calculation is invariable. Therefore, this process can be used to determine a more accurate solution of a random dispersion relationship combination. It is easy to think of the whole process as an iterative method, so we can try to perform multiple iterations on the random initial condition to obtain a near-true dispersion relation and effective constitutive law. For instance, we take a 1D elastic layered case as an example, the dispersion relationship ζ can be expressed as the ratio of the effective elastic modulus C^{eff} and the effective density ρ^{eff}:

$$\zeta(k, w) = \{\ \zeta \mid \zeta^2 = (\frac{w}{k})^2 = \frac{C^{eff}}{\rho^{eff}},\ kl \leqslant \pi\},$$

with a cell size l. With the expression of effective tensors (2.15), it is easy to get

$$\rho^e \zeta^2 + (S^e - T^e)\zeta - C^e = 0. \tag{2.17}$$

In Table (2.1), we summarized a numerical method to determine the dispersion relationship through Willis' dynamic homogenization theory. In the first step, in view of the frequency dependence of the effective constitutive relationship of the homogenized dynamic equation, we need to determine an initial combination of dispersion relations $(\boldsymbol{k}, w_{old})$. It

is worth noting that the choice of the initial dispersion relationship combination greatly affects the number of numerical calculation iterations. Without loss of generality, we use the results of the Quasi-static case as initial conditions in this example. In the second step, we can use two basic combinations of eigenstrain field $\tilde{\boldsymbol{E}}_0$ and volume force $\tilde{\boldsymbol{f}}$ to determine tensors $\mathcal{L}$ and $\boldsymbol{M}$. The third step is to determine the components of the effective constitutive coefficient matrix according to Eqs.(2.7a). Then, in the fourth step, the zero-determinant of effective impedance (2.14) or (2.16) of the homogenization equation can give a new dispersion relationship $(\boldsymbol{k}, w_{new})$. Finally, in the fifth step, we compare the updated result of the fourth step with the initial combination in the first step, and then choose to export the result or redefine the initial combination. Obviously, in this step, we decided to redefine the mean value of the old and updated result as the initial combination, that we called "mean value iteration". Generally, such a definition seems to slow down the convergence of iterative results. However, this is not the case. The redefinition like that is to avoid some "rude" fluctuations of iteration results (such as positive and negative fluctuations), thereby improving the convergence speed.

In summary, the above five steps constitute a complete iterative system for determining the exact solution of the constitutive relationship and dispersion relationship. In fact, this iterative scheme is some extensions based on the finite element method, and its significance lies in providing a reference from a different perspective to the asymptotic method of dynamic homogenization theory and its numerical simulation.

2.3 Numerical example of 1D shear wave

In this section, we consider the dynamic homogenization of a 1D shear wave in a three-phase layered composite. The shear wave gives the dynamic equation and constitutive relationship as

$$\boldsymbol{\nabla} \cdot \tilde{\boldsymbol{\sigma}} + \tilde{f} = -w^2 \rho \tilde{u}, \quad \tilde{\boldsymbol{\sigma}} = G \boldsymbol{\nabla} \tilde{u},$$

where G is the shear modulus. The three-phases model gives: the shear modulus $G_1 = 3.0 \times 10^8 (Pa)$, $G_2 = 2.0 \times 10^{11} (Pa)$, and $G_3 = 1.0 \times 10^{10} (Pa)$; the mass density $\rho_1 = 1000 (kg/m^3)$, $\rho_2 = 3000 (kg/m^3)$, and $\rho_3 = 900 (kg/m^3)$. The thicknesses of the compo-

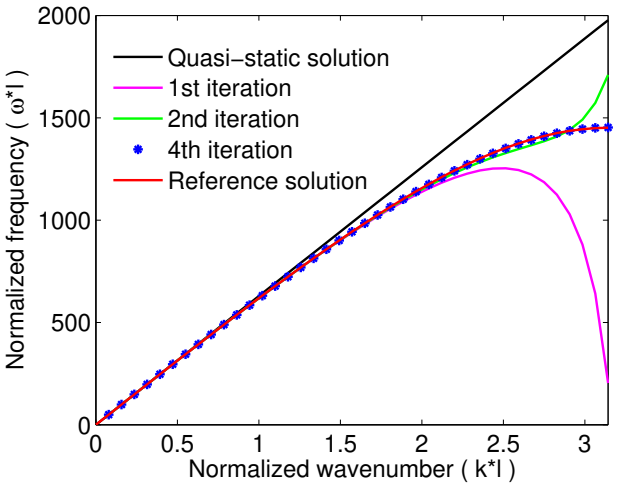

Figure 2.1: *Dispersion curves for Willis' theory (black line for Quasi-static solution, red line for Reference solution): Some iterative solutions based on Willis theory (pink line for first iteration, green line for second iteration and blue asterisk for fourth iteration).*

nents satisfy $\alpha_1 l : \alpha_2 l : \alpha_3 l = 0.52 : 0.23 : 0.25$, and the periodic RVE size is set to $l = 0.01(m)$.

2.3.1 Dispersion relationship

For the above-layered model, the analytical solution of the dispersion curve has been solved in chapter 1. In addition, the effective constitutive law can be determined by Eq.(2.7a). Then, the effective shear modulus G^{eff} and effective density ρ^{eff} can be determined according to Eq.(2.16). In this case, the effective dispersion relationship will be solved by Eq.(2.17).

Fig.(2.1) shows the dispersion curves of the Willis' theory after first (pink line), second (green line) and third (blue points) iterations using the quasi-static dispersion relationship as the initial condition. The reference solution is the finite element numerical solution that ensures accuracy. In these iterative solutions, the fourth iteration can reduce the error to 0.2%. In fact, in order to get the result of convergence faster, we try to use a "mean value iteration", which defines the mean value of the above two iterations as the initial condition for the next iteration. It turns out that it has excellent effects.

2.3.2 Effective tensors

According to the expressions (2.7a,b,c,d), the effective constitutive matrix components $\mathbb{C}^e$, $\boldsymbol{S}^e$, $\boldsymbol{T}^e$ and $\boldsymbol{\rho}^e$ can be determined from the tensors $\mathcal{L}$ and $\boldsymbol{M}$. In this 1D shear wave case, we can solve the solution $\mathcal{L}$ and $\boldsymbol{M}$ of the local dynamic equation (2.9) in two extremes cases, they can be expressed as the sum of a general solution $\tilde{u}_g$ and a particular solution u_{pL} or u_{pM}:

$$\mathcal{L} \Rightarrow \tilde{u}_g + \tilde{u}_{pL}, \quad \boldsymbol{M} \Rightarrow \tilde{u}_g + \tilde{u}_{pM},$$

where the general solution $\tilde{u}_g$ satisfies the format

$$\tilde{u}_g(x) = Ae^{\left(-ik+iw\sqrt{\rho/G}\right)x} + Be^{\left(-ik-iw\sqrt{\rho/G}\right)x},$$

and the particular solution u_{pL} and u_{pM} satisfy

$$\tilde{u}_{pL} = \frac{ikG}{w^2\rho - k^2G}, \quad \tilde{u}_{pM} = \frac{-1}{w^2\rho - k^2G},$$

where the denominator satisfies $w^2\langle\rho\rangle - k^2\langle G\rangle \neq 0$. Next, we try to determine all components (2.7a,b,c,d) in the effective constitutive law. With the help of the properties shown in (2.10), (2.11) and (2.12), it is easy to calculate:

$$\langle\mathcal{L}\rangle \Rightarrow \langle u_g\rangle + \langle\frac{ikG}{w^2\rho - k^2G}\rangle, \quad \langle\boldsymbol{M}\rangle \Rightarrow \langle u_g\rangle + \langle\frac{-1}{w^2\rho - k^2G}\rangle,$$

and

$$\begin{aligned}\langle\mathbb{C} : \boldsymbol{\varepsilon}_{\mathcal{L}}\rangle &\Rightarrow \langle G(\nabla + ik)u_g\rangle - \langle\frac{k^2G^2}{w^2\rho - k^2G}\rangle,\\ \langle\mathbb{C} : \boldsymbol{\varepsilon}_{\boldsymbol{M}}\rangle &\Rightarrow \langle G(\nabla + ik)u_g\rangle - \langle\frac{ikG}{w^2\rho - k^2G}\rangle.\end{aligned}$$

Finally, in this 1D shear wave case, we can give the effective constitutive law

$$\begin{bmatrix}\langle\tilde{\sigma}\rangle\\ \langle\tilde{p}\rangle\end{bmatrix} = \begin{bmatrix}G^e & S^e\\ T^e & \rho^e\end{bmatrix}_{(k,w)} \begin{bmatrix}\langle\tilde{\varepsilon}\rangle\\ \langle\tilde{v}\rangle\end{bmatrix}.$$

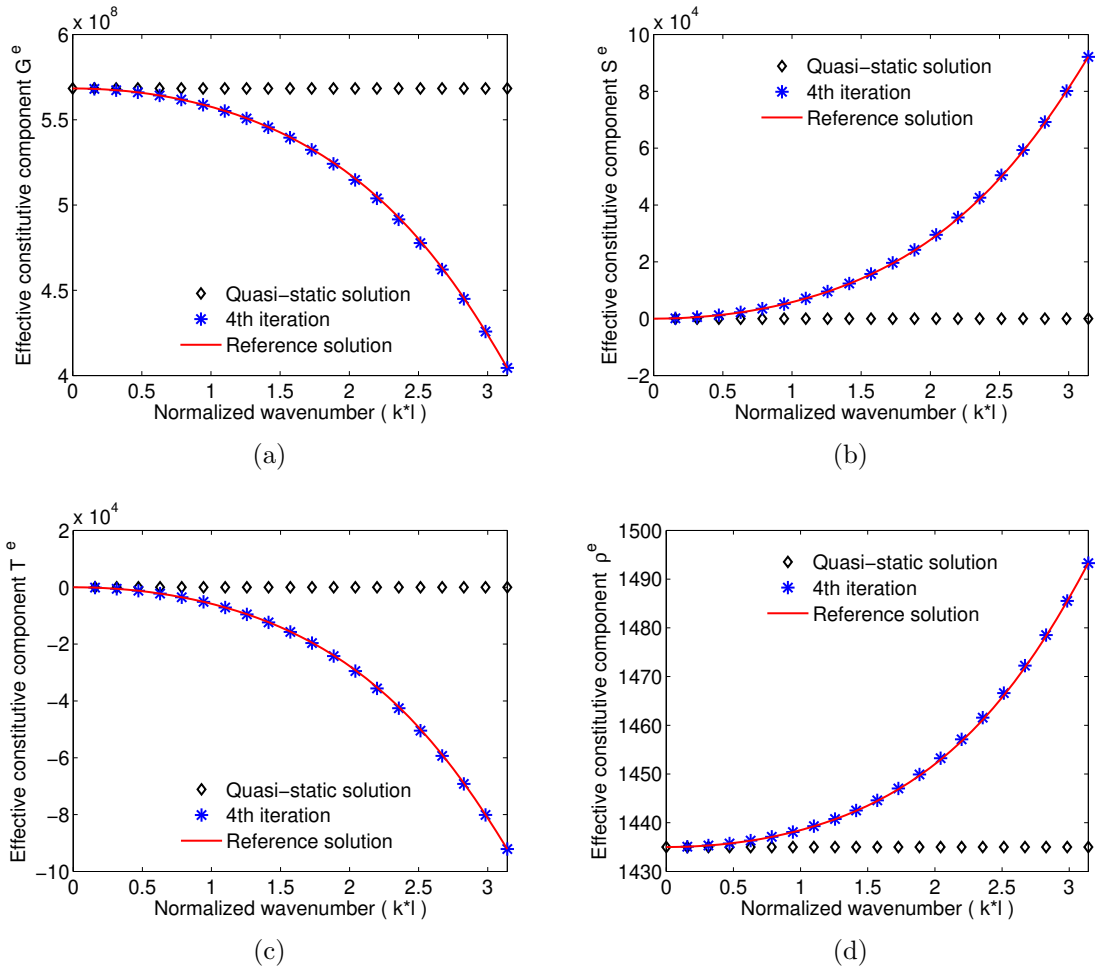

Figure 2.2: *Effective constitutive components (a) G^e, (b) S^e, (c) T^e, and (d) ρ^e: Quasi-static solution (black rhombus), Reference solution (red line), and Willis 4-th iterative solution (blue asterisk).*

As we know, the components G^e, S^e, T^e and ρ^e are calculated based on the combination $(k-w)$. Therefore, a new $(k-w)$ combination can be obtained by obtaining the coefficients of the iterative formula (2.17) through a certain initial $(k-w)$ combination (for example, the Quasi-static case).

For the above-mentioned layered material case, the iterative solution and reference solution (finite element solution) of each component are shown in Fig.(2.2). It is easy to find that the absolute values of the components S^e and T^e both start at 0 (quasi-static case) and increase with the increase of the wave number, which means that the coupling effect of the effective strain field and the effective rate field in the dynamic case will enhance with the increase of wave number.

Next, the effective shear modulus G^{eff} and mass density ρ^{eff} can be determined

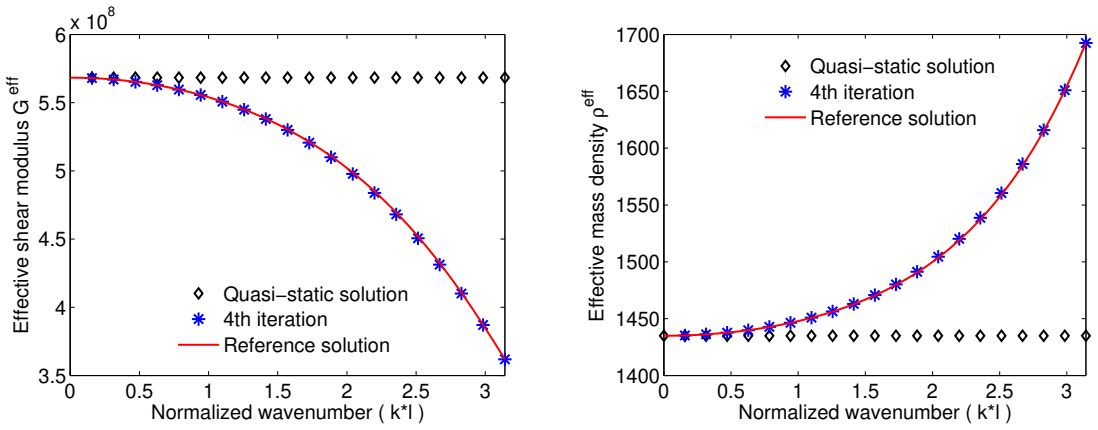

(a) (b)

Figure 2.3: *(a) Effective shear modulus G^{eff} and (b) effective mass density ρ^{eff}: Quasi-static solution (black rhombus), Reference solution (red line), and Willis 4-th iterative solution (blue asterisk).*

by Eqs.(2.15). Compared with the Reference solution (finite element solution), the frequency dependence of the effective shear modulus G^{eff} and effective density ρ^{eff} shown in Fig.(3.5a) and (3.5b). Fig.(3.5a) and (3.5b) show the frequency dependence of the effective shear modulus G^{eff} and effective density ρ^{eff}. Compared with the Reference solution (finite element solution), the iteration solutions are almost perfectly matched.

2.4 Conclusion

The Willis' dynamic homogenization method described in this chapter is a formalism that makes it possible to treat elasticity and electromagnetism problems in a unified way, which provides a systematic and complete homogenization analysis and points out the non-local coupling relationship of periodic microstructures and the frequency dependence of the effective constitutive relationship. In theory, it is not essential to use Green's function in Willis' theory. However, the use of Green's function for linear problems facilitates the solution of a large number of problems thanks to the principle of superposition. In the previous numerical examples, the numerical simulation results have also verified the accuracy of the Willis' dynamic homogenization method.

The iterative process introduced in this chapter is developed from the finite element method. For the general case, this iterative approach allows us to determine the precise

dispersion relationship through any initial combination (the quasi-static classic results are considered as initial conditions in our numerical example). It is worth noting that this iterative method is only a repeated application of the Willis theory, and its results will eventually converge to the finite element solution in Chapter 1. In short, this iterative method is not an innovation of homogenization theory or numerical asymptotic methods but provides ideas for the development of numerical asymptotic methods.

Chapter 3

Two-scale homogenization method for periodic composites

In this chapter, we mainly introduce a homogenization method based on two-scale asymptotic analysis (refer to Bensoussan et al. 2011). The high-order effective constitutive law and dispersion relationship of the homogenized equation are derived with the help of the two-scale representation of the local dynamic equation. Subsequently, a general effective impedance expression was proposed, which allowed the asymptotic expression for any-order.

3.1 Asymptotic description of local dynamic equations

3.1.1 Two-scale representation

Two-scale representation was established in Bensoussan et al. (2011, reprint of 1978), it allows us to research the macroscopic behaviour of a periodic medium by introducing a small perturbation parameter ϵ. In the work of Boutin & Auriault (1993), the physical meaning of the parameter ϵ was explained as the ratio of the micro-scale characteristic dimension l to the macroscopic wave length λ in dynamic cases, which gives $\epsilon = 2\pi l/\lambda \leqslant 1$. In this framework, we consider the propagation of harmonic waves whose wave length λ is much larger than the characteristic size l of the composite RVE.

According to the two-scale description, we introduce the macro scale variable $\boldsymbol{x}$ and the micro scale variable $\boldsymbol{y} \in T$, related by $\boldsymbol{y} = \epsilon^{-1}\boldsymbol{x}$. Within this framework, the displacement field $\boldsymbol{u}(\boldsymbol{x})$ of the periodic medium Ω will have the following definition:

$$\boldsymbol{u}(\boldsymbol{x}) \equiv \boldsymbol{u}(\boldsymbol{x}, \frac{\boldsymbol{x}}{\epsilon}) = \boldsymbol{u}(\boldsymbol{x}, \boldsymbol{y}).$$

The general dynamic equation can be shown as:

$$\boldsymbol{\nabla} \cdot [\mathbb{C}(\boldsymbol{x}, \boldsymbol{y}) : (\boldsymbol{\nabla} \otimes^s \boldsymbol{u}(\boldsymbol{x}, \boldsymbol{y}))] + \boldsymbol{f}(\boldsymbol{x}, \boldsymbol{y}) = -w^2 \boldsymbol{\rho}(\boldsymbol{x}, \boldsymbol{y}) \cdot \boldsymbol{u}(\boldsymbol{x}, \boldsymbol{y}), \tag{3.1}$$

where the periodic condition of RVE allows the material property tensor to satisfy $\mathbb{C}(\boldsymbol{x}, \boldsymbol{y}) = \mathbb{C}(\boldsymbol{y})$ and $\boldsymbol{\rho}(\boldsymbol{x}, \boldsymbol{y}) = \boldsymbol{\rho}(\boldsymbol{y})$. Next, we introduce a plane wave volume force $\boldsymbol{f}$ to satisfy the two scales description $\boldsymbol{f}(\boldsymbol{x}, \boldsymbol{y}) = \tilde{\boldsymbol{f}}(\boldsymbol{y}) e^{i\boldsymbol{k}\cdot\boldsymbol{x}} = \tilde{\boldsymbol{f}} e^{i\boldsymbol{k}\cdot\boldsymbol{x}}$. Let $\boldsymbol{u}(\boldsymbol{x}, \boldsymbol{y}) = \tilde{\boldsymbol{u}}(\boldsymbol{y}) e^{i\boldsymbol{k}\cdot\boldsymbol{x}}$ be the displacement response of the dynamic equation with the volume force $\boldsymbol{f}$, then the gradient operator can be expressed as

$$\boldsymbol{\nabla} \equiv \boldsymbol{\nabla}_{\boldsymbol{x}} + \frac{1}{\epsilon}\boldsymbol{\nabla}_{\frac{\boldsymbol{x}}{\epsilon}} = \boldsymbol{\nabla}_{\boldsymbol{x}} + \frac{1}{\epsilon}\boldsymbol{\nabla}_{\boldsymbol{y}} = i\boldsymbol{k} + \frac{1}{\epsilon}\boldsymbol{\nabla}_{\boldsymbol{y}},$$

Ignoring the $e^{i\boldsymbol{k}\cdot\boldsymbol{x}}$ part of the local dynamic equation, Eq.(3.1) can be converted to

$$(i\boldsymbol{k} + \frac{1}{\epsilon}\boldsymbol{\nabla}_{\boldsymbol{y}}) \cdot \{\mathbb{C}(\boldsymbol{y}) : [(i\boldsymbol{k} + \frac{1}{\epsilon}\boldsymbol{\nabla}_{\boldsymbol{y}}) \otimes^s \tilde{\boldsymbol{u}}(\boldsymbol{y})]\} + \tilde{\boldsymbol{f}} = -w^2 \boldsymbol{\rho}(\boldsymbol{y}) \tilde{\boldsymbol{u}}(\boldsymbol{y}), \tag{3.2}$$

where the solution $\tilde{\boldsymbol{u}}(\boldsymbol{y})$ is only related to the microscopic scale, which can be interpreted as the "local part" of $\boldsymbol{u}(\boldsymbol{x}, \boldsymbol{y})$.

Obviously, the above local dynamic equation (3.2) is similar to the one derived from Bloch-wave representation in the previous chapter. With the help of Bloch-wave representation, the displacement field has the definition $\boldsymbol{u}(\boldsymbol{x}) = \tilde{\boldsymbol{u}}(\boldsymbol{x}) e^{i\boldsymbol{k}\cdot\boldsymbol{x}}$, where $\tilde{\boldsymbol{u}}(\boldsymbol{x})$ satisfies the periodic conditions. However, the two-scale representation gives the expression $\boldsymbol{u}(\boldsymbol{x}) \equiv \boldsymbol{u}(\boldsymbol{x}, \frac{\boldsymbol{x}}{\epsilon}) = \tilde{\boldsymbol{u}}(\frac{\boldsymbol{x}}{\epsilon}) e^{i\boldsymbol{k}\cdot\boldsymbol{x}}$. From a physical point of view, both methods distinguish the macro waves and periodic micro disturbances and provide the same effect during the homogenization process.

3.1.2 Hierarchical dynamic equations

Now we consider the asymptotic expression of the local displacement solution $\tilde{\boldsymbol{u}}(\boldsymbol{y})$ related to the small parameter ϵ, which gives the displacement field as the superposition of multiple perturbed fields:

$$\tilde{\boldsymbol{u}} = \tilde{\boldsymbol{u}}_0 + \epsilon\tilde{\boldsymbol{u}}_1 + \epsilon^2\tilde{\boldsymbol{u}}_2 + ... + \epsilon^n\tilde{\boldsymbol{u}}_n, \quad n \in N, \tag{3.3}$$

where $\tilde{\boldsymbol{u}}_n$ represents the perturbed displacement field for ϵ^n order. Under the two-scaledescription, the local strain field can be shown as

$$\tilde{\boldsymbol{\varepsilon}} = \boldsymbol{\nabla}_{\boldsymbol{x}} \otimes^s \tilde{\boldsymbol{u}} + \frac{1}{\epsilon}\boldsymbol{\nabla}_{\boldsymbol{y}} \otimes^s \tilde{\boldsymbol{u}} = i\boldsymbol{k} \otimes^s \tilde{\boldsymbol{u}} + \frac{1}{\epsilon}\boldsymbol{\nabla}_{\boldsymbol{y}} \otimes^s \tilde{\boldsymbol{u}},$$

where the symbol $\boldsymbol{\nabla}_{\boldsymbol{x}}$ and $\boldsymbol{\nabla}_{\boldsymbol{y}}$ represent the gradient operators of two scales, respectively. The asymptotic expression of strain field gives:

$$\begin{aligned}
&\tilde{\boldsymbol{\varepsilon}} = \epsilon^{-1}\tilde{\boldsymbol{\varepsilon}}_{-1} + \epsilon^0\tilde{\boldsymbol{\varepsilon}}_0 + ... + \epsilon^n\tilde{\boldsymbol{\varepsilon}}_n \\
&= \epsilon^{-1}\boldsymbol{\nabla}_{\boldsymbol{y}} \otimes^s \tilde{\boldsymbol{u}}_0 + \epsilon^0(i\boldsymbol{k} \otimes^s \tilde{\boldsymbol{u}}_0 + \boldsymbol{\nabla}_{\boldsymbol{y}} \otimes^s \tilde{\boldsymbol{u}}_1) + ... + \epsilon^n(i\boldsymbol{k} \otimes^s \tilde{\boldsymbol{u}}_n + \boldsymbol{\nabla}_{\boldsymbol{y}} \otimes^s \tilde{\boldsymbol{u}}_{n+1}), \quad n \in N.
\end{aligned}$$

We consider the effective displacement field as the volume average at the micro scale $\boldsymbol{y}$. The effective displacement field is defined as $\langle\tilde{\boldsymbol{u}}(\boldsymbol{y})\rangle = \sum_n^N \epsilon^n\tilde{U}_n, (n \in N)$ with $\tilde{U}_n = \langle\tilde{\boldsymbol{u}}_n\rangle$. Extending and splitting Eq.(3.2) with different hierarchical equations according to the power of ϵ, we have

$$\begin{aligned}
\epsilon^{-2} \Rightarrow \quad & \boldsymbol{\nabla}_{\boldsymbol{y}} \cdot [\mathbb{C} : \tilde{\boldsymbol{\varepsilon}}_{-1}] = \boldsymbol{0}, \\
\epsilon^{-1} \Rightarrow \quad & i\boldsymbol{k} \cdot [\mathbb{C} : \tilde{\boldsymbol{\varepsilon}}_{-1}] + \boldsymbol{\nabla}_{\boldsymbol{y}} \cdot [\mathbb{C} : \tilde{\boldsymbol{\varepsilon}}_0] = \boldsymbol{0}, \\
\epsilon^{0} \Rightarrow \quad & i\boldsymbol{k} \cdot [\mathbb{C} : \tilde{\boldsymbol{\varepsilon}}_0] + \boldsymbol{\nabla}_{\boldsymbol{y}} \cdot [\mathbb{C} : \tilde{\boldsymbol{\varepsilon}}_1] + \tilde{\boldsymbol{f}} = -w^2\boldsymbol{\rho} \cdot \tilde{\boldsymbol{u}}_0, \\
& ..... \\
\epsilon^{n} \Rightarrow \quad & i\boldsymbol{k} \cdot [\mathbb{C} : \tilde{\boldsymbol{\varepsilon}}_n] + \boldsymbol{\nabla}_{\boldsymbol{y}} \cdot [\mathbb{C} : \tilde{\boldsymbol{\varepsilon}}_{n+1}] = -w^2\boldsymbol{\rho} \cdot \tilde{\boldsymbol{u}}_n.
\end{aligned} \tag{3.4}$$

The homogenization description of the dynamic equation needs to be performed for each hierarchical equation. This allows us to conduct a homogenization analysis for each ϵ-order of hierarchical equation. In the following two subsections (3.2) and (3.3), an effective

asymptotic analysis will be considered in the case of basic dynamic equation (without $\tilde{\boldsymbol{f}}$) and general dynamic equation (with $\tilde{\boldsymbol{f}}$), respectively.

3.2 Asymptotic description without $\tilde{\boldsymbol{f}}$

In this subsection, we analyze the asymptotic results of the dynamic equation without the volume force $\tilde{\boldsymbol{f}}$. These will be used as a basis in the next subsection (3.3). The dynamic equation is shown as

$$(i\boldsymbol{k}+\frac{1}{\epsilon}\boldsymbol{\nabla}_{\boldsymbol{y}})\cdot\{\mathbb{C}(\boldsymbol{y}):[(i\boldsymbol{k}+\frac{1}{\epsilon}\boldsymbol{\nabla}_{\boldsymbol{y}})\otimes^{s}\tilde{\boldsymbol{u}}(\boldsymbol{y})]\}=-w^{2}\boldsymbol{\rho}(\boldsymbol{y})\tilde{\boldsymbol{u}}(\boldsymbol{y}). \tag{3.5}$$

We start with the homogenization description of Willis' theory, the solution of dynamic equation $\tilde{\boldsymbol{u}}$ exhibits a coupling relationship with the effective fields $\langle\tilde{\boldsymbol{u}}\rangle$, $\langle\tilde{\boldsymbol{\varepsilon}}\rangle$, and $\langle\tilde{\boldsymbol{v}}\rangle$.

3.2.1 Localisation of hierarchical equations

As the definition of the effective filed $\langle\tilde{\boldsymbol{\varepsilon}}\rangle = i\boldsymbol{k}\otimes^{s}\langle\tilde{\boldsymbol{u}}\rangle$ and $\langle\tilde{\boldsymbol{v}}\rangle = -iw\langle\tilde{\boldsymbol{u}}\rangle$. In the following description, we try to replace this relationship with a simple expression

$$\tilde{\boldsymbol{u}}=\mathcal{T}:\langle\tilde{\boldsymbol{u}}\rangle=\langle\tilde{\boldsymbol{u}}\rangle+\boldsymbol{A}:\langle\tilde{\boldsymbol{\varepsilon}}\rangle+\boldsymbol{B}\cdot\langle\tilde{\boldsymbol{v}}\rangle, \tag{3.6}$$

where $\mathcal{T}$ is interpreted as a micro-scale related function of $(\boldsymbol{k},w,\boldsymbol{y})$. Similar to the definition of local displacement fields, the tensor $\mathcal{T}$ can also be considered as a multi-order approximate expression

$$\mathcal{T}=\mathcal{T}_{0}+\epsilon\mathcal{T}_{1}+\epsilon^{2}\mathcal{T}_{2}+...+\epsilon^{n}\mathcal{T}_{n},\quad n\in N.$$

It is easy to get the average of the tensor $\mathcal{T}$ as an identity tensor by averaging the left and right sides of Eq.(3.6). Therefore, for any ϵ order, there exists

$$\langle\mathcal{T}_{0}\rangle=\boldsymbol{I},\quad\langle\mathcal{T}_{n}\rangle=\boldsymbol{0},\quad n\geqslant 1.$$

The ϵ^{-2} order equation

First, considering only the ϵ^{-2} order equation, we have

$$\boldsymbol{\nabla}_{\boldsymbol{y}} \cdot [\mathbb{C}(\boldsymbol{y}) : (\boldsymbol{\nabla}_{\boldsymbol{y}} \otimes^s \tilde{\boldsymbol{u}}_0)] = \mathbf{0}.$$

An non-zero auxiliary test function $\delta\tilde{\boldsymbol{u}}_0$, which is periodic in the elementary cell, is introduced to solve this second-order partial differential equation. Integrate the above equation on the REV body T to get the weak form equation

$$\int_T \boldsymbol{\nabla}_{\boldsymbol{y}} \cdot [\mathbb{C}(\boldsymbol{y}) : (\boldsymbol{\nabla}_{\boldsymbol{y}} \otimes^s \tilde{\boldsymbol{u}}_0)]\delta\tilde{\boldsymbol{u}}_0 d_T = 0,$$

which has the same solution as the above equation. According to the divergence theory, we have

$$\int_{\partial T} (\mathbb{C}(\boldsymbol{y}) : \boldsymbol{\nabla}_{\boldsymbol{y}} \otimes^s \tilde{\boldsymbol{u}}_0) \cdot \boldsymbol{n} \cdot \delta\tilde{\boldsymbol{u}}_0 d_S = \int_T \mathbb{C}(\boldsymbol{y}) : \boldsymbol{\nabla}_{\boldsymbol{y}} \otimes^s \tilde{\boldsymbol{u}}_0 \cdot \boldsymbol{\nabla}_{\boldsymbol{y}} \delta\tilde{\boldsymbol{u}}_0 d_T.$$

On the local "small" scale, the displacement field $\tilde{\boldsymbol{u}}_0(\boldsymbol{y})$, $\delta\tilde{\boldsymbol{u}}_0$ and the stress field $\tilde{\boldsymbol{\sigma}}_0$ satisfy the periodic condition. Therefore, there is $\boldsymbol{\nabla}_{\boldsymbol{y}} \otimes^s \tilde{\boldsymbol{u}}_0 = \mathbf{0}$ on the right side of the equation because the periodic boundary condition causes the integral of the left side of the above equation equals to zero. This conclusion means that $\tilde{\boldsymbol{u}}_0$ does not depend on the microscopic variable $\boldsymbol{y}$, *i.e.* $\tilde{\boldsymbol{u}}_0(\boldsymbol{x}, \boldsymbol{y}) = \tilde{\boldsymbol{u}}_0(\boldsymbol{x}) = \langle \tilde{\boldsymbol{u}}_0(\boldsymbol{x}) \rangle_{\boldsymbol{y}} = \tilde{U}_0(\boldsymbol{x})$, and record the average over the cell of $\tilde{\boldsymbol{u}}_0$ as $\tilde{U}_0$. From a physical standpoint, $\tilde{\boldsymbol{u}}_0$ represents the main component of $\tilde{\boldsymbol{u}}$, but in mathematical terms, it is the lowest-order approximate part of the $\tilde{\boldsymbol{u}}$.

The ϵ^{-1} order equation

Next, expanding the ϵ^{-1} order equation, we have

$$i\boldsymbol{k} \cdot [\mathbb{C} : (\boldsymbol{\nabla}_{\boldsymbol{y}} \otimes^s \tilde{\boldsymbol{u}}_0)] + \boldsymbol{\nabla}_{\boldsymbol{y}} \cdot [\mathbb{C} : (i\boldsymbol{k} \otimes^s \tilde{\boldsymbol{u}}_0 + \boldsymbol{\nabla}_{\boldsymbol{y}} \otimes^s \tilde{\boldsymbol{u}}_1)] = \mathbf{0},$$

which can be rewritten as

$$\boldsymbol{\nabla}_{\boldsymbol{y}} \cdot [\mathbb{C} : (i\boldsymbol{k} \otimes^s \tilde{\boldsymbol{u}}_0 + \boldsymbol{\nabla}_{\boldsymbol{y}} \otimes^s \tilde{\boldsymbol{u}}_1)] = \mathbf{0},$$

Similar to the introduction of $\delta\tilde{\boldsymbol{u}}_0$, the non-zero auxiliary test function $\delta\tilde{\boldsymbol{u}}_1$ also satisfies

the periodic boundary conditions. If the $\boldsymbol{\nabla}_{\boldsymbol{y}} \otimes^s \tilde{\boldsymbol{u}}_0$ term is omitted, the ϵ^{-1} order equation becomes

$$\begin{aligned}&\int_{\partial T} [\mathbb{C} : (i\boldsymbol{k} \otimes^s \tilde{\boldsymbol{u}}_0 + \boldsymbol{\nabla}_{\boldsymbol{y}} \otimes^s \tilde{\boldsymbol{u}}_1)] \cdot \boldsymbol{n} \cdot \delta\tilde{\boldsymbol{u}}_1 d_{\partial T} \\ =&\int_T [\mathbb{C} : (i\boldsymbol{k} \otimes^s \tilde{\boldsymbol{u}}_0 + \boldsymbol{\nabla}_{\boldsymbol{y}} \otimes^s \tilde{\boldsymbol{u}}_1)] \cdot \boldsymbol{\nabla}_{\boldsymbol{y}} \delta\tilde{\boldsymbol{u}}_1 d_T.\end{aligned}$$

In addition, the traction vector $\tilde{\boldsymbol{\sigma}}_0 \cdot \boldsymbol{n} = \mathbb{C} : \tilde{\boldsymbol{\varepsilon}}_0 \cdot \boldsymbol{n} = [\mathbb{C} : (i\boldsymbol{k} \otimes^s \tilde{\boldsymbol{u}}_0 + \boldsymbol{\nabla}_{\boldsymbol{y}} \otimes^s \tilde{\boldsymbol{u}}_1)] \cdot \boldsymbol{n}$ exhibits periodic properties on the boundary, which allows the left side of the above equation to be zero. In order to solve the above equation, a position-dependent function $\mathcal{X}(\boldsymbol{y})$ is introduced to represent the correlation of $\mathcal{T}$ with the local variable $\boldsymbol{y}$. For example, when we set $\mathcal{X}_1$ to satisfy

$$\int_T \mathbb{C} : \boldsymbol{\nabla}_{\boldsymbol{y}} \mathcal{X}_1 \cdot \boldsymbol{\nabla}_{\boldsymbol{y}} \delta\tilde{\boldsymbol{u}}_1 d_T = -\int_T \mathbb{C} : \boldsymbol{\nabla}_{\boldsymbol{y}} \delta\tilde{\boldsymbol{u}}_1 d_T,$$

the solution $\tilde{\boldsymbol{u}}_1$ can be expressed as

$$\tilde{\boldsymbol{u}}_1 = \tilde{U}_1 + \mathcal{X}_1 : i\boldsymbol{k} \otimes^s \tilde{U}_0,$$

where $\tilde{U}_1 = \langle \tilde{\boldsymbol{u}}_1 \rangle$, so $\langle \mathcal{X}_1 \rangle = \boldsymbol{0}$. When we only consider first order approximation $\langle \tilde{\boldsymbol{u}} \rangle = \tilde{U}_0 + \epsilon \tilde{U}_1 + o(\epsilon^2)$ and ignore the second order ϵ^2 term. Then, the $\mathcal{T}_1$ satisfies

$$\mathcal{T}_1 : \langle \tilde{\boldsymbol{u}} \rangle = \mathcal{X}_1 : i\boldsymbol{k} \otimes^s \langle \tilde{\boldsymbol{u}} \rangle \equiv \mathcal{X}_1 \cdot i\boldsymbol{k} \cdot \langle \tilde{\boldsymbol{u}} \rangle,$$

where $\mathcal{X}_1$ is a third-order tensor with minor symmetry, i.e. $(\mathcal{X}_1)_{jkl} = (\mathcal{X}_1)_{jlk}$.

In the same way, for higher order approximation expressions of $\langle \tilde{\boldsymbol{u}} \rangle = \sum_i^n \epsilon^i \tilde{U}_i + o(\epsilon^{n+1})$, it is necessary to add some negligible high-order ϵ^{n+1} terms. For, an n-th order expression, the second-order tensors $\mathcal{T}_n$ and the $(n+2)$-order tensors $\mathcal{X}_n$ satisfy the following relationship

$$\mathcal{T}_n \cdot \langle \tilde{\boldsymbol{u}} \rangle = [\mathcal{X}_n \odot^{n-1} (i\boldsymbol{k})^{n-1}] : i\boldsymbol{k} \otimes^s \langle \tilde{\boldsymbol{u}} \rangle,\ \mathcal{X}_0 = \boldsymbol{I},\ n \in N,$$

where the tensor $\mathcal{X}_0$ is defined as an identity second-order tensor, the symbol $\odot^{n-1}$ rep-

resents an $(n-1)$-order scalar product, and $(i\boldsymbol{k})^{n-1} = i\boldsymbol{k} \otimes i\boldsymbol{k} \otimes \cdots \otimes i\boldsymbol{k}$. Recalling Eq.(3.6), the tensor $\mathcal{T}$ provides an equivalent relationship between $\tilde{\boldsymbol{u}}$ and $\langle\tilde{\boldsymbol{u}}\rangle$. In this way, we can use the effective displacement instead of the local displacement for homogenization description. Thereby avoiding the troubles caused by complex calculations of high-order approximations. For the ϵ^n-order hierarchical equation, we have the solution

$$\tilde{\boldsymbol{u}}_i = \sum_{i=0}^{n} [\mathcal{X}_i \odot^{i-1} (i\boldsymbol{k})^{i-1}] : i\boldsymbol{k} \otimes^s \tilde{U}_i, \quad \mathcal{X}_0 = \boldsymbol{I},\ (i\boldsymbol{k})^0 = 1, \tag{3.7}$$

which is equivalent to the result shown in Boutin & Auriault (1993).

3.2.2 Homogenisation of hierarchical equations

In this subsection, we will discuss the application of the above-mentioned effective displacement field hypothesis in each hierarchical equation. Part of the derivation in this chapter is omitted. For more derivation details, please refer to Annexe B.

The lowest order homogenized equation

Superimposing the ϵ^{-2} and ϵ^{-1} equations and considering the zero-order approximation expression $\langle\tilde{\boldsymbol{u}}\rangle = \tilde{U}_0 + o(\epsilon^1)$, the lowest dynamic equation will be

$$\begin{aligned} &\boldsymbol{\nabla}_{\boldsymbol{y}} \cdot \{\mathbb{C} : [i\boldsymbol{k} \otimes \mathcal{X}_1 + \boldsymbol{\nabla}_{\boldsymbol{y}}(\mathcal{X}_2 \cdot i\boldsymbol{k})]\} : i\boldsymbol{k} \otimes^s \langle\tilde{\boldsymbol{u}}\rangle \\ &+i\boldsymbol{k} \cdot [\mathbb{C} : (\mathcal{X}_0 \otimes \boldsymbol{I} + \boldsymbol{\nabla}_{\boldsymbol{y}}\mathcal{X}_1)] : i\boldsymbol{k} \otimes^s \langle\tilde{\boldsymbol{u}}\rangle = -w^2\boldsymbol{\rho}\langle\tilde{\boldsymbol{u}}\rangle. \end{aligned} \tag{3.8}$$

Averaging the left and right sides of the above equation, the lowest homogenized dynamic equation takes the form

$$i\boldsymbol{k} \cdot \langle\mathbb{C} : (\boldsymbol{I} \otimes \boldsymbol{I} + \boldsymbol{\nabla}_{\boldsymbol{y}}\mathcal{X}_1)\rangle \cdot i\boldsymbol{k} \cdot \langle\tilde{\boldsymbol{u}}\rangle = -w^2\langle\boldsymbol{\rho}\rangle\langle\tilde{\boldsymbol{u}}\rangle. \tag{3.9}$$

Combining Eqs.(3.8) and (3.9), we have

$$(\boldsymbol{\nabla}_{\boldsymbol{y}} \cdot \mathbb{C}_1 \cdot i\boldsymbol{k} + i\boldsymbol{k} \cdot \mathbb{C}_0 \cdot i\boldsymbol{k})\,\langle\boldsymbol{\rho}_0\rangle = \boldsymbol{\rho}_0(i\boldsymbol{k} \cdot \langle\mathbb{C}_0\rangle \cdot i\boldsymbol{k}), \tag{3.10}$$

where $\mathbb{C}_0$, $\mathbb{C}_1$ and $\boldsymbol{\rho}_0$ satisfy the following definitions:

$$\mathbb{C}_0 = \mathbb{C} : (\boldsymbol{I} \otimes \boldsymbol{I} + \boldsymbol{\nabla}_{\boldsymbol{y}} \mathcal{X}_1), \quad \mathbb{C}_1 = \mathbb{C} : [i\boldsymbol{k} \otimes \mathcal{X}_1 + \boldsymbol{\nabla}_{\boldsymbol{y}} (\mathcal{X}_2 \cdot i\boldsymbol{k})], \quad \boldsymbol{\rho}_0 = \boldsymbol{\rho} \ .$$

According to the assumption of the lowest order homogenization: the displacement field maintains an undisturbed form $\langle \tilde{\boldsymbol{u}} \rangle = \tilde{U}_0$. This means that we consider that the local models are undisturbed, that is the dynamic physical properties of different media are exactly the same (e.g. wave speed, wavelength). Obviously, under dynamic conditions, this result is true if and only if the local model of composites has the same material (not applicable to composite materials with different phases). Coincidentally, for the quasi-static case, there is no frequency dependence of different media in the local model, so the lowest order homogenization results (3.9) are available.

The first order homogenized equation

With the approximation expression $\langle \tilde{\boldsymbol{u}} \rangle = \tilde{U}_0 + \epsilon \tilde{U}_1 + o(\epsilon^2)$, all the ϵ^2 terms are considered as negligible under this approximation. Combining the lowest order dynamic equation (3.8), the first dynamic equation can be rewritten as

$$\boldsymbol{\nabla}_{\boldsymbol{y}} \cdot [(\mathbb{C}_1 + \epsilon \mathbb{C}_2) : i\boldsymbol{k} \otimes^s \langle \tilde{\boldsymbol{u}} \rangle] + i\boldsymbol{k} \cdot [(\mathbb{C}_0 + \epsilon \mathbb{C}_1) : i\boldsymbol{k} \otimes^s \langle \tilde{\boldsymbol{u}} \rangle] = -w^2 (\boldsymbol{\rho}_0 + \epsilon \boldsymbol{\rho}_1) \langle \tilde{\boldsymbol{u}} \rangle, \quad (3.11)$$

where $\mathbb{C}_2$ and $\boldsymbol{\rho}_1$ satisfy the definitions:

$$\mathbb{C}_2 = \mathbb{C} : \{i\boldsymbol{k} \otimes (\mathcal{X}_2 \cdot i\boldsymbol{k}) + \boldsymbol{\nabla}_{\boldsymbol{y}} [\mathcal{X}_3 : (i\boldsymbol{k})^2]\}, \quad \boldsymbol{\rho}_1 = \boldsymbol{\rho} (\mathcal{X}_1 \cdot i\boldsymbol{k}) \ .$$

It is worth noting that equation (3.11) only holds when the approximate order is ϵ^2. After the average operation, the first homogenized dynamic equation is given by

$$i\boldsymbol{k} \cdot (\langle \mathbb{C}_0 \rangle + \epsilon \langle \mathbb{C}_1 \rangle) \cdot i\boldsymbol{k} \cdot \langle \tilde{\boldsymbol{u}} \rangle = -w^2 \left(\langle \boldsymbol{\rho}_0 \rangle + \epsilon \langle \boldsymbol{\rho}_1 \rangle \right) \langle \tilde{\boldsymbol{u}} \rangle. \quad (3.12)$$

Note that the necessary condition for the above equation to hold is to limit the asymptotic order to the ϵ^n-order approximation. Thanks to this hypothesis, a relation for solving the tensor $\mathbb{C}_2$ can be derived from the equations (3.11) and (3.12) (only pay attention to all

terms of ϵ^1):

$$\begin{aligned}(\boldsymbol{\nabla}_{\boldsymbol{y}} \cdot \mathbb{C}_2 \cdot i\boldsymbol{k} + i\boldsymbol{k} \cdot \mathbb{C}_1 \cdot i\boldsymbol{k}) \langle \boldsymbol{\rho}_0 \rangle + (\boldsymbol{\nabla}_{\boldsymbol{y}} \cdot \mathbb{C}_1 \cdot i\boldsymbol{k} + i\boldsymbol{k} \cdot \mathbb{C}_0 \cdot i\boldsymbol{k}) \langle \boldsymbol{\rho}_1 \rangle \\ = \boldsymbol{\rho}_0 (i\boldsymbol{k} \cdot \langle \mathbb{C}_1 \rangle \cdot i\boldsymbol{k}) + \boldsymbol{\rho}_1 (i\boldsymbol{k} \cdot \langle \mathbb{C}_0 \rangle \cdot i\boldsymbol{k}) .\end{aligned} \tag{3.13}$$

The n-th order homogenized equation

Superimposing all the previous hierarchical equations and ignoring the ϵ^{n+1} and higher order ϵ terms for the assumption $\langle \tilde{\boldsymbol{u}} \rangle = \sum_i^n \epsilon^i \tilde{U}_i + o(\epsilon^{n+1})$, the ϵ^n order dynamic equation satisfies

$$\boldsymbol{\nabla}_{\boldsymbol{y}} \cdot \left(\mathbb{C}^{hom}_{[n+1]} : i\boldsymbol{k} \otimes^s \langle \tilde{\boldsymbol{u}} \rangle \right) + i\boldsymbol{k} \cdot \left(\mathbb{C}^{hom}_{n} : i\boldsymbol{k} \otimes^s \langle \tilde{\boldsymbol{u}} \rangle \right) = -w^2 \boldsymbol{\rho}^{hom}_n \langle \tilde{\boldsymbol{u}} \rangle, \tag{3.14}$$

with the definitions

$$\mathbb{C}^{hom}_{[n+1]} = \mathbb{C}_1 + \epsilon \mathbb{C}_2 + \epsilon^2 \mathbb{C}_3 + ... \epsilon^n \mathbb{C}_{n+1} + o(\epsilon^{n+1}), \tag{3.15a}$$

$$\mathbb{C}^{hom}_{n} = \mathbb{C}_0 + \epsilon \mathbb{C}_1 + \epsilon^2 \mathbb{C}_2 + ... \epsilon^n \mathbb{C}_n + o(\epsilon^{n+1}), \tag{3.15b}$$

$$\boldsymbol{\rho}^{hom}_n = \boldsymbol{\rho}_0 + \epsilon \boldsymbol{\rho}_1 + \epsilon^2 \boldsymbol{\rho}_2 + ... \epsilon^n \boldsymbol{\rho}_n + o(\epsilon^{n+1}), \tag{3.15c}$$

where $\mathbb{C}_n$ and $\boldsymbol{\rho}_n$ for $n \geqslant 1$ satisfy the definitions:

$$\mathbb{C}_n = \mathbb{C} : \{ i\boldsymbol{k} \otimes (\mathcal{X}_n \odot^{n-1} (i\boldsymbol{k})^{n-1}) + \boldsymbol{\nabla}_{\boldsymbol{y}} [\mathcal{X}_{n+1} \odot^n (i\boldsymbol{k})^n] \}, \tag{3.16a}$$

$$\boldsymbol{\rho}_n = \boldsymbol{\rho} [\mathcal{X}_n \odot^{n-1} (i\boldsymbol{k})^{n-1}] . \tag{3.16b}$$

The ϵ^n order homogenized dynamic equation is

$$i\boldsymbol{k} \cdot \langle \mathbb{C}^{hom}_n \rangle \cdot i\boldsymbol{k} \cdot \langle \tilde{\boldsymbol{u}} \rangle = -w^2 \langle \boldsymbol{\rho}^{hom}_n \rangle \langle \tilde{\boldsymbol{u}} \rangle. \tag{3.17}$$

According to Eqs.(3.14) and (3.17), a general relation between $\mathbb{C}^{hom}$ and $\boldsymbol{\rho}^{hom}$ can be obtained as

$$\left(\boldsymbol{\nabla}_{\boldsymbol{y}} \cdot \mathbb{C}^{hom}_{[n+1]} \cdot i\boldsymbol{k} + i\boldsymbol{k} \cdot \mathbb{C}^{hom}_n \cdot i\boldsymbol{k} \right) \langle \boldsymbol{\rho}^{hom}_n \rangle = \boldsymbol{\rho}^{hom}_n (i\boldsymbol{k} \cdot \langle \mathbb{C}^{hom}_n \rangle \cdot i\boldsymbol{k}). \tag{3.18}$$

Extending the above expression and consider only the terms of ϵ^n, we have

$$\sum_{j=0}^{n}(\boldsymbol{\nabla}_{\boldsymbol{y}}\cdot\mathbb{C}_{n+1-j}\cdot i\boldsymbol{k}+i\boldsymbol{k}\cdot\mathbb{C}_{n-j}\cdot i\boldsymbol{k})\langle\boldsymbol{\rho}_j\rangle=\sum_{j=0}^{n}\boldsymbol{\rho}_j(i\boldsymbol{k}\cdot\langle\mathbb{C}_{n-j}\rangle\cdot i\boldsymbol{k}). \tag{3.19}$$

This general solution shows the relationship between all tensors $\mathbb{C}_n$ and $\boldsymbol{\rho}_n$. That means the $\mathbb{C}_{n+1}$ can be easily obtained for any approximate order. According to the definition of tensors $\mathbb{C}_n$ (3.16a) and $\boldsymbol{\rho}_n$ (3.16b), the more important work is to get the function $\mathcal{X}_n$. Therefore, the next more important task is to seek for the tensors $\mathcal{X}_n$.

3.2.3 Effective behaviour

Thanks to the method shown in the previous subsection, considering all approximate order displacement fields as a whole, more complex derivative calculations were successfully avoided. In fact, this assumption circumvents a "confuse" that exists in the solution process of $\tilde{\boldsymbol{u}}$. For example, in the ϵ^1 homogenized dynamic equation, we have

$$i\boldsymbol{k}\cdot\langle\mathbb{C}_0\rangle:i\boldsymbol{k}\otimes^s\tilde{U}_1+i\boldsymbol{k}\cdot\langle\mathbb{C}_1\rangle:i\boldsymbol{k}\otimes^s\tilde{U}_0=-w^2\langle\boldsymbol{\rho}_0\rangle\tilde{U}_1-w^2\langle\boldsymbol{\rho}_1\rangle\tilde{U}_0. \tag{3.20}$$

In this equation, $\tilde{U}_0$ is a necessary condition for obtaining $\tilde{U}_1$, which means that the higher-order expression can only be obtained in a progressive manner. This will undoubtedly cost a lot of work. Therefore, by combining the hierarchical equations, the method in the previous subsection avoids the complexity and tedious derivation work caused by the relationship between each U_n term. Then, Eq.(3.20) can be rewritten as the following expression that is applicable up to the order ϵ^2:

$$i\boldsymbol{k}\cdot[(\langle\mathbb{C}_0\rangle+\epsilon\langle\mathbb{C}_1\rangle):i\boldsymbol{k}\otimes^s(\tilde{U}_0+\epsilon\tilde{U}_1)]=-w^2(\langle\boldsymbol{\rho}_0\rangle+\epsilon\langle\boldsymbol{\rho}_1\rangle)(\tilde{U}_0+\epsilon\tilde{U}_1)+O(\epsilon^2),$$

where the correction $O(\epsilon^2)=\epsilon^2\left\{i\boldsymbol{k}\cdot[\langle\mathbb{C}_0\rangle:\left(i\boldsymbol{k}\otimes^s\tilde{U}_1\right)]+w^2\langle\boldsymbol{\rho}\rangle\tilde{U}_1\right\}$. Similarly, the n-th order local homogenized equation (3.17) can be obtained with the definition of $\langle\tilde{\boldsymbol{u}}\rangle=\sum_i^n\epsilon^i\tilde{U}_i+o(\epsilon^{n+1})$.

In the general relationship (3.19), the determination of $\mathcal{X}$ requires all periodic boundary conditions and the continuous conditions of the REV. When we consider that all interfaces

of the composite material are perfect interfaces, the satisfaction of continuous conditions are necessary on the interface $\mathcal{S}$ (two sides of the interface $\mathcal{S}$ are denoted as $\mathcal{S}^{(-)}$ and $\mathcal{S}^{(+)}$). At the same time, the periodic conditions must be satisfied on the boundary $\partial\Omega$ (two sides corresponding to the medium Ω are denoted as $\partial\Omega^{(-)}$ and $\partial\Omega^{(+)}$ with $\partial\Omega = \partial\Omega^{(-)} + \partial\Omega^{(+)}$). In this elastic problem, the continuous conditions are given on the displacement field $\tilde{\boldsymbol{u}}$ and the traction vector $\tilde{\boldsymbol{\tau}} = \tilde{\boldsymbol{\sigma}} \cdot \boldsymbol{n}$. There are

- Periodic boundary conditions:

$$\tilde{\boldsymbol{u}}_n(\boldsymbol{y} \in \partial\Omega^{(-)}) = \tilde{\boldsymbol{u}}_n(\boldsymbol{y} \in \partial\Omega^{(+)}), \quad \tilde{\boldsymbol{\tau}}_{n-1}(\boldsymbol{y} \in \partial\Omega^{(-)}) = \tilde{\boldsymbol{\tau}}_{n-1}(\boldsymbol{y} \in \partial\Omega^{(+)});$$

- Continuous boundary conditions

$$\tilde{\boldsymbol{u}}_n(\boldsymbol{y} \in \mathcal{S}^{(-)}) = \tilde{\boldsymbol{u}}_n(\boldsymbol{y} \in \mathcal{S}^{(+)}), \quad \tilde{\boldsymbol{\tau}}_{n-1}(\boldsymbol{y} \in \mathcal{S}^{(-)}) = \tilde{\boldsymbol{\tau}}_{n-1}(\boldsymbol{y} \in \mathcal{S}^{(+)});$$

- Zero-average condition: $\langle \mathcal{X}_n \rangle = \boldsymbol{0}$.

After solving the tensors $\mathcal{X}_n$, the perturbation expression of the local displacement field (3.7) can be solved. The n-th order approximation tensors $\mathbb{C}_n^{hom}$ and $\boldsymbol{\rho}_n^{hom}$ will be determined by Eqs.(3.15b) and (3.15c). Rewriting the homogenized dynamic equation as the form $\mathcal{Z}\langle\tilde{\boldsymbol{u}}\rangle = \boldsymbol{0}$, where $\mathcal{Z}$ stands for the effective impedance, the lowest order effective impedance $\mathcal{Z}_0$ reads

$$\mathcal{Z}_0 = iw\langle\boldsymbol{\rho}\rangle iw - i\boldsymbol{k} \cdot \langle \mathbb{C} : (\boldsymbol{I} \otimes \boldsymbol{I} + \boldsymbol{\nabla}_{\boldsymbol{y}}\mathcal{X}_1)\rangle \cdot i\boldsymbol{k}.$$

It is necessary to state here that the lowest order effective elastic tensor $\langle \mathbb{C} : (\boldsymbol{I} \otimes \boldsymbol{I} + \boldsymbol{\nabla}_{\boldsymbol{y}}\mathcal{X}_1)\rangle$ represents the expression of the lowest order asymptotic analysis, which is also the effective elastic tensor for a "quasi-static" case or non-dynamic homogenization. Eq.(3.17) gives the n-th order effective impedance

$$\mathcal{Z}_n = iw\boldsymbol{\rho}^{eff} iw - i\boldsymbol{k} \cdot \mathbb{C}^{eff} \cdot i\boldsymbol{k}, \tag{3.21}$$

where the effective tensors $\mathbb{C}^{eff}$ and effective density $\boldsymbol{\rho}^{eff}$ can be obtained by averaging

the expressions $\mathbb{C}_n^{hom}$ and $\boldsymbol{\rho}_n^{hom}$ shown in Eqs.(3.15b) and (3.15c). Precisely,

$$\mathbb{C}^{eff} = \langle \mathbb{C}_n^{hom} \rangle = \langle \mathbb{C}_0 \rangle + \epsilon \langle \mathbb{C}_1 \rangle + \epsilon^2 \langle \mathbb{C}_2 \rangle + ... + \epsilon^{n-1} \langle \mathbb{C}_{n-1} \rangle + \epsilon^n \langle \mathbb{C}_n \rangle \ , \tag{3.22a}$$

$$\boldsymbol{\rho}^{eff} = \langle \boldsymbol{\rho}_n^{hom} \rangle = \langle \boldsymbol{\rho}_0 \rangle + \epsilon \langle \boldsymbol{\rho}_1 \rangle + \epsilon^2 \langle \boldsymbol{\rho}_2 \rangle + ... + \epsilon^{n-1} \langle \boldsymbol{\rho}_{n-1} \rangle + \epsilon^n \langle \boldsymbol{\rho}_n \rangle \ . \tag{3.22b}$$

So far, the only remaining problem is to solve the tensor $\mathcal{X}_n$ by using the above boundary periodic conditions and interface continuity conditions. Once the tensor $\mathcal{X}_n$ is determined, the expressions $\mathbb{C}_n^{hom}$ and $\boldsymbol{\rho}_n^{hom}$ can be obtained according to the expressions (3.22a, 3.22b) and the definitions (3.16a, 3.16b).

In fact, in the numerical case we found that only the even-numbered items in the above expressions are real numbers. The reason is that the stiffness tensor $\mathbb{C}$ and density $\boldsymbol{\rho}$ of each phase of composites are real terms, their effective stiffness tensor $\mathbb{C}^{eff}$ and effective density $\boldsymbol{\rho}^{eff}$ expressions contain complex terms that come from the $i\boldsymbol{k}$ odd power items in the definitions (3.16a, 3.16b). When we only consider the real part of $\mathbb{C}^{eff}$ and $\boldsymbol{\rho}^{eff}$, they can be shown as all the even terms (with $n = 2m$):

$$\mathbb{C}^{eff} = \langle \mathbb{C}_0 \rangle + \epsilon^2 \langle \mathbb{C}_2 \rangle + \epsilon^4 \langle \mathbb{C}_4 \rangle + ... + \epsilon^{2m} \langle \mathbb{C}_{2m} \rangle \ , \tag{3.23a}$$

$$\boldsymbol{\rho}^{eff} = \langle \boldsymbol{\rho}_0 \rangle + \epsilon^2 \langle \boldsymbol{\rho}_2 \rangle + \epsilon^4 \langle \boldsymbol{\rho}_4 \rangle + ... + \epsilon^{2m} \langle \boldsymbol{\rho}_{2m} \rangle \ . \tag{3.23b}$$

It is worth mentioning that in the work of many researchers (e.g. Fish et al., 2002a, 2002b; Wautier & Guzina, 2015), for a two-phase layered composite model, the odd terms are ignored, because the odd parts $\langle \mathbb{C}_n \rangle$ and $\langle \boldsymbol{\rho}_n \rangle$ are both zero. But in fact, this result holds only for the two-phase layered composites, and the result is not absolutely zero for the more phase layered model. Beyond that, more discussion on the imaginary part of $\mathbb{C}^{eff}$ and $\boldsymbol{\rho}^{eff}$ will be shown in Appendix B and Appendix C.

Thanks to the aforementioned two-scale representation, a clear and general wave number-dependent effective asymptotic expression can be obtained. Generally, any order effective impedance expression can be derived using Eq.(3.19). It is worth noting that the accuracy of the effective impedance in the above equation is directly related to the asymptotic order n.

3.3 Asymptotic description with $\tilde{\boldsymbol{f}}$

The free strain $\tilde{\boldsymbol{E}}_0$ and the volume force $\tilde{\boldsymbol{f}}$ are considered to determine two localization tensors $\boldsymbol{A}$ and $\boldsymbol{B}$. The tensors $\mathcal{L}$ and $\mathcal{M}$ are derived from two extremes combination modes. The effective impedance expression for the dynamic equation without the volume force has been obtained in the previous subsection. When considering the general dynamic equation with the volume force $\tilde{\boldsymbol{f}}$, it is necessary to rewrite the representation of the local displacement $\tilde{\boldsymbol{u}}$ as

$$\tilde{\boldsymbol{u}} = \mathcal{H} : \langle \tilde{\boldsymbol{u}} \rangle + \mathcal{F} \cdot \tilde{\boldsymbol{f}}, \tag{3.24}$$

where the term of $\tilde{\boldsymbol{f}}$ shows a "independent" effect with $\langle \tilde{\boldsymbol{u}} \rangle$. When we consider that the volume force $\tilde{\boldsymbol{f}} = \boldsymbol{0}$, this assumption will degenerate into the aforementioned case of without $\tilde{\boldsymbol{f}}$. Therefore, the tensors $\mathcal{H}$ and $\mathcal{F}$ satisfy

$$\langle \mathcal{H} \rangle = \boldsymbol{I}, \quad \langle \mathcal{F} \rangle = \boldsymbol{0}.$$

The general dynamic equation is expressed as:

$$(i\boldsymbol{k} + \frac{1}{\epsilon}\boldsymbol{\nabla}_{\boldsymbol{y}}) \cdot [\mathbb{C} : ((i\boldsymbol{k} + \frac{1}{\epsilon}\boldsymbol{\nabla}_{\boldsymbol{y}}) \otimes^s \tilde{\boldsymbol{u}})] + \tilde{\boldsymbol{f}} = -w^2 \boldsymbol{\rho} \cdot \tilde{\boldsymbol{u}}. \tag{3.25}$$

Similar to the approximate description Eq.(3.3), the tensors $\mathcal{H}$ and $\mathcal{F}$ also have the approximate expressions:

$$\mathcal{H} = \mathcal{H}_0 + \epsilon \mathcal{H}_1 + \epsilon^2 \mathcal{H}_2 + \dots, \quad \mathcal{F} = \mathcal{F}_0 + \epsilon \mathcal{F}_1 + \epsilon^2 \mathcal{F}_2 + \dots .$$

Averaging both sides of Eq.(3.24) yields

$$\langle \mathcal{H}_0 \rangle = \boldsymbol{I}, \ \langle \mathcal{H}_n \rangle = \boldsymbol{0}, \ (n \geqslant 1); \quad \langle \mathcal{F}_n \rangle = \boldsymbol{0}, \ (n \geqslant 0).$$

According to the assumption (3.24), the tensor $\mathcal{H}$ can be solved in the same way as the tensor $\mathcal{T}$. Similarly, the tensor $\mathcal{F}$ can also be obtained by comparing the hierarchical equations.

3.3.1 localisation of hierarchical equations

The ϵ^{-2} order equation

First, extend Eq.(3.25) to get the ϵ^{-2} order hierarchical equation:

$$\boldsymbol{\nabla_y} \cdot [\mathbb{C} : \boldsymbol{\nabla_y} \mathcal{H}_0 \langle \tilde{\boldsymbol{u}} \rangle] + \boldsymbol{\nabla_y} \cdot [\mathbb{C} : \boldsymbol{\nabla_y} \mathcal{F}_0 \tilde{\boldsymbol{f}}] = \mathbf{0},$$

where the effective displacement corresponds to the approximation $\langle \tilde{\boldsymbol{u}} \rangle = \tilde{U}_0 + o(\epsilon)$. Considering the "independent" relationship between the terms of $\mathcal{H}$ and $\mathcal{F}$, it follows that

$$\boldsymbol{\nabla_y} \cdot [\mathbb{C} : \boldsymbol{\nabla_y} \mathcal{H}_0 \langle \tilde{\boldsymbol{u}} \rangle] = \mathbf{0}, \quad \boldsymbol{\nabla_y} \cdot [\mathbb{C} : \boldsymbol{\nabla_y} \mathcal{F}_0 \tilde{\boldsymbol{f}}] = \mathbf{0}. \tag{3.26}$$

The ϵ^{-1} order equation

Superimposing the hierarchical equation of ϵ^{-2} and ϵ^{-1} and append the negligible terms of ϵ^2, the ϵ^{-1} order general dynamic equation reads

$$\begin{aligned} &\boldsymbol{\nabla_y} \cdot [\mathbb{C} : (\boldsymbol{\nabla_y} \mathcal{H}_1 + i\boldsymbol{k}\mathcal{H}_0) \langle \tilde{\boldsymbol{u}} \rangle] + i\boldsymbol{k} \cdot (\mathbb{C} : \boldsymbol{\nabla_y} \mathcal{H}_0 \langle \tilde{\boldsymbol{u}} \rangle) \\ +&\boldsymbol{\nabla_y} \cdot [\mathbb{C} : (\boldsymbol{\nabla_y} \mathcal{F}_1 + i\boldsymbol{k}\mathcal{F}_0) \tilde{\boldsymbol{f}}] + i\boldsymbol{k} \cdot (\mathbb{C} : \boldsymbol{\nabla_y} \mathcal{F}_0 \tilde{\boldsymbol{f}}) = \mathbf{0}, \end{aligned}$$

where the effective displacement is of a first order approximation $\langle \tilde{\boldsymbol{u}} \rangle = \tilde{U}_0 + \epsilon \tilde{U}_1 + o(\epsilon^2)$. Its homogenized equations are given by

$$i\boldsymbol{k} \cdot \langle \mathbb{C} : \boldsymbol{\nabla_y} \mathcal{H}_0 \rangle \langle \tilde{\boldsymbol{u}} \rangle = \mathbf{0}, \quad i\boldsymbol{k} \cdot \langle \mathbb{C} : \boldsymbol{\nabla_y} \mathcal{F}_0 \rangle \tilde{\boldsymbol{f}} = \mathbf{0}. \tag{3.27}$$

Thanks to the Eqs.(3.26) and (3.27), the tensors $\mathcal{H}_0$ and $\mathcal{F}_0$ can be determined as $\mathcal{H}_0 = \boldsymbol{I}$ and $\mathcal{F}_0 = \mathbf{0}$.

3.3.2 Homogenisation of hierarchical equations

The lowest order homogenized equation

Considering the lowest approximation $\langle \tilde{\boldsymbol{u}} \rangle = \tilde{U}_0 + o(\epsilon)$, the lowest order general dynamic

equation can be derived as:

$$\begin{aligned}
&\boldsymbol{\nabla_y} \cdot [\mathbb{C} : (\boldsymbol{\nabla}_y \mathcal{H}_2 + i\boldsymbol{k} \otimes^s \mathcal{H}_1)]\langle \tilde{\boldsymbol{u}} \rangle + i\boldsymbol{k} \cdot [\mathbb{C} : (\boldsymbol{\nabla_y} \mathcal{H}_1 + i\boldsymbol{k} \otimes^s \mathcal{H}_0)]\langle \tilde{\boldsymbol{u}} \rangle \\
&+\boldsymbol{\nabla_y} \cdot [\mathbb{C} : (\boldsymbol{\nabla}_y \mathcal{F}_2 + i\boldsymbol{k} \otimes^s \mathcal{F}_1)]\tilde{\boldsymbol{f}} + i\boldsymbol{k} \cdot [\mathbb{C} : (\boldsymbol{\nabla_y} \mathcal{F}_1 + i\boldsymbol{k} \otimes^s \mathcal{F}_0)]\tilde{\boldsymbol{f}} + \tilde{\boldsymbol{f}} \\
&= -w^2 \boldsymbol{\rho} \mathcal{H}_0 \langle \tilde{\boldsymbol{u}} \rangle - w^2 \boldsymbol{\rho} \mathcal{F}_0 \tilde{\boldsymbol{f}}.
\end{aligned} \tag{3.28}$$

We know that the first order homogenized dynamic equation takes the form

$$i\boldsymbol{k} \cdot \langle \mathbb{C} : (\boldsymbol{\nabla_y} \mathcal{H}_1 + i\boldsymbol{k} \otimes^s \mathcal{H}_0)] \rangle \langle \tilde{\boldsymbol{u}} \rangle + \tilde{\boldsymbol{f}} = -w^2 \langle \boldsymbol{\rho} \mathcal{H}_0 \rangle \langle \tilde{\boldsymbol{u}} \rangle. \tag{3.29}$$

Then,

$$i\boldsymbol{k} \cdot \langle \mathbb{C} : (\boldsymbol{\nabla_y} \mathcal{F}_1 + i\boldsymbol{k} \otimes^s \mathcal{F}_0) \rangle \tilde{\boldsymbol{f}} = -w^2 \langle \boldsymbol{\rho} \mathcal{F}_0 \rangle \tilde{\boldsymbol{f}}.$$

Its easy to get $\mathcal{F}_1 = \mathbf{0}$. For the solution of $\mathcal{F}_n (n \geq 2)$, we introduce two polynomial functions $\mathcal{X}$ and $\boldsymbol{\eta}$ to represent the $\boldsymbol{y}$-variable correlation portions of the tensors $\mathcal{H}$ and $\mathcal{F}$:

$$\begin{aligned}
\mathcal{H}_n \cdot \langle \tilde{\boldsymbol{u}} \rangle &= (\mathcal{X}_n \odot^{n-1} (i\boldsymbol{k})^{n-1}) : i\boldsymbol{k} \otimes^s \langle \tilde{\boldsymbol{u}} \rangle, \ n \geq 1, \ \mathcal{X}_0 = \boldsymbol{I}, \\
\mathcal{F}_n \tilde{\boldsymbol{f}} &= \boldsymbol{\eta}_n \odot^{n-2} (i\boldsymbol{k})^{n-2} \tilde{\boldsymbol{f}}, \ n \geq 2, \ \boldsymbol{\eta}_0 = \boldsymbol{\eta}_1 = \mathbf{0},
\end{aligned}$$

where $\boldsymbol{\eta}$, which is similar to $\mathcal{X}$, is an n-th order tensor related to the variable $\boldsymbol{y}$. The determination of $\boldsymbol{\eta}$ also needs to be based on the periodic boundary conditions and continuity conditions mentioned in the previous section.

With the definition of $\mathcal{H}$ and $\mathcal{F}$, the lowest order general dynamic equation can be written as

$$\boldsymbol{\nabla_y} \cdot (\mathbb{C}_1 : i\boldsymbol{k} \otimes^s \langle \tilde{\boldsymbol{u}} \rangle) + i\boldsymbol{k} \cdot (\mathbb{C}_0 : i\boldsymbol{k} \otimes^s \langle \tilde{\boldsymbol{u}} \rangle) + \boldsymbol{\nabla_y} \cdot (\mathbb{C} : \boldsymbol{\nabla}_y \boldsymbol{\eta}_2) \cdot \tilde{\boldsymbol{f}} + \tilde{\boldsymbol{f}} = -w^2 \boldsymbol{\rho} \langle \tilde{\boldsymbol{u}} \rangle,$$

and the lowest order homogenized dynamic equation reads

$$i\boldsymbol{k} \cdot \langle \mathbb{C}_0 \rangle \cdot i\boldsymbol{k} \cdot \langle \tilde{\boldsymbol{u}} \rangle + \tilde{\boldsymbol{f}} = -w^2 \langle \boldsymbol{\rho}_0 \rangle \langle \tilde{\boldsymbol{u}} \rangle.$$

According to Eq.(3.10) and comparing Eqs.(3.28) and (3.29), $\boldsymbol{\eta}_2$ can be determined to satisfy the following relationship:

$$\boldsymbol{\nabla}_{\boldsymbol{y}} \cdot [\mathbb{C} : \boldsymbol{\nabla}_{\boldsymbol{y}} \boldsymbol{\eta}_2] \langle \boldsymbol{\rho} \rangle = \boldsymbol{\rho} - \langle \boldsymbol{\rho} \rangle. \tag{3.30}$$

The first order homogenized equation

In the same way, combining the lowest order equations and adding some negligible ϵ^2 terms, the first dynamic equation relative to the approximation expression $\langle \tilde{\boldsymbol{u}} \rangle = \tilde{U}_0 + \epsilon \tilde{U}_1 + o(\epsilon^2)$ can be expressed as

$$\begin{aligned} &\boldsymbol{\nabla}_{\boldsymbol{y}} \cdot [(\mathbb{C}_1 + \epsilon \mathbb{C}_2) : i\boldsymbol{k} \otimes^s \langle \tilde{\boldsymbol{u}} \rangle] + i\boldsymbol{k} \cdot [(\mathbb{C}_0 + \epsilon \mathbb{C}_1) : i\boldsymbol{k} \otimes^s \langle \tilde{\boldsymbol{u}} \rangle] \\ &+ \boldsymbol{\nabla}_{\boldsymbol{y}} \cdot (\mathbb{C}_1^f + \epsilon \mathbb{C}_2^f) \cdot \tilde{\boldsymbol{f}} + i\boldsymbol{k} \cdot \epsilon \mathbb{C}_1^f \cdot \tilde{\boldsymbol{f}} + \tilde{\boldsymbol{f}} = -w^2 (\boldsymbol{\rho}_0 + \epsilon \boldsymbol{\rho}_1) \langle \tilde{\boldsymbol{u}} \rangle, \end{aligned} \tag{3.31}$$

where the third-order tensors $\mathbb{C}_1^f$ and $\mathbb{C}_2^f$ are defined by

$$\mathbb{C}_1^f = \mathbb{C} : \boldsymbol{\nabla}_{\boldsymbol{y}} \boldsymbol{\eta}_2, \quad \mathbb{C}_2^f = \mathbb{C} : [\boldsymbol{\eta}_2 + \boldsymbol{\nabla}_{\boldsymbol{y}} (\boldsymbol{\eta}_3 \cdot i\boldsymbol{k})].$$

The first order homogenized dynamic equation is given by

$$i\boldsymbol{k} \cdot \langle \mathbb{C}_0 + \epsilon \mathbb{C}_1 \rangle : i\boldsymbol{k} \otimes^s \langle \tilde{\boldsymbol{u}} \rangle + \epsilon i\boldsymbol{k} \cdot \langle \mathbb{C}_1^f \rangle \cdot \tilde{\boldsymbol{f}} + \tilde{\boldsymbol{f}} = -w^2 \langle \boldsymbol{\rho}_0 + \epsilon \boldsymbol{\rho}_1 \rangle \langle \tilde{\boldsymbol{u}} \rangle. \tag{3.32}$$

According to Eqs.(3.31), (3.32) and (3.13), the function $\boldsymbol{\eta}_3$ can be determined by

$$\left(\boldsymbol{\nabla}_{\boldsymbol{y}} \cdot (\mathbb{C}_1^f + \epsilon \boldsymbol{C}_2^f) + \epsilon i\boldsymbol{k} \cdot \mathbb{C}_1^f + \boldsymbol{I} \right) \tilde{\boldsymbol{f}} \left(\langle \boldsymbol{\rho}_0 \rangle + \epsilon \langle \boldsymbol{\rho}_1 \rangle \right) = (\boldsymbol{\rho}_0 + \epsilon \boldsymbol{\rho}_1)(\epsilon i\boldsymbol{k} \cdot \langle \mathbb{C}_1^f \rangle) \tilde{\boldsymbol{f}}. \tag{3.33}$$

Extending the above equation using a constant definition of $\tilde{\boldsymbol{f}}$, the ϵ^1 order equation gives

$$(\boldsymbol{\nabla}_{\boldsymbol{y}} \cdot \mathbb{C}_2^f + i\boldsymbol{k} \cdot \mathbb{C}_1^f) \langle \boldsymbol{\rho}_0 \rangle + (\boldsymbol{\nabla}_{\boldsymbol{y}} \cdot \mathbb{C}_1^f + \boldsymbol{I}) \langle \boldsymbol{\rho}_1 \rangle = \boldsymbol{\rho}_0 (i\boldsymbol{k} \cdot \langle \mathbb{C}_1^f \rangle) + \boldsymbol{\rho}_1. \tag{3.34}$$

The n-th order homogenized equation

Consider the approximation $\langle \tilde{\boldsymbol{u}} \rangle = \sum_{i=0}^{n} \epsilon^i \tilde{U}_i + o(\epsilon^{n+1})$ and superimpose all hierarchical

equations to get

$$\begin{aligned}\left(\boldsymbol{\nabla}_{\boldsymbol{y}}\cdot\mathbb{C}_{[n+1]}^{hom}+i\boldsymbol{k}\cdot\mathbb{C}_{n}^{hom}\right):i\boldsymbol{k}\otimes^{s}\langle\tilde{\boldsymbol{u}}\rangle\ &+\left(\boldsymbol{\nabla}_{\boldsymbol{y}}\cdot\mathbb{C}_{[n+1]}^{f.hom}+i\boldsymbol{k}\cdot\mathbb{C}_{n}^{f.hom}\right)\cdot i\boldsymbol{k}\cdot\tilde{\boldsymbol{f}}+\tilde{\boldsymbol{f}}\\&=-w^{2}\boldsymbol{\rho}_{n}^{hom}\langle\tilde{\boldsymbol{u}}\rangle-w^{2}\boldsymbol{\rho}_{n}^{f.hom}\tilde{\boldsymbol{f}},\end{aligned}\tag{3.35}$$

where the tensors $\mathbb{C}_{[n+1]}^{f.hom}$, $\mathbb{C}_{n}^{f.hom}$ and $\boldsymbol{\rho}_{n}^{f.hom}$ satisfy the expressions

$$\begin{aligned}\mathbb{C}_{[n+1]}^{f.hom}\cdot i\boldsymbol{k}&=\mathbb{C}_{1}^{f}+\epsilon\mathbb{C}_{2}^{f}+\epsilon^{2}\mathbb{C}_{3}^{f}+\epsilon^{3}\mathbb{C}_{4}^{f}+...+\epsilon^{n}\mathbb{C}_{n+1}^{f},\\\mathbb{C}_{n}^{f.hom}i\boldsymbol{k}&=\epsilon\mathbb{C}_{1}^{f}+\epsilon^{2}\mathbb{C}_{2}^{f}+\epsilon^{3}\mathbb{C}_{3}^{f}+...+\epsilon^{n}\mathbb{C}_{n}^{f},\\\boldsymbol{\rho}_{n}^{f.hom}&=\epsilon^{2}\boldsymbol{\rho}_{2}^{f}+\epsilon^{3}\boldsymbol{\rho}_{3}^{f}+...+\epsilon^{n}\boldsymbol{\rho}_{n}^{f},\end{aligned}$$

where $\mathbb{C}_{1}^{f}=\mathbb{C}:\boldsymbol{\nabla}_{\boldsymbol{y}}\boldsymbol{\eta}_{2}$ and

$$\mathbb{C}_{n}^{f}=\mathbb{C}:\{[\boldsymbol{\eta}_{n}\odot^{n-2}(i\boldsymbol{k})^{n-2}]+\boldsymbol{\nabla}_{\boldsymbol{y}}[\boldsymbol{\eta}_{n+1}\odot^{n-2}(i\boldsymbol{k})^{n-2}]\},\quad\boldsymbol{\rho}_{n}^{f}=\boldsymbol{\rho}[\boldsymbol{\eta}_{n}\odot^{n-2}(i\boldsymbol{k}^{n-2})],$$

for all $n\geqslant 2$. And the homogenized dynamic equation can be expressed as

$$\begin{aligned}&i\boldsymbol{k}\cdot\langle\mathbb{C}_{n}^{hom}\rangle:i\boldsymbol{k}\otimes^{s}\langle\tilde{\boldsymbol{u}}\rangle+\left(i\boldsymbol{k}\cdot\langle\mathbb{C}_{n}^{f.hom}\rangle\cdot i\boldsymbol{k}+\boldsymbol{I}\right)\tilde{\boldsymbol{f}}\\&=-w^{2}\langle\boldsymbol{\rho}_{n}^{hom}\rangle\langle\tilde{\boldsymbol{u}}\rangle-w^{2}\langle\boldsymbol{\rho}_{n}^{f.hom}\rangle\tilde{\boldsymbol{f}}.\end{aligned}\tag{3.36}$$

According to Eqs.(3.35), (3.36), (3.18), we have

$$\begin{aligned}&\left(\boldsymbol{\nabla}_{\boldsymbol{y}}\cdot\mathbb{C}_{[n+1]}^{f.hom}\cdot i\boldsymbol{k}+i\boldsymbol{k}\cdot\mathbb{C}_{n}^{f.hom}\cdot i\boldsymbol{k}+\boldsymbol{I}\right)\langle\boldsymbol{\rho}_{n}^{hom}\rangle\\&=\boldsymbol{\rho}_{n}^{hom}\left(i\boldsymbol{k}\cdot\langle\mathbb{C}_{n}^{f.hom}\rangle\cdot i\boldsymbol{k}+\boldsymbol{I}\right)-w^{2}\left(\boldsymbol{\rho}_{n}^{f.hom}\langle\boldsymbol{\rho}_{n}^{hom}\rangle-\langle\boldsymbol{\rho}_{n}^{f.hom}\rangle\boldsymbol{\rho}_{n}^{hom}\right),\end{aligned}\tag{3.37}$$

this general expression has the same format as Eq.(3.18), which allows $(n+1)$-th order asymptotic expressions to be solved by solutions of n-order.

3.3.3 The w-correlation of higher-order expressions

A general relation between $\mathbb{C}_n^f$ and $\boldsymbol{\rho}_n^f$ is given by Eq.(3.37). When $n = 1$ (because $\boldsymbol{\eta}_0$ and $\boldsymbol{\eta}_1$ are null), this expression gives

$$\left(\boldsymbol{\nabla}_{\boldsymbol{y}} \cdot \mathbb{C}_{[2]}^{f.hom} \cdot i\boldsymbol{k} + i\boldsymbol{k} \cdot \mathbb{C}_1^{f.hom} \cdot i\boldsymbol{k} + \boldsymbol{I}\right) \langle \boldsymbol{\rho}_1^{hom} \rangle = \boldsymbol{\rho}_1^{hom} \left(i\boldsymbol{k} \cdot \langle \mathbb{C}_1^{f.hom} \rangle \cdot i\boldsymbol{k} + \boldsymbol{I}\right),$$

which is the asymptotic result of the first order dynamic equation. However, when $n \geqslant 2$, the tensor $\boldsymbol{\rho}_n^{f.hom}$ is not zero ($\boldsymbol{\eta}_n$ is not null). Therefore, the solution of $\boldsymbol{\eta}$ is related to frequency w (or wave number $\boldsymbol{k}$), and we introduce $\boldsymbol{\xi}$ to represent these terms. Similar to $\boldsymbol{\eta}_n$, the tensors $\boldsymbol{\xi}_n$ can be determined by periodic boundary conditions and continuity conditions, and $\langle \boldsymbol{\xi}_n \rangle = \boldsymbol{0}$. It is easy to prove that $\boldsymbol{\xi}_0$, $\boldsymbol{\xi}_1$, $\boldsymbol{\xi}_2$ and $\boldsymbol{\xi}_3$ are zero. Then, the general expression for this case reads

$$\begin{aligned}\left(\boldsymbol{\nabla}_{\boldsymbol{y}} \cdot \mathbb{C}_{[n+1]}^{fw.hom} \cdot i\boldsymbol{k} + i\boldsymbol{k} \cdot \mathbb{C}_n^{fw.hom} \cdot i\boldsymbol{k} + \boldsymbol{I}\right) \langle \boldsymbol{\rho}_n^{hom} \rangle = \boldsymbol{\rho}_n^{hom} \left(i\boldsymbol{k} \cdot \langle \mathbb{C}_n^{fw.hom} \rangle \cdot i\boldsymbol{k} + \boldsymbol{I}\right) \\ -w^2[(\boldsymbol{\rho}_n^{f.hom} + \boldsymbol{\rho}_n^{fw.hom})\langle \boldsymbol{\rho}_n^{hom} \rangle - \boldsymbol{\rho}_n^{hom}(\langle \boldsymbol{\rho}_n^{f.hom} \rangle + \langle \boldsymbol{\rho}_n^{fw.hom} \rangle)],\end{aligned} \tag{3.38}$$

where

$$\begin{aligned}\mathbb{C}_{[n+1]}^{fw.hom} \cdot i\boldsymbol{k} &= \epsilon^2 \mathbb{C}_3^{fw} + \epsilon^3 \mathbb{C}_4^{fw} + ...\epsilon^n \mathbb{C}_{n+1}^{fw}, \\ \mathbb{C}_n^{fw.hom} \cdot i\boldsymbol{k} &= \epsilon^3 \mathbb{C}_3^{fw} + \epsilon^4 \mathbb{C}_4^{fw} + ...\epsilon^n \mathbb{C}_n^{fw}, \\ \boldsymbol{\rho}_n^{fw.hom} &= \epsilon^4 \boldsymbol{\rho}_4^{fw} + \epsilon^5 \boldsymbol{\rho}_5^{fw} + ...\epsilon^n \boldsymbol{\rho}_n^{fw},\end{aligned}$$

with $\mathbb{C}_3^{fw} = \mathbb{C} : \boldsymbol{\nabla}\boldsymbol{\xi}_4$ and

$$\mathbb{C}_n^{fw} = \mathbb{C} : \{\boldsymbol{\xi}_n \odot^{n-4} (i\boldsymbol{k})^{n-4} + \boldsymbol{\nabla}_{\boldsymbol{y}}[\boldsymbol{\xi}_{n+1} \odot^{n-4} (i\boldsymbol{k})^{n-4}]\}, \quad \boldsymbol{\rho}_n^{fw} = \boldsymbol{\rho} \cdot [\boldsymbol{\xi}_n \odot^{n-4} (i\boldsymbol{k})^{n-4}],$$

for all $n \leqslant 4$. As shown in Eq.(3.38), $\boldsymbol{\nabla}_{\boldsymbol{y}} \cdot \mathbb{C}_{[n+1]}^{fw.hom}$ is affected by w^n. And then, the terms $w^{2+4n}\tilde{\boldsymbol{f}}$ needs to satisfy:

$$\begin{aligned}\left(\boldsymbol{\nabla}_{\boldsymbol{y}} \cdot \mathbb{C}_{[n+1]}^{f.hom} \cdot i\boldsymbol{k} + i\boldsymbol{k} \cdot \mathbb{C}_n^{f.hom} \cdot i\boldsymbol{k} + \boldsymbol{I}\right) \langle \boldsymbol{\rho}_n^{hom} \rangle = \boldsymbol{\rho}_n^{hom} \left(i\boldsymbol{k} \cdot \langle \mathbb{C}_n^{f.hom} \rangle \cdot i\boldsymbol{k} + \boldsymbol{I}\right) \\ -w^2 \left(\boldsymbol{\rho}_n^{f.hom} \langle \boldsymbol{\rho}_n^{hom} \rangle - \boldsymbol{\rho}_n^{hom} \langle \boldsymbol{\rho}_n^{f.hom} \rangle\right),\end{aligned}$$

and the terms $w^{2+4n}\tilde{\boldsymbol{f}}$ also meets the equation:

$$\left(\boldsymbol{\nabla}_{\boldsymbol{y}}\cdot\mathbb{C}^{f.hom}_{[n+1]}\cdot i\boldsymbol{k}+i\boldsymbol{k}\cdot\mathbb{C}^{f.hom}_{n}\cdot i\boldsymbol{k}+\boldsymbol{I}\right)\langle\boldsymbol{\rho}^{hom}_{n}\rangle=\boldsymbol{\rho}^{hom}_{n}\left(i\boldsymbol{k}\cdot\langle\mathbb{C}^{f.hom}_{n}\rangle\cdot i\boldsymbol{k}+\boldsymbol{I}\right)$$
$$-w^{2}\left(\boldsymbol{\rho}^{fw.hom}_{n}\langle\boldsymbol{\rho}^{hom}_{n}\rangle-\boldsymbol{\rho}^{hom}_{n}\langle\boldsymbol{\rho}^{fw.hom}_{n}\rangle\right).$$

That means the solution $\boldsymbol{\xi}$ contains all the $w^{2n}\tilde{\boldsymbol{f}}$ terms. We show each part of $\tilde{\boldsymbol{u}}_0$ in a table ($\times$ means in general non zero, $\circ$ means zero):

	$\tilde{\boldsymbol{u}}_0$	$\tilde{\boldsymbol{u}}_1$	$\tilde{\boldsymbol{u}}_2$	$\tilde{\boldsymbol{u}}_3$	$\tilde{\boldsymbol{u}}_4$	$\tilde{\boldsymbol{u}}_5$	$\tilde{\boldsymbol{u}}_6$	$\tilde{\boldsymbol{u}}_7$	$\tilde{\boldsymbol{u}}_8$	$\tilde{\boldsymbol{u}}_9$	$\tilde{\boldsymbol{u}}_{10}$	...
$\langle\tilde{\boldsymbol{u}}\rangle$	$\circ$	$\circ$	$\circ$	$\circ$	$\circ$	$\circ$	$\circ$	$\circ$	$\circ$	$\circ$	$\circ$	...
$\tilde{\boldsymbol{f}}$	$\times$	$\times$	$\circ$	$\circ$	$\circ$	$\circ$	$\circ$	$\circ$	$\circ$	$\circ$	$\circ$	...
$w^2\tilde{\boldsymbol{f}}$	$\times$	$\times$	$\times$	$\times$	$\circ$	$\circ$	$\circ$	$\circ$	$\circ$	$\circ$	$\circ$	...
$w^4\tilde{\boldsymbol{f}}$	$\times$	$\times$	$\times$	$\times$	$\times$	$\times$	$\circ$	$\circ$	$\circ$	$\circ$	$\circ$	...
$w^6\tilde{\boldsymbol{f}}$	$\times$	$\times$	$\times$	$\times$	$\times$	$\times$	$\times$	$\times$	$\circ$	$\circ$	$\circ$	...
$w^8\tilde{\boldsymbol{f}}$	$\times$	$\times$	$\times$	$\times$	$\times$	$\times$	$\times$	$\times$	$\times$	$\times$	$\circ$	...

As shown in the table, for the local displacement $\tilde{\boldsymbol{u}}_n$, when $n\geqslant 2$, it contains the volume force terms $\tilde{\boldsymbol{f}}$, and when $n\geqslant 4$, it contains the frequency-dependent term.

After obtaining all the coefficient matrices $\mathcal{X}_n$, $\boldsymbol{\eta}_n$ and $\boldsymbol{\xi}_n$, the solution of the general dynamic equation can be expressed as

$$\tilde{\boldsymbol{u}}_n=\sum_{i=0}^{n}[\mathcal{X}_i\odot^{i-1}(i\boldsymbol{k})^{i-1}]:i\boldsymbol{k}\otimes^{s}U_{n-i}+[\boldsymbol{\eta}_n\odot^{n-2}(i\boldsymbol{k})^{n-2}]\tilde{\boldsymbol{f}}+[\boldsymbol{\xi}_n\odot^{n-4}(i\boldsymbol{k}^{n-4})]\tilde{\boldsymbol{f}},\quad(3.39)$$

with $\boldsymbol{\eta}_0=\boldsymbol{\eta}_1=\boldsymbol{0}$ and $\boldsymbol{\xi}_0=\boldsymbol{\xi}_1=\boldsymbol{\xi}_2=\boldsymbol{\xi}_3=\boldsymbol{0}$. In the three parts of this expression, unlike $\mathcal{X}_n$ and $\boldsymbol{\eta}_n$, the coefficient $\boldsymbol{\xi}_n$ provides all frequency-dependent terms. For example, the local displacement fields $\tilde{\boldsymbol{u}}_n$ are specified by

$$\begin{aligned}
\tilde{\boldsymbol{u}}_2&=\tilde{U}_2+\mathcal{X}_1:i\boldsymbol{k}\otimes^{s}\tilde{U}_1+(\mathcal{X}_2\cdot i\boldsymbol{k}):i\boldsymbol{k}\otimes^{s}\tilde{U}_0+\boldsymbol{\eta}_2\tilde{\boldsymbol{f}},\\
\tilde{\boldsymbol{u}}_3&=\tilde{U}_3+\mathcal{X}_1:i\boldsymbol{k}\otimes^{s}\tilde{U}_2+(\mathcal{X}_2\cdot i\boldsymbol{k}):i\boldsymbol{k}\otimes^{s}\tilde{U}_1+[\mathcal{X}_3:(i\boldsymbol{k})^2]:i\boldsymbol{k}\otimes^{s}\tilde{U}_0+(\boldsymbol{\eta}_3\cdot i\boldsymbol{k})\tilde{\boldsymbol{f}},\\
\tilde{\boldsymbol{u}}_4&=\tilde{U}_4+\mathcal{X}_1:i\boldsymbol{k}\otimes^{s}\tilde{U}_3+(\mathcal{X}_2\cdot i\boldsymbol{k}):i\boldsymbol{k}\otimes^{s}\tilde{U}_2+[\mathcal{X}_3:(i\boldsymbol{k})^2]:i\boldsymbol{k}\otimes^{s}\tilde{U}_1\\
&\quad+[\mathcal{X}_4\odot^{3}(i\boldsymbol{k})^3]:i\boldsymbol{k}\otimes^{s}\tilde{U}_0+[\boldsymbol{\eta}_4:(i\boldsymbol{k})^2]\tilde{\boldsymbol{f}}+\boldsymbol{\xi}_4\tilde{\boldsymbol{f}}.
\end{aligned}$$

Obviously, this expression easily degenerates into the classic local asymptotic expression (3.7) in the case of $\tilde{\boldsymbol{f}} = \mathbf{0}$.

3.3.4 Effective behavior

According to the general relation Eq.(3.36), the general homogenized dynamic equation has the following form:

$$\left(iw\langle\boldsymbol{\rho}^{hom}\rangle iw - i\boldsymbol{k}\cdot\langle\mathbb{C}^{hom}\rangle\cdot i\boldsymbol{k}\right)\langle\tilde{\boldsymbol{u}}\rangle = (i\boldsymbol{k}\cdot\langle\mathbb{C}_n^{f.hom}\rangle\cdot i\boldsymbol{k} + \boldsymbol{I} - iw\langle\boldsymbol{\rho}_n^{f.hom}\rangle iw)\tilde{\boldsymbol{f}}. \quad (3.40)$$

The tensors $\mathcal{X}$, $\boldsymbol{\eta}$ and $\boldsymbol{\xi}$ of $\mathbb{C}^{hom}$ and $\boldsymbol{\rho}^{hom}$ can be obtained through periodic boundary conditions and interface continuity conditions. In addition, the zero-average conditions are given as

$$\langle\mathcal{X}_n\rangle = \mathbf{0}, \quad \langle\boldsymbol{\eta}_n\rangle = \mathbf{0}, \quad \langle\boldsymbol{\xi}_n\rangle = \mathbf{0}.$$

Rewriting the effective dynamic equation in the form $\mathcal{Z}\langle\tilde{\boldsymbol{u}}\rangle = \tilde{\boldsymbol{f}}$, then the effective impedance $\mathcal{Z}$ is calculated by

$$\mathcal{Z} = (\mathcal{Z}_n^f)^{-1}\mathcal{Z}_n$$

where $\mathcal{Z}_n$ represents the n-th asymptotic expression (3.21) of the effective impedance in the case of null volume force, and $\mathcal{Z}_n^f$ represents the n-th order asymptotic effective impedance correction factor including volume force, which is given as

$$\mathcal{Z}^f = \boldsymbol{I} + i\boldsymbol{k}\cdot\langle\mathbb{C}_n^{f.hom}\rangle\cdot i\boldsymbol{k} - iw\langle\boldsymbol{\rho}_n^{f.hom}\rangle iw.$$

3.4 Numerical example of 1D shear wave

In this section, we consider the shear wave model in the previous chapter. The three-layer model is specified by the shear modulus $G_1 = 3.0\times10^8(Pa), G_2 = 2.0\times10^{11}(Pa)$, and $G_3 = 1.0\times10^{10}(Pa)$; the mass density $\rho_1 = 1000(kg/m^3), \rho_2 = 3000(kg/m^3)$, and $\rho_3 = 900(kg/m^3)$. The size of the periodic RVE is set to $l = 0.01(m)$, and the thicknesses

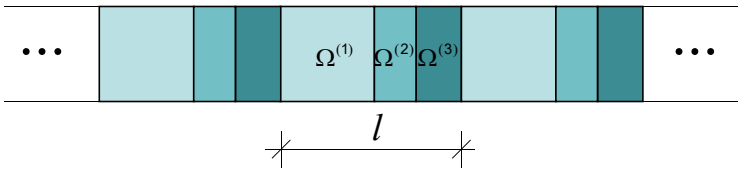

Figure 3.1: *1D three-phase layered composite model.*

of the components satisfy $\alpha_1 l : \alpha_2 l : \alpha_3 l = 0.52 : 0.23 : 0.25$. The effective expressions (3.23a) and (3.23b) can be used to solve the effective shear modulus G^{eff} and effective mass density ρ^{eff}. Of course, before that, we need to determine the tensor $\mathcal{X}_n$ based on periodic conditions and interface continuity conditions. The shear wave is governed by the local dynamic equation and constitutive relationship

$$\boldsymbol{\nabla} \cdot \tilde{\boldsymbol{\sigma}} + \tilde{f} = -w^2 \rho \tilde{u}, \quad \tilde{\boldsymbol{\sigma}} = G \boldsymbol{\nabla} \tilde{u}.$$

The solution $\tilde{\boldsymbol{u}}_n$ has the form (3.39). In this 1D case, we can rewrite the solution as

$$\tilde{u}_n = \sum_{i=0}^{n} \mathcal{X}_i (ik)^i U_{n-i} + \boldsymbol{\eta}_n (ik)^{n-2} \tilde{f} + \boldsymbol{\xi}_n (ik)^{n-4} \tilde{f},$$

where the tensors $\mathcal{X}$, $\boldsymbol{\eta}$ and $\boldsymbol{\xi}$ are degraded to scalar coefficients. As mentioned earlier, the effective dispersion relationship of the local equation depends on the results of the effective tensors $\mathbb{C}^{eff}$ and $\boldsymbol{\rho}^{eff}$. However, these effective tensors are related to the value of $\mathcal{X}$. Therefore, in the subsequent analysis, we only show the solution for $\mathcal{X}$.

3.4.1 Polynomial asymptotic expression of $\mathcal{X}_n$

According to the properties mentioned in the previous section, the tensor $\mathcal{X}_n$ should satisfy all continuity and periodic conditions. In layered case, we can try to represent $\mathcal{X}_n$ by a polynomial related to the coordinate variable $\boldsymbol{y}$. Then, we can define $\mathcal{X}_n$ (for $n \geqslant 1$, $\mathcal{X}_0 = \mathbf{1}$) as a polynomial function of order $\boldsymbol{y}^n$:

$$\begin{aligned} \mathcal{X}_1 &= \boldsymbol{a}_1^1 \boldsymbol{y} + \boldsymbol{a}_1^0, \\ &\dots \\ \mathcal{X}_n &= \boldsymbol{a}_n^n \boldsymbol{y}^n + \dots + \boldsymbol{a}_n^1 \boldsymbol{y} + \boldsymbol{a}_n^0, \end{aligned}$$

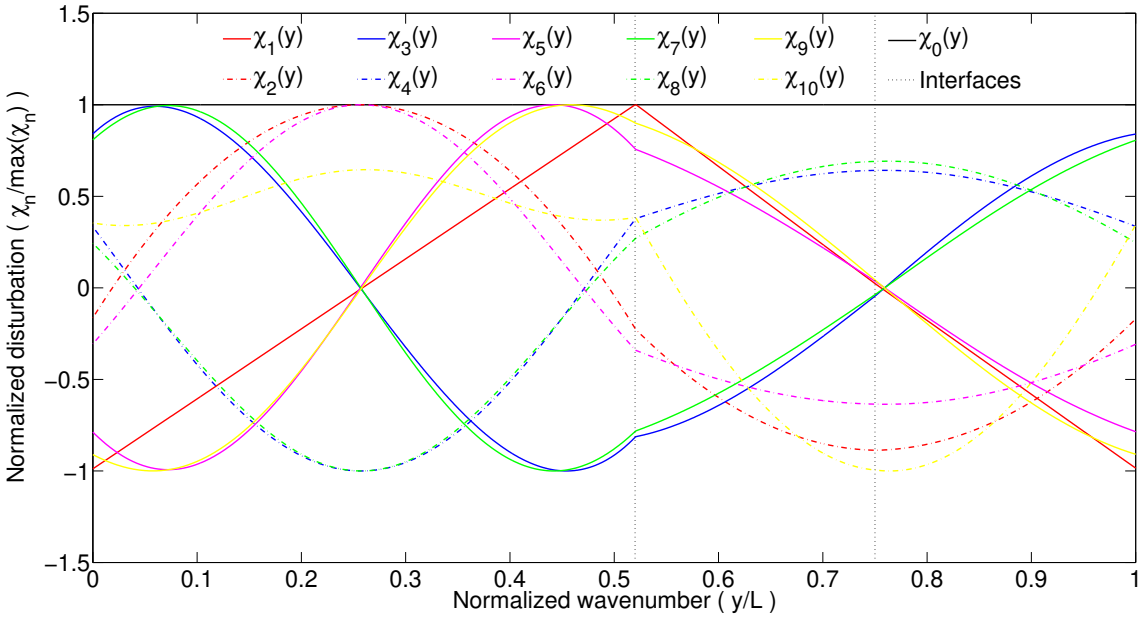

Figure 3.2: *1D polynomial approximation function $\mathcal{X}_n$ (up to order 10).*

where the polynomial coefficients $\boldsymbol{a}_n^i (i = 0, 1, ..., n)$ are the constant vectors to be determined, and the size of the vector $\boldsymbol{a}_n^i$ depends on the number of layers of the layered composite model.

In numerical applications, the magnitude of the function $\mathcal{X}_n$ differs greatly. Therefore, we consider standardizing it, that is, considering only the changing characteristics of the function. Fig.(3.2) shows the curves of each order function $\mathcal{X}_n$ in this 1D layered case. As shown by the curves, the functions $\mathcal{X}_n$ related to the local coordinate $\boldsymbol{y}$ are always continuous on each interface.

3.4.2 Dispersion relationship and effective tensors

The dispersion curve can be obtained from the zero determinant of the effective impedance $\mathcal{Z}$. As shown in Fig.(3.3), the ϵ^2 (pink line) and ϵ^4 (green line) order approximation have some reluctant results. However, as the asymptotic order increases, the high-order approximation results have an extremely good match (the maximum error is less than 0.01%) with the reference (analytical) solution (red line).

On the other hand, in order to exhibit the asymptotic error easily, we define the error

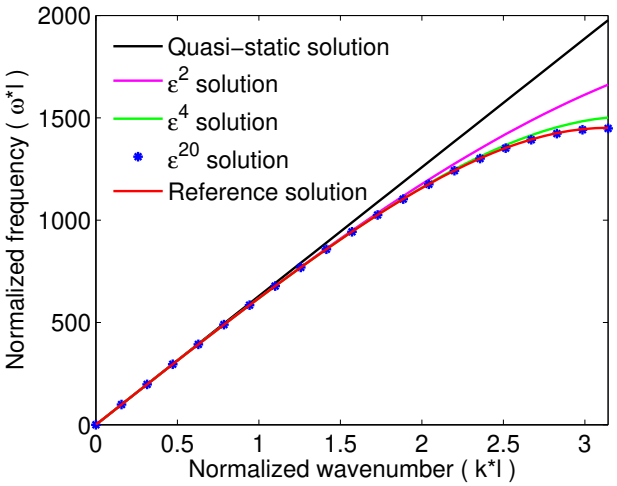

Figure 3.3: *Dispersion curves for two-scalemethod (black line for Quasi-static solution, red line for Reference solution): The asymptotic results of orders* ϵ^2, ϵ^4 *and* ϵ^{20} *are shown.*

function of the dispersion curve as

$$Err(\boldsymbol{k}, w) = \frac{||w - w_{num}||}{||w_{num}||} \times 100\%,$$

where w and w_{num} represent asymptotic and numerical results of the angular frequency when the wave number is $\boldsymbol{k}$, respectively. The maximum errors of different asymptotic orders are shown in Fig.(3.4). The maximum error of the dispersion relationship decreases quickly at the low-order epsilon and stabilizes after a small fluctuation. It is worth noting that the fluctuations in the error curve do not mean that the higher asymptotic level will have a better matching result in the higher asymptotic stage ($\epsilon^4 - \epsilon^{12}$). On the contrary, the asymptotic results in the volatility phase may have errors that cannot be ignored. After numerical verification, the fluctuation stage like that is more obvious for the high-contrast model.

According to Eqs.(3.23a) and (3.23b), the asymptotic results of G^{eff} and ρ^{eff} are shown in Fig.(3.5) under the normalized wave number (kl). The asymptotic result with a sufficient order of ϵ (about ϵ^{20}) can guarantee a good matching result with the reference solution (numerical solution determined by the finite element method).

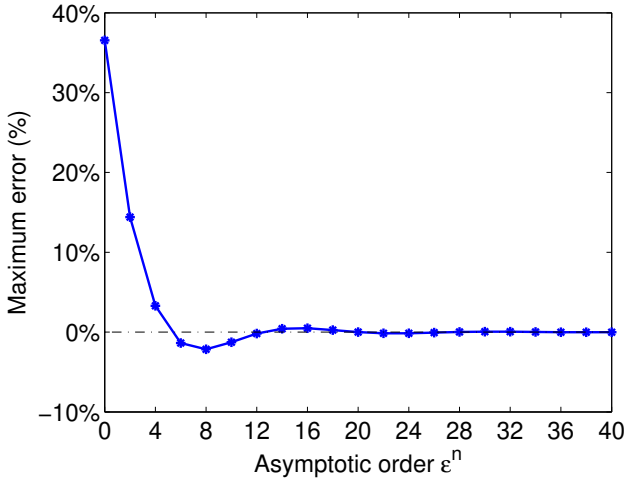

Figure 3.4: *The relationship between the maximum error of the dispersion curve and the asymptotic order ϵ.*

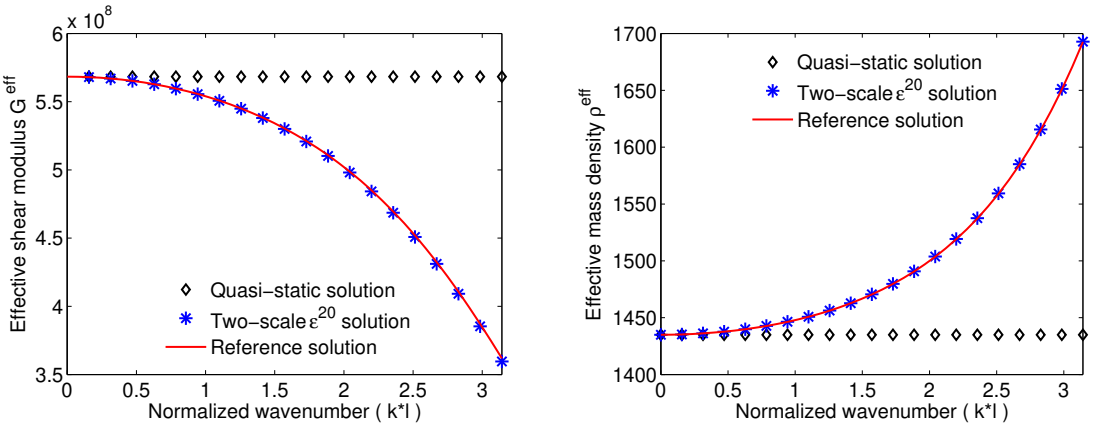

(a) (b)

Figure 3.5: *Comparison of asymptotic results for (a) effective shear modulus G^{eff} and (b) effective mass density ρ^{eff}: Quasi-static solution (black rhombus), Reference solution (red line), two-scaleasymptotic solution at ϵ^{20} order (blue asterisk).*

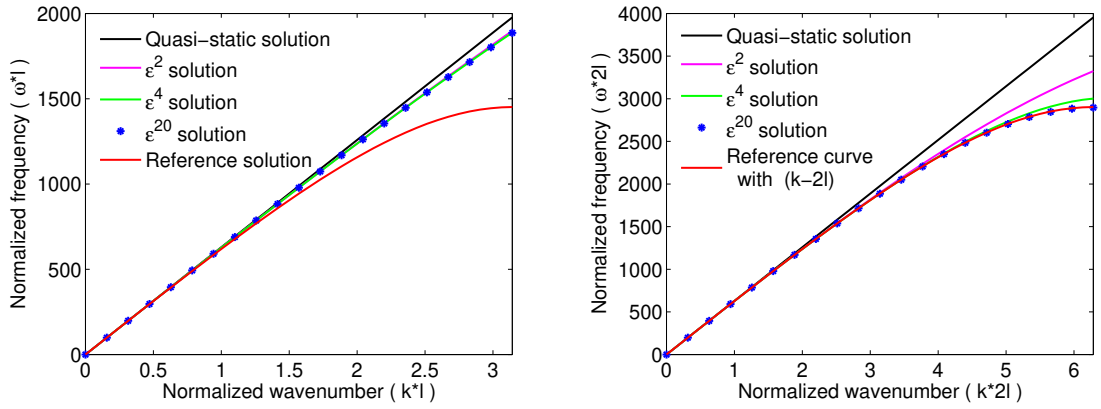

(a) (b)

Figure 3.6: *Asymptotic dispersion curves (a) and comparison of complete dispersion curves (in the double wave number range) (b) for the case of* $\epsilon = 0.5$.

3.4.3 Discussion on the small parameter ϵ

As previously described, the small parameter ϵ is defined to be the ratio of the microscopic characteristic dimension l to the macroscopic characteristic dimension L (or macroscopic wave length λ). At the same time, we know that the small parameter ϵ needs to satisfy the condition $\epsilon \leqslant 1$. In an extreme case, the smaller parameter $\epsilon = 1$ means that the characteristic dimension L is equal to the cell size l, and then the two scales ($\boldsymbol{x}$ and $\boldsymbol{y}$) will degenerate to the same scale. Under this assumption, Eq.(3.3) represents the superposition of perturbation fields of the same scale. For the general case, we define the size of the RVE as the macroscopic characteristic dimension L, and the value of ϵ can be redefined as the ratio of the size of the microscopic characteristic dimension l to the size of the RVE. Therefore, different small parameter values indicate different RVE sizes. For example, when we set $\epsilon = 0.5$, the RVE at this time is defined as two basic cells. In this case, the wave number range becomes twice the original one, that is, the normalized wave number $k * 2l \leqslant \pi$, which comes from the wave number limitation in Nassar et al. (2015). In summary, the value of the small parameter ϵ determines the degree of homogenization at the microscale, or it can determine the homogenization effect when the wavelength is greater than the representative cell size.

3.5 Conclusion

The advantage of the two-scale description is that it allows analysis of macro-scale behavior through the micro-scale description of composites. Thanks to the two-scale description of local dynamic equations and the asymptotic analysis of effective displacement fields, we obtained a general higher-order asymptotic expression of the effective impedance through the hierarchical analysis of dynamic equations. Apart from that, this general expression is verified to be applicable to any asymptotic order.

The hierarchical equations are developed based on the small parameter ϵ. The definition of the small parameter and its homogenization effect on the infinite periodic structure model are explained in this chapter. The final numerical simulation indicates that the asymptotic performance of the two-scale method in the low-order asymptotic stage (less than ϵ^{12}) is not perfect, but after a small fluctuation, the numerical results in the high-order asymptotic stage (large than ϵ^{20}) becomes extremely matched. The two-scale method borrows the asymptotic polynomial of the tensor $\mathcal{X}$, and its results do not depend on the model mesh, so its numerical calculation cost is lower than the finite element method. On the other hand, with the help of the analytical solution expressions of the layered model in chapter 1, we found that the results of the two-scale method in the higher-order asymptotic stage are even better than those of the finite element method with a sufficiently dense mesh. Unfortunately, because the current development of the two-scale method is not profound, we have not applied it to the general 2D situation for the time being. The core difficulty lies in the 2D solution of the tensor $\mathcal{X}$, which will be considered in future work.

Part II

Elastodynamic imperfect interface models for composites

Chapter 4

Elastic wave propagation through a perfect interface

This chapter mainly considers the perfect interface and uses the finite-difference time-domain method (FDTD) to carry out numerical simulations. The 2D anti-plane shear wave is taken as a prototype, and the finite difference method relies on the distribution of difference-points, which is not suitable for general interface shapes. To solve this problem, the Explicit Simplified Interface Method (ESIM) proposed in the work of Lombard & Piraux (2004) provides a good matching scheme.

4.1 Interface conditions

4.1.1 Interface geometry

A smooth surface $\mathcal{S}$ in a three-dimensional Euclidean space $\mathbb{R}^3$ can be defined as a zero-level set of the function $F(\boldsymbol{x})$ with $\boldsymbol{x} = (x, y, z) \in \mathbb{R}^3$:

$$\mathcal{S} = \{\boldsymbol{x} \in \mathbb{R}^3 | F(\boldsymbol{x}) = 0\}.$$

Taking a point $\boldsymbol{x} = (x_0, y_0, z_0)$ on the surface, the curve $\Gamma(x, y, z)$ passing the point $\boldsymbol{x}$ satisfies

$$x = f_1(t), \quad y = f_2(t), \quad z = f_3(t),$$

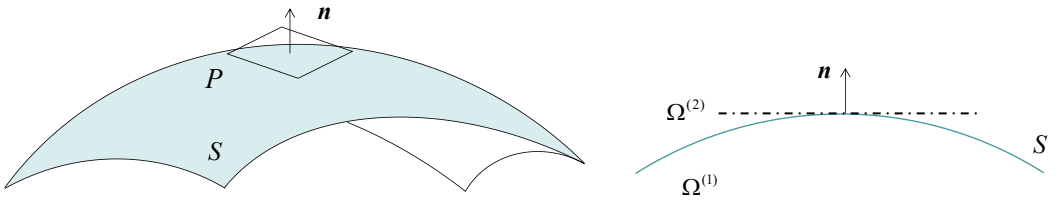

(a) 3D smooth surface model (b) 2D interface section

Figure 4.1: *(a) Let $\boldsymbol{x}$ be a point on the smooth surface $\mathcal{S}$, where $\mathcal{P}$ and $\boldsymbol{n}$ are the tangent plane and outer normal. (b) Consider $\mathcal{S}$ being the interface of media $\Omega^{(1)}$ and $\Omega^{(2)}$ in plane (e_1, e_2).*

where f_1, f_2 and f_3 represent three functions that satisfy $F(f_1(t), f_2(t), f_3(t)) = 0$, and t is the variable corresponding to the point on the curve Γ. There are $x_0 = f_1(t_0), y_0 = f_2(t_0)$ and $z_0 = f_3(t_0)$. Let $\mathcal{P}$ be the tangent plane of the smooth surface $\mathcal{S}$ at position $\boldsymbol{x}$, the expression of the tangent plane $\mathcal{P}(\boldsymbol{x})$ reads

$$F_x(x_0, y_0, z_0)(x - x_0) + F_y(x_0, y_0, z_0)(y - y_0) + F_z(x_0, y_0, z_0)(z - z_0) = 0.$$

In addition, the normal vector $\boldsymbol{n}$ and the tangent vector $\boldsymbol{t}$ at the point $\boldsymbol{x}$ are

$$\boldsymbol{n}(\boldsymbol{x}) = \frac{(F_x(\boldsymbol{x}), F_y(\boldsymbol{x}), F_z(\boldsymbol{x}))}{||\,(F_x(\boldsymbol{x}), F_y(\boldsymbol{x}), F_z(\boldsymbol{x}))\,||}\Big|_{\boldsymbol{x}=(x_0,y_0,z_0)}, \quad \boldsymbol{t}(\boldsymbol{x}) = \frac{(f_1'(t), f_2'(t), f_3'(t))}{||\,(f_1'(t), f_2'(t), f_3'(t))\,||}\Big|_{t=t_0},$$

where $F_x = \frac{\partial F}{\partial x}$, and same operations as F_y and F_z.

4.1.2 Two orthogonal projection operators

For any smooth interface or surface, we can introduce two orthogonal projection operators associated with the normal vector $\boldsymbol{n}(\boldsymbol{x})$, which are defined as

$$\boldsymbol{N} = \boldsymbol{n} \otimes \boldsymbol{n}, \quad \boldsymbol{T} = \boldsymbol{I} - \boldsymbol{n} \otimes \boldsymbol{n},$$

where $\boldsymbol{I}$ stands for the second-order identity tensor, $\boldsymbol{N}$ and $\boldsymbol{T}$ represent the normal and tangent projection operators, respectively.

Next, we consider $\varphi(\boldsymbol{x})$ is a scalar function and $\boldsymbol{\phi}(\boldsymbol{x})$ is a continuously differentiable

vector function. Their gradient fields admit the following decompositions

$$\boldsymbol{\nabla}\varphi = \boldsymbol{\nabla}\varphi(\boldsymbol{N}+\boldsymbol{T}) \equiv \boldsymbol{\nabla}_n\varphi + \boldsymbol{\nabla}_t\varphi, \quad \boldsymbol{\nabla}\boldsymbol{\phi} = \boldsymbol{\nabla}\boldsymbol{\phi}(\boldsymbol{N}+\boldsymbol{T}) \equiv \boldsymbol{\nabla}_n\boldsymbol{\phi} + \boldsymbol{\nabla}_t\boldsymbol{\phi},$$

where the operator $\boldsymbol{\nabla}_n$ and $\boldsymbol{\nabla}_t$ are defined as the normal derivative operator and tangent derivative operator. The normal derivatives are defined by

$$\boldsymbol{\nabla}_n\varphi \equiv (\boldsymbol{\nabla}\varphi)\boldsymbol{N} = (\boldsymbol{\nabla}\varphi\cdot\boldsymbol{n})\boldsymbol{n}, \quad \boldsymbol{\nabla}_n\boldsymbol{\phi} \equiv (\boldsymbol{\nabla}\boldsymbol{\phi}) : \boldsymbol{N} = (\boldsymbol{\nabla}\boldsymbol{\phi}\cdot\boldsymbol{n})\boldsymbol{n}.$$

Similarly, the divergence fields of $\boldsymbol{\phi}(\boldsymbol{x})$ and the tensor function $\boldsymbol{\tau}(\boldsymbol{x})$ can be decomposed as follows :

$$\boldsymbol{\nabla}\cdot\boldsymbol{\phi} = \boldsymbol{\nabla}\boldsymbol{\phi} : (\boldsymbol{N}+\boldsymbol{T}) \equiv \boldsymbol{\nabla}_n\cdot\boldsymbol{\phi} + \boldsymbol{\nabla}_t\cdot\boldsymbol{\phi}, \quad \boldsymbol{\nabla}\cdot\boldsymbol{\tau} = \boldsymbol{\nabla}\boldsymbol{\tau} : (\boldsymbol{N}+\boldsymbol{T}) \equiv \boldsymbol{\nabla}_n\cdot\boldsymbol{\tau} + \boldsymbol{\nabla}_t\cdot\boldsymbol{\tau},$$

where

$$\boldsymbol{\nabla}_n\cdot\boldsymbol{\phi} \equiv \boldsymbol{\nabla}\boldsymbol{\phi} : \boldsymbol{N} = \boldsymbol{\nabla}(\boldsymbol{\phi}\cdot\boldsymbol{n})\boldsymbol{n}, \quad \boldsymbol{\nabla}_n\cdot\boldsymbol{\tau} \equiv \boldsymbol{\nabla}\boldsymbol{\tau} : \boldsymbol{N} = \boldsymbol{\nabla}(\boldsymbol{\tau}\cdot\boldsymbol{n})\boldsymbol{n}.$$

Let $\boldsymbol{\Omega}^{(1)}$ and $\boldsymbol{\Omega}^{(2)}$ are the two sub-domains separated by $\mathcal{S}$. Considering a vector function $\boldsymbol{\phi}(\boldsymbol{x})$ with $(\boldsymbol{x}\in\mathcal{S})$ is continuous across $\mathcal{S}$:

$$\boldsymbol{\phi}^{(1)}(\boldsymbol{x}) = \boldsymbol{\phi}^{(2)}(\boldsymbol{x}),$$

where the superscript $(\cdot)^{(1)}$ and $(\cdot)^{(2)}$ represent the value in the sub-domain $\boldsymbol{\Omega}^{(1)}$ and $\boldsymbol{\Omega}^{(2)}$. The Hadamard relationship gives

$$\boldsymbol{\nabla}\boldsymbol{\phi}^{(2)}(\boldsymbol{x}) - \boldsymbol{\nabla}\boldsymbol{\phi}^{(1)}(\boldsymbol{x}) = \boldsymbol{\alpha}\otimes\boldsymbol{n}, \quad \boldsymbol{\nabla}\cdot\boldsymbol{\phi}^{(2)}(\boldsymbol{x}) - \boldsymbol{\nabla}\cdot\boldsymbol{\phi}^{(1)}(\boldsymbol{x}) = \boldsymbol{\alpha}\cdot\boldsymbol{n}.$$

where $\boldsymbol{\alpha}$ is a constant vector generally different from $\boldsymbol{0}$, $\boldsymbol{n}$ is the outer normal vector of $\mathcal{S}$. It follows from the Hadamard relation that

$$\boldsymbol{\nabla}_t\boldsymbol{\phi}^{(1)}(\boldsymbol{x}) = \boldsymbol{\nabla}_t\boldsymbol{\phi}^{(2)}(\boldsymbol{x}), \quad \boldsymbol{\nabla}_t\cdot\boldsymbol{\phi}^{(1)}(\boldsymbol{x}) = \boldsymbol{\nabla}_t\cdot\boldsymbol{\phi}^{(2)}(\boldsymbol{x}). \tag{4.1}$$

4.1.3 Continuous conditions for the perfect interface

Taking a 3D elasticity problem as an example, we denote the displacement field and the stress field as $\boldsymbol{u}$ and $\boldsymbol{\sigma}$, respectively. The following continuity conditions are met on the perfect interface $\mathcal{S}$ at the point $\boldsymbol{x}$:

$$\boldsymbol{u}^{(1)}(\boldsymbol{x}) = \boldsymbol{u}^{(2)}(\boldsymbol{x}), \quad \boldsymbol{\nabla u}^{(1)}(\boldsymbol{x}) \cdot \boldsymbol{T} = \boldsymbol{\nabla u}^{(2)}(\boldsymbol{x}) \cdot \boldsymbol{T}, \quad \boldsymbol{\sigma}^{(1)}(\boldsymbol{x}) \cdot \boldsymbol{N} = \boldsymbol{\sigma}^{(2)}(\boldsymbol{x}) \cdot \boldsymbol{N},$$

where the superscript indicate the physical fields in the media $\boldsymbol{\Omega}^{(1)}$ and $\boldsymbol{\Omega}^{(2)}$ on both sides of the interface $\mathcal{S}$. In a 3D elastic case with the base vectors $(\boldsymbol{e}_1, \boldsymbol{e}_2, \boldsymbol{e}_3)$, the displacement field is given as $\boldsymbol{u}(\boldsymbol{x}) = u_1(\boldsymbol{x})\boldsymbol{e}_1 + u_2(\boldsymbol{x})\boldsymbol{e}_2 + u_3(\boldsymbol{x})\boldsymbol{e}_3$, and the gradient operator is written as $\boldsymbol{\nabla} = (\frac{\partial}{\partial x}, \frac{\partial}{\partial y}, \frac{\partial}{\partial z})$. When we set the normal vector at the point $\boldsymbol{x} \in \mathcal{S}$ to $\boldsymbol{n}(\boldsymbol{x}) = (1, 0, 0)$, there exist the continuity conditions:

$$\begin{bmatrix} 0 & u_{2,1}^{(1)} & u_{3,1}^{(1)} \\ 0 & u_{2,2}^{(1)} & u_{3,2}^{(1)} \\ 0 & u_{2,3}^{(1)} & u_{3,3}^{(1)} \end{bmatrix} = \begin{bmatrix} 0 & u_{2,1}^{(2)} & u_{3,1}^{(2)} \\ 0 & u_{2,2}^{(2)} & u_{3,2}^{(2)} \\ 0 & u_{2,3}^{(2)} & u_{3,3}^{(2)} \end{bmatrix}, \quad \begin{bmatrix} \sigma_{11}^{(1)} & 0 & 0 \\ \sigma_{21}^{(1)} & 0 & 0 \\ \sigma_{31}^{(1)} & 0 & 0 \end{bmatrix} = \begin{bmatrix} \sigma_{11}^{(2)} & 0 & 0 \\ \sigma_{21}^{(2)} & 0 & 0 \\ \sigma_{31}^{(2)} & 0 & 0 \end{bmatrix},$$

where $(u_{,1}, u_{,2}, u_{,3})$ represents the partial derivative operator $(\frac{\partial u}{\partial x}, \frac{\partial u}{\partial y}, \frac{\partial u}{\partial z})$, and σ_{ij} are components of $\boldsymbol{\sigma}$ with $(i, j = 1, 2, 3)$. According to the the small strain hypothesis $\boldsymbol{\varepsilon} = \frac{1}{2}(\boldsymbol{\nabla u} + \boldsymbol{\nabla}^T \boldsymbol{u})$ and the symmetry property of stress field $\boldsymbol{\sigma} = \boldsymbol{\sigma}^T$, the continuity conditions of the point $\boldsymbol{x}$ for $(\boldsymbol{x} \in \mathcal{S})$ can also be expressed as

$$\begin{bmatrix} 0 & 0 & 0 \\ 0 & \varepsilon_{22}^{(1)} & \varepsilon_{32}^{(1)} \\ 0 & \varepsilon_{23}^{(1)} & \varepsilon_{33}^{(1)} \end{bmatrix} = \begin{bmatrix} 0 & 0 & 0 \\ 0 & \varepsilon_{22}^{(2)} & \varepsilon_{32}^{(2)} \\ 0 & \varepsilon_{23}^{(2)} & \varepsilon_{33}^{(2)} \end{bmatrix}, \quad \begin{bmatrix} \sigma_{11}^{(1)} & \sigma_{12}^{(1)} & \sigma_{12}^{(1)} \\ \sigma_{21}^{(1)} & 0 & 0 \\ \sigma_{31}^{(1)} & 0 & 0 \end{bmatrix} = \begin{bmatrix} \sigma_{11}^{(2)} & \sigma_{12}^{(2)} & \sigma_{12}^{(2)} \\ \sigma_{21}^{(2)} & 0 & 0 \\ \sigma_{31}^{(2)} & 0 & 0 \end{bmatrix}.$$

4.1.4 Jump conditions for the imperfect interfaces

In the above elasticity problem, the continuity conditions given by the perfect interface $\mathcal{S}$ can be summarized as the continuity of the displacement field $\boldsymbol{u}$ and traction vector $\boldsymbol{\tau} = \boldsymbol{\sigma} \cdot \boldsymbol{n}$ (the normal component of the stress field). We denote the difference between the physical fields on both sides of the interface as $[[\boldsymbol{u}]]$ and $[[\boldsymbol{\tau}]]$, that is, $[[\boldsymbol{u}]] = \boldsymbol{u}^{(2)} - \boldsymbol{u}^{(1)}$ and $[[\boldsymbol{\tau}]] = \boldsymbol{\tau}^{(2)} - \boldsymbol{\tau}^{(1)}$, where the superscripts (1) and (2) indicate the physical fields of the

materials on both sides. Then, the continuity conditions provided by the perfect interface can be expressed as $[[\boldsymbol{u}]] = \mathbf{0}$ and $[[\boldsymbol{\tau}]] = \mathbf{0}$. Conversely, the imperfect interface does not provide continuity for both fields, i.e. $[[\boldsymbol{u}]] \neq 0$ or/and $[[\boldsymbol{\tau}]] \neq \mathbf{0}$. It is worth discussing two extreme imperfect interfaces: *the spring-layer model* and *the interface stress model*. The first spring-layer model allows the traction vector to be continuous at the interface ($[[\boldsymbol{\tau}]] = \mathbf{0}$), while the displacement field has a jump relationship ($[[\boldsymbol{u}]] \neq \mathbf{0}$) that is linear with the traction vectors on both sides of the interface. The second interface stress model defines that the displacement field is continuous at the interface ($[[\boldsymbol{u}]] = \mathbf{0}$), but the traction vector has a discontinuous jump relationship ($[[\boldsymbol{\tau}]] \neq \mathbf{0}$) and satisfies the Young-Laplace equation.

4.2 Reflection coefficient $\mathcal{R}$ and transmission coefficient $\mathcal{T}$

In this section, we discussed the amplitudes of the reflected and transmitted waves on both sides of the perfect interface, namely the reflection coefficient $\mathcal{R}$ and the transmission coefficient $\mathcal{T}$. Take an anti-shear plane wave (the SH wave) in the 2D plane (x, y) as an example, and let $u(x, y, t)$ be the propagation solution of the dynamic equation in the homogeneous medium, the dynamic equation reads

$$\boldsymbol{\nabla} \cdot \boldsymbol{\sigma} = \rho \ddot{u}, \quad \boldsymbol{\sigma} = G \boldsymbol{\nabla} u, \tag{4.2}$$

where the double dot symbol represents the second derivative of time. In the frequency domain, the harmonic wave equation reads

$$\boldsymbol{\nabla} \cdot \boldsymbol{\sigma} = -w^2 \rho u, \quad \boldsymbol{\sigma} = G \boldsymbol{\nabla} u,$$

where w is the angular frequency. The wave number gives $k = w/c$ and the wave velocity is $c = \sqrt{G/\rho}$. The harmonic displacement solution $u(x, y, t)$ can be split into a time dependence part e^{-iwt} (the time dependence part will be omitted in the following discussion) and a wave number dependence part $e^{ik(x,y)}$.

4.2.1 Single perfect interface model

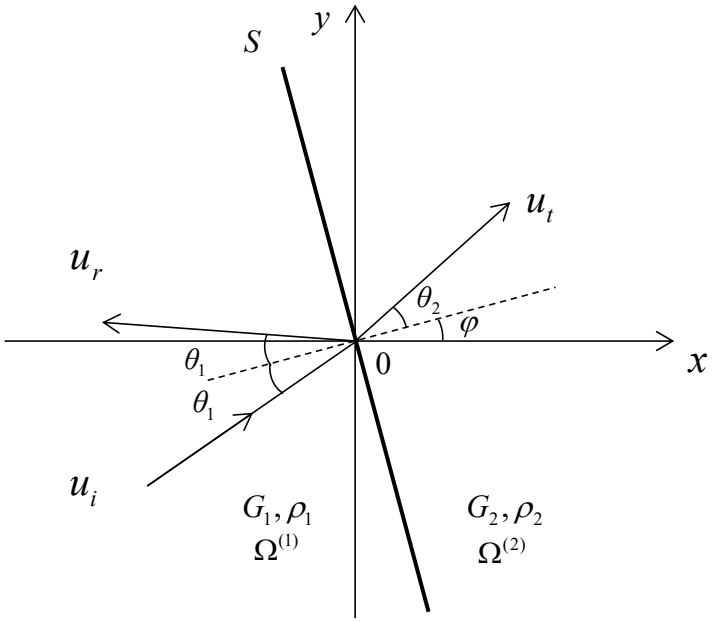

Figure 4.2: *A simple bi-phase interface model contains two media $\Omega^{(1)}$ (G_1, ρ_1) and $\Omega^{(2)}$ (G_2, ρ_2). The interface $\mathcal{S}$ has an angle φ. The incident, reflected wave in $\Omega^{(1)}$ and the transmitted wave in $\Omega^{(2)}$ are denoted as u_i, u_r and u_t, respectively.*

We first consider the single perfect interface model shown in Fig.(4.2), which contains two semi-infinite matrices $\Omega^{(1)}$, $\Omega^{(2)}$ and a perfect interface $\mathcal{S}$ with an angle φ. The normal and tangent vectors of the interface $\mathcal{S}$ are $\boldsymbol{n} = (cos(\varphi), sin(\varphi))$ and $\boldsymbol{t} = (-sin(\varphi), cos(\varphi))$. Setting the shear modulus (G_1, G_2) and the mass density (ρ_1, ρ_2) for each media $(\Omega^{(1)}, \Omega^{(2)})$. The incident wave u_i and the reflected wave u_r (with the reflection coefficient $\mathcal{R}$) in the medium $\Omega^{(1)}$ and the transmitted wave u_t (with the transmission coefficient $\mathcal{T}$) in the medium $\Omega^{(2)}$ can be respectively represented as

$$
\begin{aligned}
u_i &= e^{ik_1 cos(\theta_1+\varphi)x + ik_1 sin(\theta_1+\varphi)y}, \\
u_r &= \mathcal{R} e^{-ik_1 cos(\theta_1-\varphi)x + ik_1 sin(\theta_1-\varphi)y}, \\
u_t &= \mathcal{T} e^{ik_2 cos(\theta_2+\varphi)x + ik_2 sin(\theta_2+\varphi)y},
\end{aligned}
$$

where θ_1 indicates the angle of incidence and reflection in $\Omega^{(1)}$, and θ_2 represent the transmission angle in $\Omega^{(2)}$. Snell's law gives the relationship $k_1 sin(\theta_1) = k_2 sin(\theta_2)$.

According to the continuous conditions of the perfect interface $[[u]] = 0$ and $[[\tau]] = 0$, It is easy to get the reflection coefficient $\mathcal{R}$ and transmission coefficient $\mathcal{T}$ of the wave

propagating from the medium $\Omega^{(1)}$ to the medium $\Omega^{(2)}$ as

$$\mathcal{R} = \frac{\eta_1 cos(\theta_1) - \eta_2 cos(\theta_2)}{\eta_1 cos(\theta_1) + \eta_2 cos(\theta_2)}, \quad \mathcal{T} = \frac{2\eta_1 cos(\theta_1)}{\eta_1 cos(\theta_1) + \eta_2 cos(\theta_2)},$$

where η represents the impedance, defined as $\eta_i = \sqrt{G_i \rho_i}$ for $(i = 1, 2)$.

4.2.2 Double perfect interface model

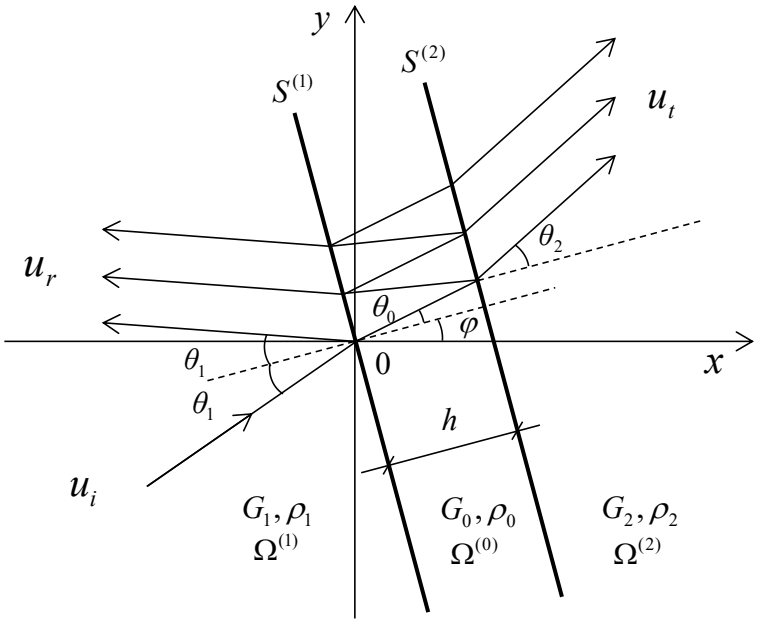

Figure 4.3: *A simple thin interphase layer model contains a thin layer $\Omega^{(0)}$ (G_0, ρ_0) with a small thickness h . The parallel interfaces $\mathcal{S}^1$ and $\mathcal{S}^2$ have an angle φ. The incident, reflected wave in $\Omega^{(1)}$ (G_1, ρ_1) and the transmitted wave in $\Omega^{(2)}$ (G_2, ρ_2) are denoted as u_i, u_r and u_t, respectively.*

Next, we consider a double perfect interface model shown in Fig.(4.3), which contains two semi-infinite matrices $\Omega^{(1)}$, $\Omega^{(2)}$ and a homogeneous interphase layer $\Omega^{(0)}$ with the thickness h. The parallel interfaces $\mathcal{S}^{(1)}$ and $\mathcal{S}^{(2)}$ have an angle φ. Similar to the single interface model, the normal and tangent vectors are the same. The incident wave u_1, the reflected wave u_r and the transmitted wave u_t can be expressed as

$$\begin{aligned} u_i &= e^{ik_1 cos(\theta_1+\varphi)x + ik_1 sin(\theta_1+\varphi)y}, \\ u_r &= \mathcal{R} e^{i\Delta\Phi_1 - ik_1 cos(\theta_1-\varphi)x + ik_1 sin(\theta_1-\varphi)y}, \\ u_t &= \mathcal{T} e^{ik_0 cos(\theta_0)h} e^{i\Delta\Phi_4 + ik_2 cos(\theta_2+\varphi)x + ik_2 sin(\theta_2+\varphi)y}, \end{aligned} \tag{4.3}$$

where θ_1 indicates the angle of incidence and reflection in $\Omega^{(1)}$, and θ_0 and θ_2 represent the transmission angle in $\Omega^{(0)}$ and $\Omega^{(2)}$, respectively. Snell's law gives the relationship $k_1 sin(\theta_1) = k_0 sin(\theta_0) = k_2 sin(\theta_2)$. In the above expressions, $\Delta\Phi_1$ and $\Delta\Phi_4$ are two supplementary terms. They make the reflected and transmitted waves meet the phase-matching condition at two perfect interfaces (*the waves must have the same phase when passing through a perfect interface*).

Multiple reflections of waves between two perfect interfaces

When the incident wave (u_i) reaches the left interface $\mathcal{S}^{(1)}$ for the first time, it will generate reflected wave ($u_{Lr}^{(1)}$) and transmitted wave ($u_{Lt}^{(1)}$), and then the transmitted wave ($u_{Lt}^{(1)}$) reaches the right interface $\mathcal{S}^{(2)}$ for the first time, it will also generate reflected wave ($u_{Rr}^{(1)}$) and transmitted wave ($u_{Rt}^{(1)}$). In this process, the wave reaches the left and right interfaces for the first time, which we record the superscript as $n = 1$. The superscript (n) indicates that the incident wave reaches the interface for the n-th time after being transmitted or refracted. Then the reflected wave ($u_{Rr}^{(1)}$) will return to the left interface to be reflected and transmitted again, and so on (see Fig.(4.4)).

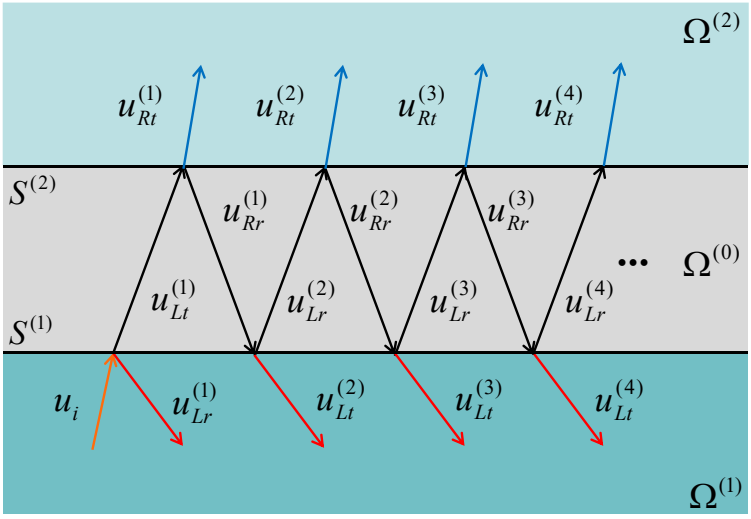

Figure 4.4: *A simple double interface model. The incident wave u_i passes through the two interfaces $\mathcal{S}^{(1)}$ and $\mathcal{S}^{(2)}$ from bottom to top, $u_{Lr}^{(1)}$ and $u_{Lt}^{(n)}$ $(n \geqslant 2)$ generated through the interface $\mathcal{S}^{(1)}$ constitute the reflected wave u_r, and $u_{Rt}^{(n)}$ $(n \geqslant 1)$ through the interface $\mathcal{S}^{(2)}$ constitute the transmitted wave u_t.*

Set the coordinates of the points where the waves reach the interfaces $\mathcal{S}^{(1)}$ and $\mathcal{S}^{(2)}$ are $O_L^{(n)}$ and $O_R^{(n)}$ (with the initial point (x_1, y_1)), their expressions related to n can be

determined as

$$O_L^{(n)} = (x_1 + 2(n-1)\Delta x, y_1 + 2(n-1)\Delta y),$$
$$O_R^{(n)} = (x_2 + (2n-1)\Delta x, y_2 + (2n-1)\Delta y),$$

where the coordinates satisfy $x_2 = x_1 + hcos(\varphi)$ and $y_2 = y_1 + hsin(\varphi)$, and the differential distances are defined as $\Delta x = -htan(\theta_0)sin(\varphi)$ and $\Delta y = htan(\theta_0)cos(\varphi)$. The reflection and transmission coefficients of the perfect interface $\mathcal{S}^{(1)}$ (medium $\Omega^{(1)}$, $\Omega^{(0)}$) and $\mathcal{S}^{(2)}$ (medium $\Omega^{(0)}$, $\Omega^{(2)}$) are given as

$$\mathcal{R}_{10} = \frac{\eta_1 cos(\theta_1) - \eta_0 cos(\theta_0)}{\eta_1 cos(\theta_1) + \eta_0 cos(\theta_0)}, \quad \mathcal{T}_{10} = \frac{2\eta_1 cos(\theta_1)}{\eta_1 cos(\theta_1) + \eta_0 cos(\theta_0)},$$
$$\mathcal{R}_{02} = \frac{\eta_0 cos(\theta_0) - \eta_2 cos(\theta_2)}{\eta_0 cos(\theta_0) + \eta_2 cos(\theta_2)}, \quad \mathcal{T}_{02} = \frac{2\eta_0 cos(\theta_0)}{\eta_0 cos(\theta_0) + \eta_2 cos(\theta_2)}.$$

Among them, the reflection coefficient satisfies $\mathcal{R}_{10} = -\mathcal{R}_{01}$. At the same time, the relationships $1 + \mathcal{R}_{10} = \mathcal{T}_{10}$ and $1 + \mathcal{R}_{02} = \mathcal{T}_{02}$ are automatically satisfied.

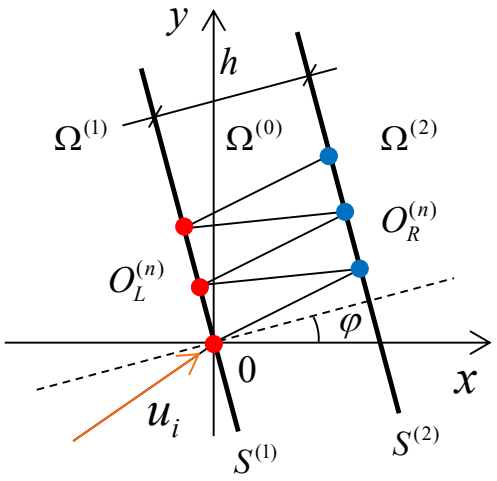

Figure 4.5: *The points $O_L^{(n)}$ (red dots) and $O_R^{(n)}$ (blue dots) when the incident wave u_i passing through the interfaces $\mathcal{S}^{(1)}$ and $\mathcal{S}^{(2)}$.*

Supplementary terms $\Delta\Phi_1$ and $\Delta\Phi_4$

Firstly, we consider the case of $n = 1$, the incident wave $u_i = e^{ik_1\mathcal{F}(\theta_1+\varphi,x,y)}$, which has

the definition $\mathcal{F}(\theta_1+\varphi,x,y)=cos(\theta_1+\varphi)x+sin(\theta_1+\varphi)y$. On the left interface, we have

$$u_{Lr}^{(1)}(x_1,y_1)=\mathcal{R}_{10}e^{ik_1\mathcal{F}(\theta_1-\varphi,-x_1,y_1)+i\Delta\phi_1},\quad u_{Lt}^{(1)}(x_1,y_1)=\mathcal{T}_{10}e^{ik_0\mathcal{F}(\theta_0+\varphi,x_1,y_1)+i\Delta\phi_2}.$$

Considering the phase-matching condition of $u_{Lr}^{(1)}$ and $u_{Lt}^{(1)}$, it is easy to get

$$\begin{aligned}\Delta\phi_1&=k_1\mathcal{F}(\theta_1+\varphi,x_1,y_1)-k_1\mathcal{F}(\theta_1-\varphi,-x_1,y_1),\\ \Delta\phi_2&=k_1\mathcal{F}(\theta_1+\varphi,x_1,y_1)-k_0\mathcal{F}(\theta_0+\varphi,x_1,y_1).\end{aligned}$$

When the transmitted wave $u_{Lt}^{(1)}$ reaches the right interface, we have

$$u_{Rr}^{(1)}(x_2)=\mathcal{T}_{10}\mathcal{R}_{02}e^{ik_0\mathcal{F}(\theta_0-\varphi,-x_2,y_2)+i\Delta\phi_3},\quad u_{Rt}^{(1)}(x_2)=\mathcal{T}_{10}\mathcal{T}_{02}e^{ik_2\mathcal{F}(\theta_2+\varphi,x_2,y_2)+i\Delta\phi_4},$$

where the supplementary items $\Delta\phi_3$ and $\Delta\phi_4$ satisfy

$$\begin{aligned}\Delta\phi_3&=k_1\mathcal{F}(\theta_1+\varphi,x_1,y_1)+k_0\mathcal{F}(\theta_0-\varphi,x_2,-y_2)+k_0hcos(\varphi),\\ \Delta\phi_4&=k_1\mathcal{F}(\theta_1+\varphi,x_1,y_1)-k_2\mathcal{F}(\theta_2+\varphi,x_2,y_2)+k_0hcos(\varphi).\end{aligned}$$

And then, the reflected wave $u_{Rr}^{(1)}$ returns to the left interface for the case of $n=2$.

Finally, the general expressions of reflected and transmitted waves for $n\geqslant 2$ can be determined as

$$\begin{aligned}u_{Lt}^{(n)}(x_1)&=\mathcal{T}_{10}\mathcal{R}_{02}(\mathcal{R}_{02}\mathcal{R}_{01})^{n-2}\mathcal{T}_{01}e^{ik_1\mathcal{F}(\theta_1-\varphi,-x_1,y_1)+i\Delta\phi_{4n-2}},\\ u_{Rt}^{(n)}(x_2)&=\mathcal{T}_{10}(\mathcal{R}_{02}\mathcal{R}_{01})^{n-1}\mathcal{T}_{02}e^{ik_2\mathcal{F}(\theta_2+\varphi,x_2,y_2)+i\Delta\phi_{4n}},\end{aligned}$$

where $\Delta\phi_{4n-2}$ and $\Delta\phi_{4n}$ satisfy

$$\begin{aligned}\Delta\phi_{4n-2}&=k_1\mathcal{F}(\theta_1+\varphi,x_1,y_1)-k_1\mathcal{F}(\theta_1-\varphi,-x_1,y_1)+2(n-1)k_0cos(\theta_0)h,\\ \Delta\phi_{4n}&=k_1\mathcal{F}(\theta_1+\varphi,x_1,y_1)-k_2\mathcal{F}(\theta_2+\varphi,x_2,y_2)+(2n-1)k_0cos(\theta_0)h.\end{aligned}$$

Coefficients $\mathcal{R}$ and $\mathcal{T}$

Integrate all the reflected waves $u_r(x,y)$ ($(x,y) \in \Omega^{(1)}$) to get

$$\begin{aligned} u_r(x,y) &= \sum_{n=1}^{N} u_r^{(n)}(x) \\ &= \left[\mathcal{R}_{01} + \left(\sum_{n=2}^{N} \left(\mathcal{R}_{02}\mathcal{R}_{01} e^{2ik_0 cos(\theta_0)h} \right)^{n-2} \right) \mathcal{T}_{10}\mathcal{R}_{02}\mathcal{T}_{01} e^{2ik_0 cos(\theta_0)h} \right] e^{ik_1 \mathcal{F}(\theta_1 - \varphi, -x, y) + i\Delta\Phi_1}, \end{aligned} \tag{4.4}$$

where $\Delta\Phi_1 = \Delta\phi_1$. And the superposition of transmitted waves $u_t(x,y)$ ($(x,y) \in \Omega^{(2)}$) can be expressed as

$$\begin{aligned} u_t(x,y) &= \sum_{n=1}^{N} u_t^{(n)}(x) \\ &= \left[\left(\sum_{n=1}^{N} \left(\mathcal{R}_{02}\mathcal{R}_{01} e^{2ik_0 cos(\theta_0)h} \right)^{n-1} \right) \mathcal{T}_{10}\mathcal{T}_{02} e^{ik_0 cos(\theta_0)h} \right] e^{ik_2 \mathcal{F}(\theta_2 + \varphi, x, y) + i\Delta\Phi_4}, \end{aligned} \tag{4.5}$$

where $\Delta\Phi_4 = \Delta\phi_4 - k_0 h cos(\theta_0)$. The analytical reflection coefficient $\mathcal{R}$ and transmission coefficient $\mathcal{T}$ are finally determined as

$$\mathcal{R} = \mathcal{R}_{10} + \alpha(N-1)\mathcal{T}_{10}\mathcal{R}_{02}\mathcal{T}_{01} e^{2ik_0 cos(\theta_0)h}, \quad \mathcal{T} = \alpha(N)\mathcal{T}_{10}\mathcal{T}_{02} e^{ik_0 cos(\theta_0)h}, \tag{4.6}$$

where the coefficient α depends on the number of times the waves crosses the left or right interface, denoted as N. The expression of α is given as

$$\alpha(0) = 0, \quad \alpha(N) = \sum_{n=1}^{N} (\mathcal{R}_{02}\mathcal{R}_{01} e^{2ik_0 cos(\theta_0)h})^{n-1}, \quad N \in \mathbb{N}^*.$$

Considering the geometric sequence expression of the analytical solution, when N is large enough, we can get the approximate expression

$$\alpha(N) = \sum_{n=1}^{N} (\mathcal{R}_{02}\mathcal{R}_{01} e^{2ik_0 cos(\theta_0)h})^{n-1} \approx \frac{1}{1 - \mathcal{R}_{02}\mathcal{R}_{01} e^{2ik_0 cos(\theta_0)h}},$$

where the condition $|\mathcal{R}_{02}\mathcal{R}_{01} e^{2ik_0 cos(\theta_0)h}| < 1$ must be guaranteed. Without loss of generality, for a small thickness h of the interphase layer (less than $\lambda_0/4$ wavelength in the medium $\Omega^{(0)}$) according to the Euler' formula. Then, the approximate reflection coefficient

$\mathcal{R}$ and transmission coefficient $\mathcal{T}$ can be derived as

$$\mathcal{R} = \mathcal{R}_{10} + \frac{\mathcal{T}_{10}\mathcal{R}_{02}\mathcal{T}_{01}e^{2ik_0cos(\theta_0)h}}{1-\mathcal{R}_{02}\mathcal{R}_{01}e^{2ik_0cos(\theta_0)h}}, \quad \mathcal{T} = \frac{\mathcal{T}_{10}\mathcal{T}_{02}e^{ik_0cos(\theta_0)h}}{1-\mathcal{R}_{02}\mathcal{R}_{01}e^{2ik_0cos(\theta_0)h}}. \tag{4.7}$$

4.3 Numerical method

In the current 2D anti-plane shear wave problem, we give the second-order hyperbolic dynamic equation (5.16) as

$$c^2(\frac{\partial^2}{\partial x^2} + \frac{\partial^2}{\partial y^2})u(x,y,t) = \frac{\partial^2 u(x,y,t)}{\partial t^2}, \tag{4.8}$$

where the wave velocity $c = \sqrt{G/\rho}$, and its value depends on which medium the wave $u(x,y)$ progresses in. We consider using the finite-difference time-domain (FDTD) method to implement the numerical modeling of the perfect interface.

4.3.1 Explicit difference scheme

We start with a 1D M-th order Taylor series expansion of the displacement field $u(x,t)$, which gives

$$u(x+p\Delta x,t) = \sum_{k=0}^{M}\frac{(p\Delta x)^k}{k!}\frac{\partial^k u(x,t)}{\partial x^k} + \mathcal{O}(\Delta x^{k+1}), \tag{4.9}$$

where Δx represents the space step, and p is a positive integer. Try to introduce two vectors U and $\mathcal{U}$, they are defined as

$$\begin{aligned} U &= [u(x-p\Delta x,t),\ \ldots,\ u(x,t),\ \ldots,\ u(x+p\Delta x,t)]^T, \\ \mathcal{U} &= [u(x,t),\ \Delta x\frac{\partial u(x,t)}{\partial x},\ \ldots,\ \Delta x^k\frac{\partial^k u(x,t)}{\partial x^k}]^T. \end{aligned}$$

Rewriting the Taylor series expression (4.9) as the form $U = \boldsymbol{E}\,\mathcal{U}$, where the coefficient matrix $\boldsymbol{E}$ gives the index form

$$E_{ij} = \frac{(i-p-1)^{j-1}}{(j-1)!},$$

The second-order coefficient matrix $\boldsymbol{E}$ have the dimension $(2p+1)*(m+1)$. For example, when we set $p=2$, the expression $U=\boldsymbol{E}\,\mathcal{U}$ is written as

$$\begin{bmatrix} u(x-2\Delta x,t) \\ u(x-\Delta x,t) \\ u(x,t) \\ u(x+\Delta x,t) \\ u(x+2\Delta x,t) \end{bmatrix} = \begin{bmatrix} 1 & -2 & 2 & -\frac{4}{3} & \frac{2}{3} \\ 1 & -1 & \frac{1}{2} & -\frac{1}{6} & \frac{1}{24} \\ 1 & 0 & 0 & 0 & 0 \\ 1 & 1 & \frac{1}{2} & \frac{1}{6} & \frac{1}{24} \\ 1 & 2 & 2 & \frac{4}{3} & \frac{2}{3} \end{bmatrix} \begin{bmatrix} u(x,t) \\ \Delta x\frac{\partial u(x,t)}{\partial x} \\ \Delta x^2\frac{\partial^2 u(x,t)}{\partial x^2} \\ \Delta x^3\frac{\partial^3 u(x,t)}{\partial x^3} \\ \Delta x^4\frac{\partial^4 u(x,t)}{\partial x^4} \end{bmatrix}.$$

Therefore, the Taylor series expression (4.9) can be rewritten as in matrix form as $\mathcal{U}=\boldsymbol{E}^{-1}U$ for $M=2p$:

$$\begin{bmatrix} u(x,t) \\ \Delta x\frac{\partial u(x,t)}{\partial x} \\ \Delta x^2\frac{\partial^2 u(x,t)}{\partial x^2} \\ \Delta x^3\frac{\partial^3 u(x,t)}{\partial x^3} \\ \Delta x^4\frac{\partial^4 u(x,t)}{\partial x^4} \end{bmatrix} = \begin{bmatrix} 0 & 0 & 1 & 0 & 0 \\ \frac{1}{12} & -\frac{2}{3} & 0 & \frac{2}{3} & -\frac{1}{12} \\ -\frac{1}{12} & \frac{4}{3} & -\frac{5}{2} & \frac{4}{3} & -\frac{1}{12} \\ -\frac{1}{2} & 1 & 0 & -1 & \frac{1}{2} \\ 1 & -4 & 6 & -4 & 1 \end{bmatrix} \begin{bmatrix} u(x-2\Delta x,t) \\ u(x-\Delta x,t) \\ u(x,t) \\ u(x+\Delta x,t) \\ u(x+2\Delta x,t) \end{bmatrix}.$$

Taking the k-th order spatial partial derivative as an example, it is expressed as

$$\Delta x^k\frac{\partial^k u_i}{\partial x^k}=\boldsymbol{e}_k U,$$

where $\boldsymbol{e}_k$ represents a coefficient vector derived from $\boldsymbol{E}^{-1}$, which is $(k+1)$-th row.

On the other hand, the two K-order Taylor series of the time derivative terms for solution $u(x,y,t)$ are

$$u(x,y,t+\Delta t)=u(x,y,t)+\sum_{k=1}^{K}\frac{\Delta t^k}{k!}\frac{\partial^k u(x,y,t)}{\partial t^k}+\mathcal{O}(\Delta t^{K+1}),$$
$$u(x,y,t-\Delta t)=u(x,y,t)+\sum_{k=1}^{K}\frac{(-\Delta t)^k}{k!}\frac{\partial^k u(x,y,t)}{\partial t^k}+\mathcal{O}(\Delta t^{K+1}),$$

where Δt is the time step. Summing the above two expressions, it is easy to get the

second-order time derivative term

$$u(x,y,t+\Delta t)-2u(x,y,t)+u(x,y,t-\Delta t)=\sum_{k=1}^{K/2}\frac{2\Delta t^{2k}}{(2k)!}\frac{\partial^{2k}u(x,y,t)}{\partial t^{2k}}+\mathcal{O}(\Delta t^{K+1}),$$

where K is an even integer. According to the above expression, we can replace the time derivative terms in equation (4.8) with space derivative terms. Setting the space step $\Delta x=\Delta y$, the explicit time-step difference form (in the order of K) can be expressed as

$$\begin{aligned}u(x,y,t+\Delta t)=&\,2u(x,y,t)-u(x,y,t-\Delta t)\\&+\sum_{k=1}^{K/2}\frac{2}{(2k)!}\left(\frac{\Delta t}{\Delta x}c\right)^{2k}\left(\sum_{m=0}^{k}\boldsymbol{L}_{(2m,2k-2m)}:\boldsymbol{U}\right),\end{aligned}\tag{4.10}$$

where the matrices $\boldsymbol{L}$ and $\boldsymbol{U}$ have definitions

$$\boldsymbol{L}_{(2m,2k-2m)}=\boldsymbol{e}_{2m}\otimes\boldsymbol{e}_{2k-2m},\quad \boldsymbol{U}=\begin{bmatrix}u(x-p\Delta x,y-p\Delta y,t) & \dots & u(x+p\Delta x,y-p\Delta y,t)\\ \dots & \dots & \dots\\ u(x-p\Delta x,y+p\Delta y,t) & \dots & u(x+p\Delta x,y+p\Delta y,t)\end{bmatrix}.$$

The above scheme is similar to the Lax-Wendroff scheme of the first-order 2D linear hyperbolic partial differential equations (Lörcher & Munz, 2007). The constant coefficient matrix $\boldsymbol{L}_{(2m,2k-2m)}$ can be determined according to the accuracy of time steps $\mathcal{O}(\Delta t^{K+1})$ and space steps $\mathcal{O}(\Delta x^{M+1})$. For example, when $p=2$, The expressions of the matrix $\boldsymbol{L}_{(2m,2k-2m)}$ are given as

$$\boldsymbol{L}_{(0,2)}=\boldsymbol{e}_0\otimes\boldsymbol{e}_2=\begin{bmatrix}0&0&0&0&0\\0&0&0&0&0\\-\frac{1}{12}&\frac{4}{3}&-\frac{5}{2}&\frac{4}{3}&-\frac{1}{12}\\0&0&0&0&0\\0&0&0&0&0\end{bmatrix},\quad \boldsymbol{L}_{(0,4)}=\boldsymbol{e}_0\otimes\boldsymbol{e}_4=\begin{bmatrix}0&0&0&0&0\\0&0&0&0&0\\1&-4&6&-4&1\\0&0&0&0&0\\0&0&0&0&0\end{bmatrix},$$

$$\boldsymbol{L}_{(2,2)} = \boldsymbol{e}_2 \otimes \boldsymbol{e}_2 = \begin{bmatrix} \frac{1}{144} & -\frac{1}{9} & \frac{5}{24} & -\frac{1}{9} & \frac{1}{144} \\ -\frac{1}{9} & \frac{16}{9} & -\frac{10}{3} & \frac{16}{9} & -\frac{1}{9} \\ \frac{5}{24} & -\frac{10}{3} & \frac{25}{4} & -\frac{10}{3} & \frac{5}{24} \\ -\frac{1}{9} & \frac{16}{9} & -\frac{10}{3} & \frac{16}{9} & -\frac{1}{9} \\ \frac{1}{144} & -\frac{1}{9} & \frac{5}{24} & -\frac{1}{9} & \frac{1}{144} \end{bmatrix},$$

Moreover, the matrix $\boldsymbol{L}$ satisfies the symmetrical relationship $\boldsymbol{L}_{(2m,2k-2m)} = \boldsymbol{L}^T_{(2k-2m,2m)}$.

4.3.2 Numerical modeling of perfect interface

Considering the explicit central difference scheme mentioned earlier, this section performs numerical simulations on the single perfect interface model and the double perfect interface model (with a small thickness of h).

Single perfect interface model

Taking the 1D model shown in Fig.(4.6) as an example, the dynamic equation (5.16) reads

$$G\frac{\partial^2 u}{\partial x^2} = \rho\frac{\partial^2 u}{\partial t^2}.$$

The continuity of the displacement field $[[u]] = 0$ and the continuity of the traction vector $[[\tau]] = 0$ at the perfect interface $\mathcal{S}$.

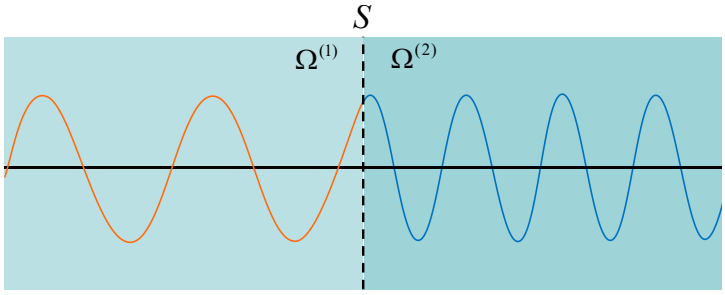

Figure 4.6: *1D perfect interface model: the wave satisfies the displacement field continuous* $[[u]] = 0$ *and the traction vector continuous* $[[t]] = 0$ *on the perfect interface* $\mathcal{S}$.

Let x be a point located on the interface $\mathcal{S}$, and $\mathcal{S}^{(+)}$ and $\mathcal{S}^{(-)}$ be two sides of $\mathcal{S}$. The displacement fields on both sides of the interface are denoted as $u(x^{(+)})$ and $u(x^{(-)})$, respectively. Using the explicit central difference scheme from the previous section, we

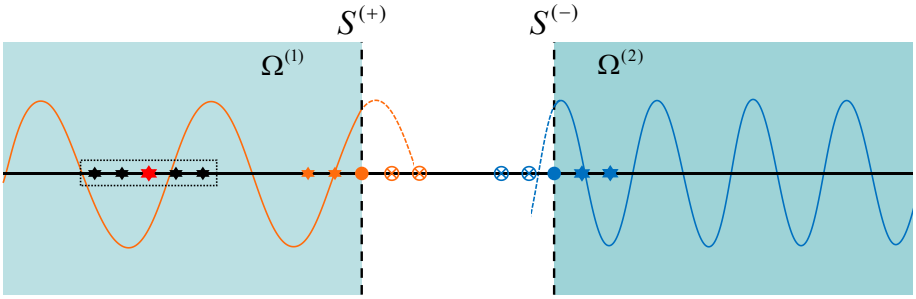

Figure 4.7: *1D center difference model: both sides of the perfect interface $\mathcal{S}$ are denoted as $\mathcal{S}^{(+)}$ and $\mathcal{S}^{(-)}$, and the displacements of the left (orange dot) and right (blue dot) points of the interface are denoted as $u(x^{(+)})$ and $u(x^{(-)})$, respectively. The symbol $*$ represents the difference grid of the medium $\Omega^{(1)}$ (orange) or $\Omega^{(2)}$ (blue), and the symbol $\otimes$ represents the corresponding virtual point. The black dotted frame represents the five-point difference stencil of red point.*

take $p = 2$ as an example. According to the continuity conditions $[[u]] = 0$ and $[[\tau]] = 0$, it is easy to prove that

$$\begin{aligned}
\frac{\partial^2[[u]]}{\partial t^2} = 0 \ &: \frac{\partial^2 u(x^{(+)})}{\partial t^2} = \frac{\partial^2 u(x^{(-)})}{\partial t^2}, \\
\frac{\partial^4[[u]]}{\partial t^4} = 0 \ &: \frac{\partial^4 u(x^{(+)})}{\partial t^4} = \frac{\partial^4 u(x^{(-)})}{\partial t^4}, \\
[[\tau]] = 0 \ &: G_1 \frac{\partial u(x^{(+)})}{\partial x} = G_2 \frac{\partial u(x^{(-)})}{\partial x}, \\
\frac{\partial^2[[\tau]]}{\partial t^2} = 0 \ &: G_1 \frac{\partial^2}{\partial t^2}\left(\frac{\partial u(x^{(+)})}{\partial x}\right) = G_2 \frac{\partial^2}{\partial t^2}\left(\frac{\partial u(x^{(-)})}{\partial x}\right).
\end{aligned}$$

We denote the displacement field of the virtual points as $u^*(x^{(+)}+p\Delta x)$ and $u^*(x^{(-)}-p\Delta x)$, they allow

$$\begin{aligned}
G_1\rho_2 \boldsymbol{e}_2 U^+ = G_2\rho_1 \boldsymbol{e}_2 U^-, \quad G_1^2\rho_2^2 \boldsymbol{e}_4 U^+ = G_2^2\rho_1^2 \boldsymbol{e}_4 U^-, \\
G_1 \boldsymbol{e}_1 U^+ = G_2 \boldsymbol{e}_1 U^-, \quad G_1^2\rho_2 \boldsymbol{e}_3 U^+ = G_2^2\rho_1 \boldsymbol{e}_3 U^-,
\end{aligned}$$

where

$$\begin{aligned}
U^+ &= [u(x^{(+)} - 2\Delta x), u(x^{(+)} - \Delta x), u(x^{(+)}), u^*(x^{(+)} + \Delta x), u^*(x^{(+)} + 2\Delta x)]^T, \\
U^- &= [u^*(x^{(-)} - 2\Delta x), u^*(x^{(-)} - \Delta x), u(x^{(-)}), u(x^{(-)} + \Delta x), u(x^{(-)} + 2\Delta x)]^T.
\end{aligned}$$

With help of the Taylor series expansion (4.9) for $p = 2$, we can get the relation

$$\begin{bmatrix} \frac{4\gamma_G}{3\gamma_\rho} & -\frac{\gamma_G}{12\gamma_\rho} & -\frac{1}{12} & \frac{4}{3} \\ -\frac{4\gamma_G^2}{\gamma_\rho^2} & \frac{\gamma_G^2}{\gamma_\rho^2} & 1 & -4 \\ \frac{2\gamma_G}{3} & -\frac{\gamma_G}{12} & \frac{1}{12} & -\frac{2}{3} \\ -\frac{\gamma_G^2}{\gamma_\rho} & \frac{\gamma_G^2}{2\gamma_\rho} & -\frac{1}{2} & 1 \end{bmatrix} U^* = \begin{bmatrix} -\frac{\gamma_G}{12\gamma_\rho} & \frac{4\gamma_G}{3\gamma_\rho} & -\frac{5\gamma_G}{2\gamma_\rho} & -\frac{5}{2} & \frac{4}{3} & -\frac{1}{12} \\ \frac{\gamma_G^2}{\gamma_\rho^2} & -\frac{4\gamma_G^2}{\gamma_\rho^2} & \frac{6\gamma_G^2}{\gamma_\rho^2} & 6 & -4 & 1 \\ \frac{\gamma_G}{12} & -\frac{2\gamma_G}{3} & 0 & 0 & \frac{2}{3} & -\frac{1}{12} \\ -\frac{\gamma_G^2}{2\gamma_\rho} & \frac{\gamma_G^2}{\gamma_\rho} & 0 & 0 & 1 & \frac{1}{2} \end{bmatrix} U$$

where $\gamma_G = \frac{G_1}{G_2}$ and $\gamma_\rho = \frac{\rho_1}{\rho_2}$, and

$$U^* = [u^*(x^{(+)} + \Delta x), u^*(x^{(+)} + 2\Delta x), u^*(x^{(-)} - 2\Delta x), u^*(x^{(-)} - \Delta x)]$$
$$U = [u(x^{(+)} - 2\Delta x), u(x^{(+)} - \Delta x), u(x^{(+)}), u(x^{(-)}), u(x^{(-)} + \Delta x), u(x^{(-)} + 2\Delta x)].$$

In this way, the displacement U^* of the virtual point can be determined by the displacement U of the difference-point on both sides of the interface $\mathcal{S}$.

Similarly, for the 2D case, the displacement of the virtual point can still be solved by this scheme. But it is worth noting that in this method, the perfect interface must pass through the difference-points (like the orange and blue dots in Fig.(4.7)). In the current work, what we discuss is the continuity conditions of the physical field at the perfect interface and its numerical modeling. For a more general 2D situation, we will discuss it in Chapter 6 of this thesis.

Considering a single interface model with the following definition: the incident shear waves propagate from medium $\Omega^{(1)}$ to medium $\Omega^{(2)}$, they have the shear modulus $G_1 = 3.0 \times 10^9(Pa), G_2 = 2.5 \times 10^9(Pa)$ and the mass density $\rho_1 = 3.0 \times 10^3(Kg/m^3), \rho_2 = 2.0 \times 10^3(Kg/m^3)$. The incident wave is set as a sinusoidal single-period wave: $u_i = -Asin(ik_1x - iwt)$, where $A = 1$, $w = 2\pi f$ and $k_1 = \frac{2\pi}{c_1 f}$ with the frequency $f = 10(Hz)$ and the wave velocity $c_1 = \sqrt{\frac{G_1}{\rho_1}}$. In the numerical model, the space step and the time step are set as $\Delta u = 1.0(m)$ and $\Delta t = 0.85(ms)$. And the Courant–Friedrichs–Lewy (CFL) condition is $\gamma = 0.95$. Fig.(4.8) shows the reflected and transmitted waves of the reference solution and the numerical solution. The reference solution is the approximate analytical solution in equations (4.2.2) and (4.2.2), and the numerical solution is determined by setting $p = 2$ of the aforementioned differential scheme.

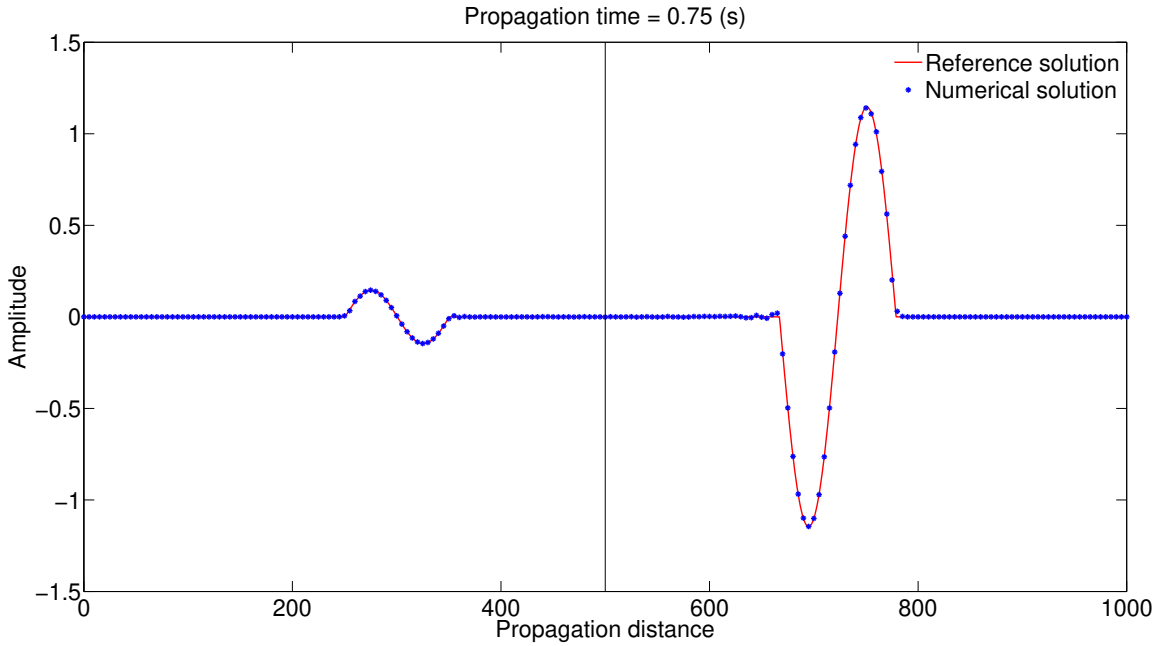

Figure 4.8: *The capture of wave propagation in Single perfect interface model at time* $t = 0.75(s)$. *The red line is the reference solution, and the blue point is the numerical solution* $(p = 2)$.

Double perfect interface model

The double perfect interface case is considered in a model with a thin homogeneous layer $\Omega^{(0)}$, whose thickness h is much smaller than the wavelength λ_0 of the wave in the intermediate layer ($h \approx 0.1\lambda_0$). Set the shear modulus of medium $\Omega^{(0)}$ to $G_0 = 2.0 \times 10^9(Pa)$ and the mass density to $\rho_0 = 1.5 \times 10^3(Kg/m^3)$. The numerical model parameters are the same as the above case. The comparison between the reference solution and the numerical solution is shown in Fig.(4.9).

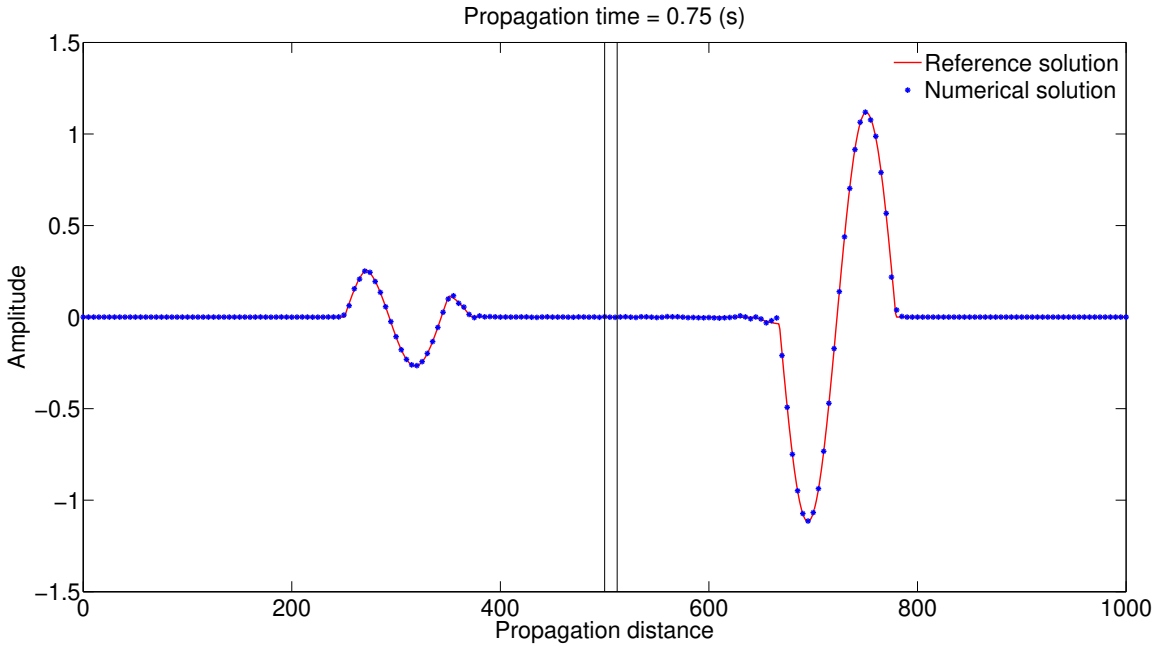

Figure 4.9: *The capture of wave propagation in Double perfect interface model at time* $t = 0.75(s)$. *The red line is the reference solution, and the blue point is the numerical solution* $(p = 2)$.

Chapter 5

Establishment of elastodynamic imperfect interface models

In this chapter, two interface operators are introduced to explain the continuity of the physical field at the perfect interface. With the help of these two interface operators, in the context of the linear elastodynamic problem of composites, we derived the jump conditions of the perfect interfaces through the thin interphase model and replaced it with an imperfect interface. The core content of this chapter is developed from the work of Gu & He (2011).

5.1 Interfacial operators

5.1.1 Two orthogonal interfacial operators

We start with the introduction of two orthogonal plane projection operators $\boldsymbol{N}$ and $\boldsymbol{T}$ mentioned in chapter 4, which are related to the normal vector $\boldsymbol{n}$ of the perfect interface. Now we define two fourth-order interfacial operators, namely the fourth-order normal operator $\mathbb{P}^{\perp}$ and the fourth-order tangent operator $\mathbb{P}^{\parallel}$:

$$\mathbb{P}^{\perp} = \boldsymbol{I}\underline{\otimes}\boldsymbol{N}, \quad \mathbb{P}^{\parallel} = \boldsymbol{I}\underline{\otimes}\boldsymbol{T},$$

where $\boldsymbol{I}$ is the second-order identity tensor. Their index form is expressed as

$$(\mathbb{P}^{\perp})_{ijkl} = \delta_{ik}N_{jl} = \delta_{ik}n_j n_l, \quad (\mathbb{P}^{\parallel})_{ijkl} = \delta_{ik}T_{jl} = \delta_{ik}(\delta_{jl} - n_j n_l), \tag{5.1}$$

where δ_{ij} is the Kronecker delta.

Remark *These two projection operators satisfy the relationships*

$$\mathbb{P}^{\perp} + \mathbb{P}^{\parallel} = \mathbb{I}, \quad \mathbb{P}^{\perp}\mathbb{P}^{\perp} = \mathbb{P}^{\perp}, \quad \mathbb{P}^{\parallel}\mathbb{P}^{\parallel} = \mathbb{P}^{\parallel}, \quad \mathbb{P}^{\perp}\mathbb{P}^{\parallel} = \mathbb{P}^{\parallel}\mathbb{P}^{\perp} = \mathbb{O}, \tag{5.2}$$

where $\mathbb{I} = \boldsymbol{I}\underline{\otimes}\boldsymbol{I}$ *is a fourth-order identity tensor satisfies the index form* $(\mathbb{I})_{ijkl} = \delta_{ik}\delta_{jl}$*, and* $\mathbb{O}$ *is a fourth-order zero-tensor.*

Let $\boldsymbol{u}$ be the response of the dynamic equation for an elastic problem, the dynamic equation gives

$$\boldsymbol{\nabla} \cdot \boldsymbol{\sigma} = \boldsymbol{\rho}\ddot{\boldsymbol{u}}, \quad \boldsymbol{\sigma} = \mathbb{C} : \boldsymbol{\nabla}\boldsymbol{u},$$

where $\mathbb{C}$ and $\boldsymbol{\rho}$ represent the stiffness (elasticity) tensor and the mass density tensor, respectively, the upper double-dot symbol represents the second derivative of time. The constitutive law satisfies $\boldsymbol{\sigma} = \mathbb{C} : \boldsymbol{\nabla}\boldsymbol{u}$, and its inverse relationship is shown as $\boldsymbol{\nabla}\boldsymbol{u} = \mathbb{S} : \boldsymbol{\sigma}$, where $\mathbb{C} : \mathbb{S} = \mathbb{I}$.

Using the definition of two orthogonal operators $\mathbb{P}^{\perp}$ and $\mathbb{P}^{\parallel}$, the displacement gradient field $\boldsymbol{\nabla}\boldsymbol{u}$ and stress field $\boldsymbol{\sigma}$ can be split as

$$\boldsymbol{\nabla}\boldsymbol{u} = \mathbb{P}^{\perp}\boldsymbol{\nabla}\boldsymbol{u} + \mathbb{P}^{\parallel}\boldsymbol{\nabla}\boldsymbol{u}, \quad \boldsymbol{\sigma} = \mathbb{P}^{\perp}\boldsymbol{\sigma} + \mathbb{P}^{\parallel}\boldsymbol{\sigma}. \tag{5.3}$$

Considering the continuity conditions of the perfect interface $\mathcal{S}$ of media $\Omega^{(1)}$ and $\Omega^{(2)}$, the displacement field $\boldsymbol{u}(\boldsymbol{x})$ is continuous on the interface $\boldsymbol{x} \in \mathcal{S}$, and also the tangential component of the displacement gradient $\boldsymbol{\nabla}\boldsymbol{u}$ and the normal component of the stress field $\boldsymbol{\sigma}$ (or traction vector $\boldsymbol{\tau}$) are continuous:

$$\boldsymbol{u}^{(1)}(\boldsymbol{x}) = \boldsymbol{u}^{(2)}(\boldsymbol{x}), \quad \mathbb{P}^{\perp}\boldsymbol{\sigma}^{(1)}(\boldsymbol{x}) = \mathbb{P}^{\perp}\boldsymbol{\sigma}^{(2)}(\boldsymbol{x}), \quad \mathbb{P}^{\parallel}\boldsymbol{\nabla}\boldsymbol{u}^{(1)}(\boldsymbol{x}) = \mathbb{P}^{\parallel}\boldsymbol{\nabla}\boldsymbol{u}^{(2)}(\boldsymbol{x}), \tag{5.4}$$

where the superscripts (1) and (2) represent the physical fields of media $\Omega^{(1)}$ and $\Omega^{(2)}$, and $\mathbb{P}^{\perp}\boldsymbol{\sigma} = \boldsymbol{\sigma}\boldsymbol{N} = (\boldsymbol{\sigma}\cdot\boldsymbol{n})\otimes\boldsymbol{n} = \boldsymbol{\tau}\otimes\boldsymbol{n}$.

5.1.2 Continuity conditions of a perfect interface

As mentioned in the previous subsection, some components of the physical field at the interface satisfy the continuity conditions, such as tangential displacement gradient component and normal stress field component (or traction vector). Next, we have necessary to discuss the relationship between the displacement gradient fields $\boldsymbol{\nabla u}$ or the stress fields $\boldsymbol{\sigma}$ on both sides of the interface $\mathcal{S}$.

According to Eq.(5.3) and the constitutive law, we can get the relations

$$\mathbb{P}^{\perp}\mathbb{C}\mathbb{P}^{\perp}\boldsymbol{\nabla u} = \mathbb{P}^{\perp}\boldsymbol{\sigma} - \mathbb{P}^{\perp}\mathbb{C}\mathbb{P}^{\parallel}\boldsymbol{\nabla u}, \quad \mathbb{P}^{\parallel}\mathbb{S}\mathbb{P}^{\parallel}\boldsymbol{\sigma} = \mathbb{P}^{\parallel}\boldsymbol{\nabla u} - \mathbb{P}^{\parallel}\mathbb{S}\mathbb{P}^{\perp}\boldsymbol{\sigma}, \tag{5.5}$$

where the part $\mathbb{P}^{\perp}\boldsymbol{\sigma}$ and $\mathbb{P}^{\parallel}\boldsymbol{\nabla u}$ satisfy the continuous conditions shown in Eq.(5.4). The normal projection $\mathbb{P}^{\perp}\mathbb{C}\mathbb{P}^{\perp}$ index form can be simplified as

$$\begin{aligned}(\mathbb{P}^{\perp}\mathbb{C}\mathbb{P}^{\perp})_{ijkl} &= (\mathbb{P}^{\perp})_{ijmn}(\mathbb{C})_{mnpq}(\mathbb{P}^{\perp})_{pqkl} = \delta_{im}n_jn_nC_{mnpq}\delta_{pk}n_qn_k \\ &= C_{inkq}n_jn_nn_ln_q = (C_{inkq}n_nn_q)n_jn_l,\end{aligned}$$

which gives the result of $\mathbb{P}^{\perp}\mathbb{C}\mathbb{P}^{\perp} = (\boldsymbol{C}\underline{:}\boldsymbol{N})\underline{\otimes}\boldsymbol{N}$ with the definition $(\boldsymbol{C}\underline{:}\boldsymbol{N})_{ij} = C_{imjn}n_mn_n$. The inverse of $\boldsymbol{C}\underline{:}\boldsymbol{N}$ satisfies $(\boldsymbol{C}\underline{:}\boldsymbol{N})\cdot(\boldsymbol{C}\underline{:}\boldsymbol{N})^{-1} = \boldsymbol{I}$, where $\boldsymbol{I}$ is the second-order identity tensor. To simplify the description, we define two second-order tensors as $\boldsymbol{Q} = \mathbb{C}\underline{:}\boldsymbol{N}$ and $\boldsymbol{Q} = (\mathbb{C}\underline{:}\boldsymbol{N})^{-1}$, they satisfy $\boldsymbol{G}\boldsymbol{Q} = \boldsymbol{I}$. It is easy to prove $(\boldsymbol{G}\underline{\otimes}\boldsymbol{I})\,(\boldsymbol{Q}\underline{\otimes}\boldsymbol{I}) = \mathbb{I}$ and

$$\begin{aligned}(\boldsymbol{G}\underline{\otimes}\boldsymbol{N})\,(\boldsymbol{Q}\underline{\otimes}\boldsymbol{N}) = (\boldsymbol{G}\underline{\otimes}\boldsymbol{N})\,(\boldsymbol{Q}\underline{\otimes}\boldsymbol{I}) = (\boldsymbol{G}\underline{\otimes}\boldsymbol{I})\,(\boldsymbol{Q}\underline{\otimes}\boldsymbol{N}) = \mathbb{P}^{\perp}, \\ (\boldsymbol{G}\underline{\otimes}\boldsymbol{T})\,(\boldsymbol{Q}\underline{\otimes}\boldsymbol{T}) = (\boldsymbol{G}\underline{\otimes}\boldsymbol{T})\,(\boldsymbol{Q}\underline{\otimes}\boldsymbol{I}) = (\boldsymbol{G}\underline{\otimes}\boldsymbol{I})\,(\boldsymbol{Q}\underline{\otimes}\boldsymbol{T}) = \mathbb{P}^{\parallel}.\end{aligned}$$

Defining a tensor $\mathbb{A} = (\boldsymbol{C}\underline{:}\boldsymbol{N})^{-1}\underline{\otimes}\boldsymbol{N}$, it have following properties

$$\mathbb{A}(\mathbb{P}^{\perp}\mathbb{C}\mathbb{P}^{\perp}) = (\mathbb{P}^{\perp}\mathbb{C}\mathbb{P}^{\perp})\mathbb{A} = \mathbb{P}^{\perp}, \quad \mathbb{A}\mathbb{P}^{\perp} = \mathbb{P}^{\perp}\mathbb{A} = \mathbb{A}.$$

For the tangent part $\mathbb{P}^{\parallel}\mathbb{S}\mathbb{P}^{\parallel}$, we will try to introduce a tensor $\mathbb{B}$, which satisfies

$$\mathbb{B}(\mathbb{P}^{\parallel}\mathbb{S}\mathbb{P}^{\parallel}) = (\mathbb{P}^{\parallel}\mathbb{S}\mathbb{P}^{\parallel})\mathbb{B} = \mathbb{P}^{\parallel}, \quad \mathbb{B}\mathbb{P}^{\parallel} = \mathbb{P}^{\parallel}\mathbb{B} = \mathbb{B}.$$

Thanks to these properties of $\mathbb{A}$ and $\mathbb{B}$, the expressions (5.5) can be rewritten as

$$\boldsymbol{\nabla u} = \mathbb{A}\mathbb{P}^{\perp}\boldsymbol{\sigma} + (\mathbb{I} - \mathbb{A}\mathbb{C})\mathbb{P}^{\parallel}\boldsymbol{\nabla u}, \quad \boldsymbol{\sigma} = \mathbb{B}\mathbb{P}^{\parallel}\boldsymbol{\nabla u} + (\mathbb{I} - \mathbb{B}\mathbb{S})\mathbb{P}^{\perp}\boldsymbol{\sigma}. \tag{5.6}$$

In this way, the displacement gradient field $\boldsymbol{\nabla u}$ and the stress field $\boldsymbol{\sigma}$ are expressed as the sum of two continuous fields ($\mathbb{P}^{\parallel}\boldsymbol{\nabla u}$ and $\mathbb{P}^{\perp}\boldsymbol{\sigma}$) on the perfect interface $\mathcal{S}$. Comparing the same components of Eq.(5.6) in constitutive law, it is easy to get an identity relationship

$$\mathbb{C}\mathbb{A} + \mathbb{B}\mathbb{S} = \mathbb{A}\mathbb{C} + \mathbb{S}\mathbb{B} = \mathbb{I}.$$

Then, the expression of $\mathbb{B}$ can be given as $\mathbb{B} = \mathbb{C} - \mathbb{C}\mathbb{A}\mathbb{C}$. We have also the relationships

$$\begin{aligned}
\mathbb{S}\mathbb{B} &= \mathbb{I} - \mathbb{A}\mathbb{C} = \mathbb{P}^{\parallel} - \mathbb{A}(\mathbb{P}^{\perp}\mathbb{C}\mathbb{P}^{\perp} - \mathbb{P}^{\perp}\mathbb{C}) = \mathbb{P}^{\parallel} + \mathbb{A}\mathbb{C}\mathbb{P}^{\parallel}, \\
\mathbb{C}\mathbb{A} &= \mathbb{I} - \mathbb{B}\mathbb{S} = \mathbb{P}^{\perp} - \mathbb{B}(\mathbb{P}^{\parallel}\mathbb{S}\mathbb{P}^{\parallel} - \mathbb{P}^{\parallel}\mathbb{S}) = \mathbb{P}^{\perp} + \mathbb{B}\mathbb{S}\mathbb{P}^{\perp}.
\end{aligned}$$

Returning to equation (5.6), the displacement gradient fields and the stress fields across the interface $\mathcal{S}$ satisfy:

$$\boldsymbol{\nabla u}^{(1)}(\boldsymbol{x}) = \mathbb{A}^{(1)}\boldsymbol{\sigma}^{(2)}(\boldsymbol{x}) + \mathbb{S}^{(1)}\mathbb{B}^{(1)}\boldsymbol{\nabla u}^{(2)}(\boldsymbol{x}), \tag{5.7a}$$

$$\boldsymbol{\sigma}^{(1)}(\boldsymbol{x}) = \mathbb{B}^{(1)}\boldsymbol{\nabla u}^{(2)}(\boldsymbol{x}) + \mathbb{C}^{(1)}\mathbb{A}^{(1)}\boldsymbol{\sigma}^{(2)}(\boldsymbol{x}). \tag{5.7b}$$

5.2 Jump conditions of thin interphase layers and equivalent imperfect interfaces

In this section, the jump conditions for a homogeneous intermediate layer with two perfect interfaces and for an equivalent imperfect interface are explained.

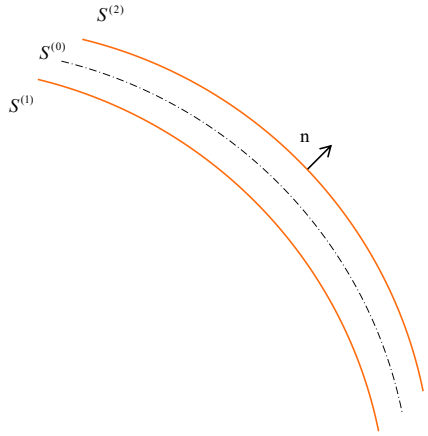

(a) Homogeneous interphase layer model

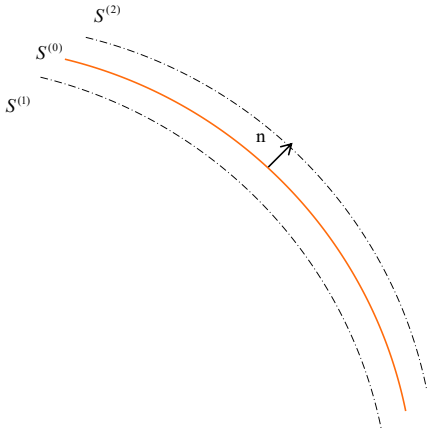

(b) Equivalent imperfect interface model

Figure 5.1: *Two interface model: (a) A sufficiently thin homogeneous layer is sandwiched between two semi-infinite domains. (b) The thin interphase layer is simplified to an equivalent imperfect interface.*

5.2.1 Analysis for an thin homogeneous interphase layer

Considering a basic model consisting of two materials $\Omega^{(1)}$ and $\Omega^{(2)}$ and a homogeneous interphase $\Omega^{(0)}$ with the thickness h, two parallel interfaces (they have the same normal vector $\boldsymbol{n}$) $\mathcal{S}^1$ and $\mathcal{S}^2$ are located between the media $\Omega^{(1)}$, $\Omega^{(0)}$ and $\Omega^{(2)}$, $\Omega^{(0)}$, respectively. And the interface $\mathcal{S}^0$ is a virtual interface between $\mathcal{S}^1$ and $\mathcal{S}^2$. Using the Taylor expansions to extend the displacement field $\boldsymbol{u}(\boldsymbol{x})$, we have

$$\begin{aligned} \boldsymbol{u}^{(0)}(\boldsymbol{x}_0) &= \boldsymbol{u}^{(0)}(\boldsymbol{x}_1) + \frac{h}{2}\boldsymbol{\nabla}\boldsymbol{u}^{(0)}(\boldsymbol{x}_1)\cdot\boldsymbol{n} + \mathcal{O}(h^2), \\ \boldsymbol{u}^{(0)}(\boldsymbol{x}_0) &= \boldsymbol{u}^{(0)}(\boldsymbol{x}_2) - \frac{h}{2}\boldsymbol{\nabla}\boldsymbol{u}^{(0)}(\boldsymbol{x}_2)\cdot\boldsymbol{n} + \mathcal{O}(h^2), \end{aligned} \tag{5.8}$$

where $\boldsymbol{x}_0 \in \mathcal{S}^0$, $\boldsymbol{x}_1 \in \mathcal{S}^1$ and $\boldsymbol{x}_2 \in \mathcal{S}^2$. The displacement jump condition of two interfaces $\mathcal{S}^1$ and $\mathcal{S}^2$ is expressed as $[[\boldsymbol{u}]]_h = \boldsymbol{u}^{(2)}(\boldsymbol{x}_2) - \boldsymbol{u}^{(1)}(\boldsymbol{x}_1)$. Owing to Eqs.(5.4), (5.7) and (5.8), the displacement jump condition $[[\boldsymbol{u}]]_h$ can be expressed as

$$[[\boldsymbol{u}]]_h = h[\mathbb{A}^{(0)}\langle\boldsymbol{\sigma}\rangle_h + \mathbb{S}^{(0)}\mathbb{B}^{(0)}\langle\boldsymbol{\nabla}\boldsymbol{u}\rangle_h]\cdot\boldsymbol{n} + \mathcal{O}(h^2), \tag{5.9}$$

where the average operator $\langle\boldsymbol{\phi}\rangle_h = [\boldsymbol{\phi}^{(1)}(\boldsymbol{x}_1) + \boldsymbol{\phi}^{(2)}(\boldsymbol{x}_2)]/2$ with $\boldsymbol{\phi} = \boldsymbol{\sigma}$ or $\boldsymbol{\nabla}\boldsymbol{u}$.

Similarly, the Taylor series expansions of the traction vector $\boldsymbol{\tau}(\boldsymbol{x})$ are given as

$$\begin{aligned}\boldsymbol{\tau}^{(0)}(\boldsymbol{x}_0) &= \boldsymbol{\tau}^{(0)}(\boldsymbol{x}_1) + \frac{h}{2}\boldsymbol{\nabla}\boldsymbol{\tau}^{(0)}(\boldsymbol{x}_1)\boldsymbol{n} + \mathcal{O}(h^2),\\ \boldsymbol{\tau}^{(0)}(\boldsymbol{x}_0) &= \boldsymbol{\tau}^{(0)}(\boldsymbol{x}_2) - \frac{h}{2}\boldsymbol{\nabla}\boldsymbol{\tau}^{(0)}(\boldsymbol{x}_2)\boldsymbol{n} + \mathcal{O}(h^2),\end{aligned} \tag{5.10}$$

where $\boldsymbol{x}_0 \in \mathcal{S}^0$, $\boldsymbol{x}_1 \in \mathcal{S}^1$ and $\boldsymbol{x}_2 \in \mathcal{S}^2$. Using the definition equation $\boldsymbol{\nabla}\cdot\boldsymbol{\sigma} = \boldsymbol{\nabla}_n\cdot\boldsymbol{\sigma} + \boldsymbol{\nabla}_t\cdot\boldsymbol{\sigma}$, the normal part $\boldsymbol{\nabla}_n \cdot \boldsymbol{\sigma}$ gives

$$\boldsymbol{\nabla}_n \cdot \boldsymbol{\sigma} = \boldsymbol{\nabla}\boldsymbol{\sigma} : \boldsymbol{N} = \boldsymbol{\nabla}(\boldsymbol{\sigma}\cdot\boldsymbol{n})\cdot\boldsymbol{n} \equiv \boldsymbol{\nabla}\boldsymbol{\tau}\cdot\boldsymbol{n} = -\boldsymbol{\nabla}_t\cdot\boldsymbol{\sigma} + \boldsymbol{\rho}\ddot{\boldsymbol{u}}.$$

Owing to Eqs.(4.1), (5.4), (5.7) and (5.10), the traction jump condition $[[\boldsymbol{\tau}]]_h = \boldsymbol{\tau}^{(2)}(\boldsymbol{x}_2) - \boldsymbol{\tau}^{(1)}(\boldsymbol{x}_1)$ can be expressed as

$$[[\boldsymbol{\tau}]]_h = h\{\boldsymbol{\rho}^{(0)}\langle\ddot{\boldsymbol{u}}\rangle_h - \boldsymbol{\nabla}_t\cdot[\mathbb{B}^{(0)}\langle\boldsymbol{\nabla}\boldsymbol{u}\rangle_h + \mathbb{C}^{(0)}\mathbb{A}^{(0)}\langle\boldsymbol{\sigma}\rangle_h]\} + \mathcal{O}(h^2), \tag{5.11}$$

where the average operator $\langle\boldsymbol{\phi}\rangle_h = [\boldsymbol{\phi}^{(1)}(\boldsymbol{x}_1) + \boldsymbol{\phi}^{(2)}(\boldsymbol{x}_2)]/2$ with $\boldsymbol{\phi} = \ddot{\boldsymbol{u}}$, $\boldsymbol{\sigma}$ or $\boldsymbol{\nabla}\boldsymbol{u}$.

5.2.2 Analysis for an equivalent imperfect interface

Try to replace the thin intermediate layer model of the previous subsection with an equivalent imperfect model. In this model, we consider the two-phase media $\Omega^{(1)}$ and $\Omega^{(2)}$ in two side of the equivalent imperfect interface $\mathcal{S}^0$, and the interfaces $\mathcal{S}^1$ and $\mathcal{S}^2$ are two virtual perfect interfaces parallel to $\mathcal{S}^0$. Let $\boldsymbol{x}_1$, $\boldsymbol{x}_2$, and $\boldsymbol{x}_0$ be the points at which the normal vectors are located on the three interfaces. Similar to equations (5.8) and (5.9), the Taylor expansions of $\boldsymbol{u}(\boldsymbol{x})$ on the interface $\mathcal{S}^1$ and $\mathcal{S}^2$ have

$$\begin{aligned}\boldsymbol{u}^{(1)}(\boldsymbol{x}_1) &= \boldsymbol{u}^{(1)}(\boldsymbol{x}_0) - \frac{h}{2}\boldsymbol{\nabla}\boldsymbol{u}^{(1)}(\boldsymbol{x}_0)\cdot\boldsymbol{n} + \mathcal{O}(h^2),\\ \boldsymbol{u}^{(2)}(\boldsymbol{x}_2) &= \boldsymbol{u}^{(2)}(\boldsymbol{x}_0) + \frac{h}{2}\boldsymbol{\nabla}\boldsymbol{u}^{(2)}(\boldsymbol{x}_0)\cdot\boldsymbol{n} + \mathcal{O}(h^2),\end{aligned} \tag{5.12}$$

where $(\cdot)^{(1)}$ and $(\cdot)^{(2)}$ represent the fields in media $\Omega^{(1)}$ and $\Omega^{(2)}$. With the help of equation (5.9), the displacement jump condition $[[\boldsymbol{u}]]_0 = \boldsymbol{u}^{(2)}(\boldsymbol{x}_0) - \boldsymbol{u}^{(1)}(\boldsymbol{x}_0)$ across the interface $\mathcal{S}^0$

reads

$$[[\boldsymbol{u}]]_0 = [[\boldsymbol{u}]]_h - h\langle \boldsymbol{\nabla u}\rangle_0 \cdot \boldsymbol{n} + \mathcal{O}(h^2),$$

where $\langle \boldsymbol{\nabla u}\rangle_0 = [\boldsymbol{\nabla u}^{(2)}(\boldsymbol{x}_0) + \boldsymbol{\nabla u}^{(1)}(\boldsymbol{x}_0)]/2$. Substitute Eqs.(5.7) and (5.9) into the above equation, we have

$$[[\boldsymbol{u}]]_0 = \frac{h}{2}[\boldsymbol{\nabla u}^{(0)}(\boldsymbol{x}_2) + \boldsymbol{\nabla u}^{(0)}(\boldsymbol{x}_1)] \cdot \boldsymbol{n} - \frac{h}{2}[\boldsymbol{\nabla u}^{(2)}(\boldsymbol{x}_0) + \boldsymbol{\nabla u}^{(1)}(\boldsymbol{x}_0)] \cdot \boldsymbol{n} + \mathcal{O}(h^2).$$

Noticed that the approximation order lock in $\mathcal{O}(h^2)$, we choose the first-order Taylor expression

$$\boldsymbol{\nabla u}^{(0)}(\boldsymbol{x}_2) \cdot \boldsymbol{n} = \boldsymbol{\nabla u}^{(0)}(\boldsymbol{x}_0) \cdot \boldsymbol{n} + \mathcal{O}(h), \quad \boldsymbol{\nabla u}^{(0)}(\boldsymbol{x}_1) \cdot \boldsymbol{n} = \boldsymbol{\nabla u}^{(0)}(\boldsymbol{x}_0) \cdot \boldsymbol{n} + \mathcal{O}(h).$$

They can also be expressed as

$$\begin{aligned}
\boldsymbol{\nabla u}^{(0)}(\boldsymbol{x}_2) \cdot \boldsymbol{n} &= [\mathbb{A}^{(0)}\boldsymbol{\sigma}^{(2)}(\boldsymbol{x}_2) + \mathbb{S}^{(0)}\mathbb{B}^{(0)}\boldsymbol{\nabla u}^{(2)}(\boldsymbol{x}_2)] \cdot \boldsymbol{n} \\
&= [\mathbb{A}^{(0)}\boldsymbol{\sigma}^{(2)}(\boldsymbol{x}_0) + \mathbb{S}^{(0)}\mathbb{B}^{(0)}\boldsymbol{\nabla u}^{(2)}(\boldsymbol{x}_0)] \cdot \boldsymbol{n}, \\
\boldsymbol{\nabla u}^{(0)}(\boldsymbol{x}_1) \cdot \boldsymbol{n} &= [\mathbb{A}^{(0)}\boldsymbol{\sigma}^{(1)}(\boldsymbol{x}_1) + \mathbb{S}^{(0)}\mathbb{B}^{(0)}\boldsymbol{\nabla u}^{(1)}(\boldsymbol{x}_1)] \cdot \boldsymbol{n} \\
&= [\mathbb{A}^{(0)}\boldsymbol{\sigma}^{(1)}(\boldsymbol{x}_0) + \mathbb{S}^{(0)}\mathbb{B}^{(0)}\boldsymbol{\nabla u}^{(1)}(\boldsymbol{x}_0)] \cdot \boldsymbol{n}.
\end{aligned}$$

Finally, using Eqs.(5.7) and (5.9), the displacement jump condition $[[\boldsymbol{u}]]$ of the imperfect interface can be rewritten as

$$\begin{aligned}
[[\boldsymbol{u}]]_0 = &\frac{h}{2}[(\mathbb{A}^{(0)} - \mathbb{A}^{(2)})\boldsymbol{\sigma}^{(2)}(\boldsymbol{x}_0) + (\mathbb{S}^{(0)}\mathbb{B}^{(0)} - \mathbb{S}^{(2)}\mathbb{B}^{(2)})\boldsymbol{\nabla u}^{(2)}(\boldsymbol{x}_0)] \cdot \boldsymbol{n} \\
&+ \frac{h}{2}[(\mathbb{A}^{(0)} - \mathbb{A}^{(1)})\boldsymbol{\sigma}^{(1)}(\boldsymbol{x}_0) + (\mathbb{S}^{(0)}\mathbb{B}^{(0)} - \mathbb{S}^{(1)}\mathbb{B}^{(1)})\boldsymbol{\nabla u}^{(1)}(\boldsymbol{x}_0)] \cdot \boldsymbol{n} + \mathcal{O}(h^2).
\end{aligned} \tag{5.13}$$

Similarly, the Taylor expansions of $\boldsymbol{\tau}(\boldsymbol{x})$ on the interface $\mathcal{S}^1$ and $\mathcal{S}^2$ have

$$\begin{aligned}
\boldsymbol{\tau}^{(1)}(\boldsymbol{x}_1) &= \boldsymbol{\tau}^{(1)}(\boldsymbol{x}_0) - \frac{h}{2}\boldsymbol{\nabla}\boldsymbol{\tau}^{(1)}(\boldsymbol{x}_0) \cdot \boldsymbol{n} + \mathcal{O}(h^2), \\
\boldsymbol{\tau}^{(2)}(\boldsymbol{x}_2) &= \boldsymbol{\tau}^{(2)}(\boldsymbol{x}_0) + \frac{h}{2}\boldsymbol{\nabla}\boldsymbol{\tau}^{(2)}(\boldsymbol{x}_0) \cdot \boldsymbol{n} + \mathcal{O}(h^2).
\end{aligned}$$

The traction jump condition $[[\boldsymbol{\tau}]]_0 = \boldsymbol{\tau}^{(2)}(\boldsymbol{x}_0) - \boldsymbol{\tau}^{(1)}(\boldsymbol{x}_0)$ gives

$$[[\boldsymbol{\tau}]]_0 = [\boldsymbol{\tau}^{(2)}(\boldsymbol{x}_2) - \boldsymbol{\tau}^{(1)}(\boldsymbol{x}_1)] - \frac{h}{2}[\boldsymbol{\nabla}\boldsymbol{\tau}^{(2)}(\boldsymbol{x}_0) + \boldsymbol{\nabla}\boldsymbol{\tau}^{(1)}(\boldsymbol{x}_0)] \cdot \boldsymbol{n} + \mathcal{O}(h^2).$$

Substitute Eqs.(5.7) and (5.11) into above equation, the traction jump condition $[[\boldsymbol{t}]]$ of the imperfect interface can be rewritten as

$$\begin{aligned}
[[\boldsymbol{\tau}]]_0 =& \frac{h}{2}[(\boldsymbol{\rho}^{(0)} - \boldsymbol{\rho}^{(2)})\ddot{\boldsymbol{u}}^{(2)}(\boldsymbol{x}_0) + (\boldsymbol{\rho}^{(0)} - \boldsymbol{\rho}^{(1)})\ddot{\boldsymbol{u}}^{(1)}(\boldsymbol{x}_0)] \\
&-\frac{h}{2}\{\boldsymbol{\nabla}_t \cdot [(\mathbb{B}^{(0)} - \mathbb{B}^{(2)})\boldsymbol{\nabla}\boldsymbol{u}^{(2)}(\boldsymbol{x}_0) + (\mathbb{C}^{(0)}\mathbb{A}^{(0)} - \mathbb{C}^{(2)}\mathbb{A}^{(2)})\boldsymbol{\sigma}^{(2)}(\boldsymbol{x}_0)] \\
&+ \boldsymbol{\nabla}_t \cdot [(\mathbb{B}^{(0)} - \mathbb{B}^{(1)})\boldsymbol{\nabla}\boldsymbol{u}^{(1)}(\boldsymbol{x}_0) + (\mathbb{C}^{(0)}\mathbb{A}^{(0)} - \mathbb{C}^{(1)}\mathbb{A}^{(1)})\boldsymbol{\sigma}^{(1)}(\boldsymbol{x}_0)]\} + \mathcal{O}(h^2).
\end{aligned} \tag{5.14}$$

Equivalent thickness models of jump conditions

The thin interphase layer are replaced with an equivalent imperfect interface in the above section. At the same time, we consider also the generality of this idea, that the thin interphase layer is transformed into another equivalent empty layer with a thickness of a by repositioning the interfaces $\mathcal{S}_a^1$ and $\mathcal{S}_a^2$. According to the limitation of the aforementioned jump conditions of the thickness h, the equivalent thickness a can be defined in the interval $[0, 2h]$, where we choose the maximum value of a equal to $2h$ to avoid unreasonable errors caused by large equivalent thickness. Then we introduce a coefficient $\epsilon = (h - a)/h$, the jump conditions for this equivalent empty layer related to ϵ can be expressed as

$$\begin{aligned}
[[\boldsymbol{u}]]_a =& \frac{h}{2}[(\mathbb{A}^{(0)} - \epsilon\mathbb{A}^{(2)})\boldsymbol{\sigma}^{(2)}(\boldsymbol{x}_2^*) + (\mathbb{S}^{(0)}\mathbb{B}^{(0)} - \epsilon\mathbb{S}^{(2)}\mathbb{B}^{(2)})\boldsymbol{\nabla}\boldsymbol{u}^{(2)}(\boldsymbol{x}_2^*)] \cdot \boldsymbol{n} \\
&+\frac{h}{2}[(\mathbb{A}^{(0)} - \epsilon\mathbb{A}^{(1)})\boldsymbol{\sigma}^{(1)}(\boldsymbol{x}_1^*) + (\mathbb{S}^{(0)}\mathbb{B}^{(0)} - \epsilon\mathbb{S}^{(1)}\mathbb{B}^{(1)})\boldsymbol{\nabla}\boldsymbol{u}^{(1)}(\boldsymbol{x}_1^*)] \cdot \boldsymbol{n} + \mathcal{O}(h^2),
\end{aligned} \tag{5.15a}$$

$$\begin{aligned}
[[\boldsymbol{\tau}]]_a =& \frac{h}{2}[(\boldsymbol{\rho}^{(0)} - \epsilon\boldsymbol{\rho}^{(2)})\ddot{\boldsymbol{u}}^{(2)}(\boldsymbol{x}_2^*) + (\boldsymbol{\rho}^{(0)} - \epsilon\boldsymbol{\rho}^{(1)})\ddot{\boldsymbol{u}}^{(1)}(\boldsymbol{x}_1^*)] \\
&-\frac{h}{2}\{\boldsymbol{\nabla}_t \cdot [(\mathbb{B}^{(0)} - \epsilon\mathbb{B}^{(2)})\boldsymbol{\nabla}\boldsymbol{u}^{(2)}(\boldsymbol{x}_2^*) + (\mathbb{C}^{(0)}\mathbb{A}^{(0)} - \epsilon\mathbb{C}^{(2)}\mathbb{A}^{(2)})\boldsymbol{\sigma}^{(2)}(\boldsymbol{x}_2^*)] \\
&+ \boldsymbol{\nabla}_t \cdot [(\mathbb{B}^{(0)} - \epsilon\mathbb{B}^{(1)})\boldsymbol{\nabla}\boldsymbol{u}^{(1)}(\boldsymbol{x}_1^*) + (\mathbb{C}^{(0)}\mathbb{A}^{(0)} - \epsilon\mathbb{C}^{(1)}\mathbb{A}^{(1)})\boldsymbol{\sigma}^{(1)}(\boldsymbol{x}_1^*)]\} + \mathcal{O}(h^2),
\end{aligned} \tag{5.15b}$$

where $\boldsymbol{x}_1^*$ and $\boldsymbol{x}_2^*$ represent the corresponding points on the virtual interfaces $\mathcal{S}_a^{(1)}$ and $\mathcal{S}_a^{(2)}$, respectively. Obviously, when we set the equivalent thickness $a = 0$, these jump conditions will degenerate into the imperfect interface model in the previous section.

5.2.3 Two extreme cases of imperfect interfaces

Due to the influence of the interphase layer, the jump conditions of the double perfect interface with the distance h can be expressed as

$$[[\boldsymbol{u}]]_h = \frac{h}{2}\left(\boldsymbol{\nabla}\boldsymbol{u}^{(0)}(\boldsymbol{x}_1) + \boldsymbol{\nabla}\boldsymbol{u}^{(0)}(\boldsymbol{x}_2)\right)\cdot\boldsymbol{n}, \quad [[\boldsymbol{\tau}]]_h = \frac{h}{2}\boldsymbol{\nabla}\left[\left(\boldsymbol{\sigma}^0(\boldsymbol{x}_1) + \boldsymbol{\sigma}^0(\boldsymbol{x}_2)\right)\cdot\boldsymbol{n}\right]\cdot\boldsymbol{n},$$

The tensors $\mathbb{A}$ and $\mathbb{B}$ are two fourth-order tensors related to the stiffness tensor $\mathbb{C}$ and the compliance tensor $\mathbb{S}$. It is easy to think that the jump conditions have two extreme cases when the properties of the intermediate layer are extremely "hard" or "soft" compared to the materials on both sides. We can compare these two extreme models by jump conditions (5.9) and (5.11). The first case is that the interphase is very "hard", namely $\mathbb{C}^{(0)} \gg \mathbb{C}^{(1)}$ and $\mathbb{C}^{(2)}$. That gives $\left(\boldsymbol{\nabla}\boldsymbol{u}^{(0)}(\boldsymbol{x}_1)\cdot\boldsymbol{n}, \boldsymbol{\nabla}\boldsymbol{u}^{(0)}(\boldsymbol{x}_2)\cdot\boldsymbol{n}\right) \ll \boldsymbol{\nabla}\boldsymbol{u}^{(1)}(\boldsymbol{x}_1)\cdot\boldsymbol{n}$ and $\boldsymbol{\nabla}\boldsymbol{u}^{(2)}(\boldsymbol{x}_2)\cdot\boldsymbol{n}$, but $\left(\boldsymbol{\sigma}^{(0)}(\boldsymbol{x}_1)\cdot\boldsymbol{n}, \boldsymbol{\sigma}^{(0)}(\boldsymbol{x}_2)\cdot\boldsymbol{n}\right)$ have the same order of magnitude with $\boldsymbol{\sigma}^{(1)}(\boldsymbol{x}_1)\cdot\boldsymbol{n}$ and $\boldsymbol{\sigma}^{(2)}(\boldsymbol{x}_2)\cdot\boldsymbol{n}$. Therefore, in the approximate expression, the jump conditions at (h)-order are given as

$$\begin{aligned}
[[\boldsymbol{u}]]_h &= \frac{h}{2}\left(\boldsymbol{\nabla}\boldsymbol{u}^{(0)}(\boldsymbol{x}_1) + \boldsymbol{\nabla}\boldsymbol{u}^{(0)}(\boldsymbol{x}_2)\right)\cdot\boldsymbol{n} \approx \boldsymbol{0},\\
[[\boldsymbol{\tau}]]_h &= \frac{h}{2}\boldsymbol{\nabla}\left[\left(\boldsymbol{\sigma}^0(\boldsymbol{x}_1) + \boldsymbol{\sigma}^0(\boldsymbol{x}_2)\right)\cdot\boldsymbol{n}\right]\cdot\boldsymbol{n}\\
&= \frac{h}{2}\boldsymbol{\nabla}\left[\mathbb{C}^{(0)} : \left(\boldsymbol{\nabla}\boldsymbol{u}^0(\boldsymbol{x}_1) + \boldsymbol{\nabla}\boldsymbol{u}^0(\boldsymbol{x}_2)\right)\cdot\boldsymbol{n}\right]\cdot\boldsymbol{n}\\
&= \frac{h}{2}\{\boldsymbol{\rho}^{(0)}\left(\ddot{\boldsymbol{u}}(\boldsymbol{x}_1) + \ddot{\boldsymbol{u}}(\boldsymbol{x}_2)\right) - \boldsymbol{\nabla}_t\cdot\left[\mathbb{C}^{(0)} : \left(\boldsymbol{\nabla}\boldsymbol{u}^0(\boldsymbol{x}_1) + \boldsymbol{\nabla}\boldsymbol{u}^0(\boldsymbol{x}_2)\right)\right]\}.
\end{aligned}$$

Conversely, in the second case, the "soft" interphase satisfies $\mathbb{C}^{(0)} \ll \mathbb{C}^{(1)}$ and $\mathbb{C}^{(2)}$, which is the opposite of the first one. That gives $\left(\boldsymbol{\nabla}\boldsymbol{u}^{(0)}(\boldsymbol{x}_1)\cdot\boldsymbol{n}, \boldsymbol{\nabla}\boldsymbol{u}^{(0)}(\boldsymbol{x}_2)\cdot\boldsymbol{n}\right) \gg \boldsymbol{\nabla}\boldsymbol{u}^{(1)}(\boldsymbol{x})\cdot\boldsymbol{n}$ and $\boldsymbol{\nabla}\boldsymbol{u}^{(2)}(\boldsymbol{x})\cdot\boldsymbol{n}$. At the same time, the traction vector $\left(\boldsymbol{\sigma}^{(0)}(\boldsymbol{x}_1)\cdot\boldsymbol{n}, \boldsymbol{\sigma}^{(0)}(\boldsymbol{x}_2)\cdot\boldsymbol{n}\right)$ have the same order of magnitude with $\boldsymbol{\sigma}^{(1)}(\boldsymbol{x}_1)\cdot\boldsymbol{n}$ and $\boldsymbol{\sigma}^{(2)}(\boldsymbol{x}_2)\cdot\boldsymbol{n}$. However, the gradient of traction vector satisfies $\left(\boldsymbol{\nabla}\left(\boldsymbol{\sigma}^{(0)}(\boldsymbol{x}_1)\cdot\boldsymbol{n}\right), \boldsymbol{\nabla}\left(\boldsymbol{\sigma}^{(0)}(\boldsymbol{x}_2)\cdot\boldsymbol{n}\right)\right) \ll \boldsymbol{\nabla}\left(\boldsymbol{\sigma}^{(1)}(\boldsymbol{x})\cdot\boldsymbol{n}\right)$ and $\boldsymbol{\nabla}\left(\boldsymbol{\sigma}^{(1)}(\boldsymbol{x})\cdot\boldsymbol{n}\right)$. Therefore, the jump conditions at (h)-order are given as

$$\begin{aligned}
[[\boldsymbol{u}]]_h &= \frac{h}{2}\left(\boldsymbol{\nabla}\boldsymbol{u}^{(0)}(\boldsymbol{x}_1) + \boldsymbol{\nabla}\boldsymbol{u}^{(0)}(\boldsymbol{x}_2)\right)\cdot\boldsymbol{n} = \frac{h}{2}\mathbb{S}^{(0)}\left(\boldsymbol{\sigma}^{(0)}(\boldsymbol{x}_1) + \boldsymbol{\sigma}^{(0)}(\boldsymbol{x}_2)\right)\cdot\boldsymbol{n},\\
[[\boldsymbol{\tau}]]_h &= \frac{h}{2}\boldsymbol{\nabla}\left[\left(\boldsymbol{\sigma}^0(\boldsymbol{x}_1) + \boldsymbol{\sigma}^0(\boldsymbol{x}_2)\right)\cdot\boldsymbol{n}\right]\cdot\boldsymbol{n} \approx \boldsymbol{0}.
\end{aligned}$$

In fact, These two interphase layer models correspond to two typical imperfect interface models: the interface stress model and the spring-layer model. The first model provides continuity of the displacement field across the interface, but the normal stress field (or traction vector) satisfies the Young-Laplace equation. The second model is that the normal stress field (or traction vector) is continuous at the interface, while the displacement field satisfies the linear relationship between the traction vectors on both sides of the interface.

5.3 Example for 2D anti-plane shear wave

In this section, we consider an anti-plane shear wave (SH wave) propagates in the plane (x, y), which contains two semi-infinite matrices $\Omega^{(1)}$, $\Omega^{(2)}$ and a homogeneous interphase layer $\Omega^{(0)}$ with the thickness h. The model has the shear modulus (G_1, G_2, G_0) and the mass density (ρ_1, ρ_2, ρ_0) for each medium $(\Omega^{(1)}, \Omega^{(2)}, \Omega^{(0)})$. Considering the interphase layer model shown in Fig.(5.2), two parallel perfect interfaces represent the interfaces of the mediums $(\Omega^{(1)}, \Omega^{(0)})$ and $(\Omega^{(1)}, \Omega^{(0)})$. Let $u(x, y, t)$ be the solution of the dynamic equation

$$\boldsymbol{\nabla} \cdot \boldsymbol{\sigma} = \rho \ddot{u}, \quad \boldsymbol{\sigma} = G \boldsymbol{\nabla} u. \tag{5.16}$$

5.3.1 Equivalent jump conditions

As the dynamic equation of the shear wave shown in Eq.(5.16), the displacement field $u(x, y, t)$ is a scalar function. Therefore, in the jump conditions shown in Eqs.(5.15a) and

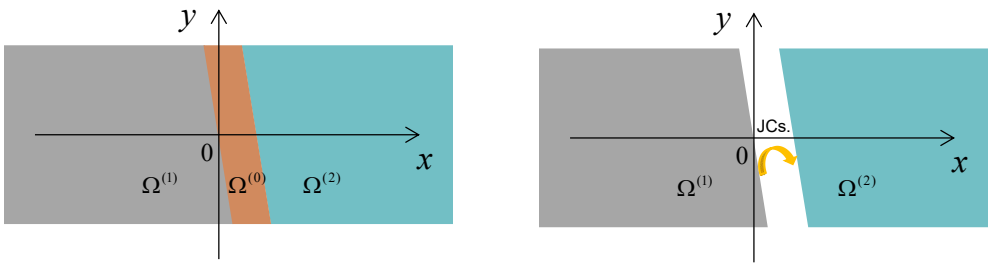

(a) Heterogeneous interphase layer model (b) Equivalent jump conditions model

Figure 5.2: *Consider a 2D anti-plane shear wave case, comparison with two model: (a) two semi-matrices Ω_1 and Ω_2 with a homogeneous interphase layer Ω_0, (b) two semi-matrix Ω_1 and Ω_2 with the equivalent Jump Conditions.*

(5.15b), the tensor $\mathbb{C}$, $\mathbb{S}$, $\mathbb{A}$ and $\mathbb{B}$ can be greatly simplified to

$$\mathbb{C} \Rightarrow G\boldsymbol{I}, \quad \mathbb{S} \Rightarrow G^{-1}\boldsymbol{I}, \quad \mathbb{A} \Rightarrow G^{-1}\boldsymbol{N}, \quad \mathbb{B} = G\boldsymbol{T},$$

where $\boldsymbol{I}$ is the second-order identity vector, and $\boldsymbol{N}$ and $\boldsymbol{T}$ are two projection operators defined by $\boldsymbol{N} = \boldsymbol{n} \otimes \boldsymbol{n}$ and $\boldsymbol{T} = \boldsymbol{I} - \boldsymbol{N}$, respectively. Subsequently, the jump conditions of this equivalent empty layer model can be simply expressed as

$$[[u]]_a = \frac{h}{2}[(\frac{G_1}{G_0} - \epsilon)\boldsymbol{\nabla} u(x_1) \cdot \boldsymbol{n} + (\frac{G_2}{G_0} - \epsilon)\boldsymbol{\nabla} u(x_2) \cdot \boldsymbol{n}] + \mathcal{O}(h^2), \tag{5.17a}$$

$$\begin{aligned}[[\tau]]_a = &\frac{h}{2}[G_1 \left(\frac{\rho_0}{\rho_1} - \epsilon\right) \boldsymbol{\Delta} u(x_1) + G_2 \left(\frac{\rho_0}{\rho_2} - \epsilon\right) \boldsymbol{\Delta} u(x_2)] \\ &- \frac{h}{2}[(G_0 - \epsilon G_1)\boldsymbol{\Delta}_t u(x_1) + (G_0 - \epsilon G_2)\boldsymbol{\Delta}_t u(x_2)] + \mathcal{O}(h^2),\end{aligned} \tag{5.17b}$$

where the Laplace operator is given as $\boldsymbol{\Delta} u = \boldsymbol{\nabla} \cdot (\boldsymbol{\nabla} u)$ and $\boldsymbol{\Delta}_t u = \boldsymbol{\nabla}_t \cdot (\boldsymbol{\nabla}_t u)$. (See the section 4.1.2 for the definition of $\boldsymbol{\Delta}_t$.)

5.3.2 Reflection and transmission coefficients for jump conditions

When we consider the model shown in Figs.(5.2), the interfaces $\mathcal{S}^{(1)}$ and $\mathcal{S}^{(2)}$ have an angle φ with the vertical axis. Then, the normal and tangent vectors are $\boldsymbol{n} = (cos(\varphi), sin(\varphi))$ and $\boldsymbol{t} = (-sin(\varphi), cos(\varphi))$, respectively. The incident wave u_i and the reflected wave u_r (with the reflection coefficient $\mathcal{R}$) in the medium $\Omega^{(1)}$ and the transmitted wave u_t (with the transmission coefficient $\mathcal{T}$) in the medium $\Omega^{(2)}$ can be respectively represented as Eqs.(4.3). The reflection coefficient and transmission coefficient can be easily obtained through the jump conditions of the homogeneous interphase layer. For the model shown in Fig.(5.2b) with the thickness a, the jump conditions Eqs.(5.17a) and (5.17b) can be

rewritten as

$$[[u]]_a = \left(\frac{\partial}{\partial x}cos(\varphi) + \frac{\partial}{\partial y}sin(\varphi)\right)(A_1u(x_1) + A_2u(x_2)), \tag{5.18a}$$

$$\begin{aligned}[[\tau]]_a = &\left(\frac{\partial^2}{\partial x^2} + \frac{\partial^2}{\partial y^2}\right)(B_1u(x_1) + B_2u(x_2)) \\ &- \left(\frac{\partial}{\partial x}sin(\varphi) - \frac{\partial}{\partial y}cos(\varphi)\right)^2 (C_1u(x_1) + C_2u(x_2)),\end{aligned} \tag{5.18b}$$

where the coefficients A, B and C are defined as

$$\begin{aligned} A_1 &= \frac{h}{2}(\frac{G_1}{G_0} - \epsilon), \quad B_1 = \frac{h}{2}G_1(\frac{\rho_0}{\rho_1} - \epsilon), \quad C_1 = \frac{h}{2}(G_0 - \epsilon G_1), \\ A_2 &= \frac{h}{2}(\frac{G_2}{G_0} - \epsilon), \quad B_2 = \frac{h}{2}G_2(\frac{\rho_0}{\rho_2} - \epsilon), \quad C_2 = \frac{h}{2}(G_0 - \epsilon G_2). \end{aligned}$$

The above expressions can be degenerated into the jump condition model when $\epsilon = 0$, or the imperfect interface model when $\epsilon = 1$. According to these jump conditions and the wave expressions (4.3), we have

$$\mathcal{R} = \frac{(1-a_2)(b_1+d_1) - (1+a_1)(b_2-d_2)}{(1-a_2)(b_1-d_1) + (1-a_1)(b_2-d_2)}, \quad \mathcal{T} = \frac{(1+a_1)(b_1-d_1) + (1-a_1)(b_1+d_1)}{(1-a_2)(b_1-d_1) + (1-a_1)(b_2-d_2)},$$

where

$$\begin{aligned} a_1 &= A_1ik_1cos(\theta_1), \quad b_1 = G_1ik_1cos(\theta_1), \quad d_1 = (C_1sin^2(\theta_1) - B_1)k_1^2, \\ a_2 &= A_1ik_2cos(\theta_2), \quad b_2 = G_2ik_2cos(\theta_2), \quad d_2 = (C_2sin^2(\theta_2) - B_2)k_2^2. \end{aligned}$$

5.3.3 Numerical examples

Considering a three-phase composite model with a thin interphase layer, the modeling parameters are given as: the shear modulus $G_1 = 3 \times 10^{11}(Pa)$, $G_2 = 4 \times 10^{11}(Pa)$ and $G_0 = 2 \times 10^{11}(Pa)$; the mass density $\rho_1 = 3000(Kg/m^3)$, $\rho_2 = 3500(Kg/m^3)$ and $\rho_0 = 3300(Kg/m^3)$. The reflection and transmission coefficients of the analytical solution (with $N = 4$), approximate solution and equivalent jump conditions of this model will be compared. As shown in Figs.(5.3), when the ratio of the thickness of interphase layer h to the wavelength λ_0 is small, the equivalent jump conditions have a comfortable equivalent

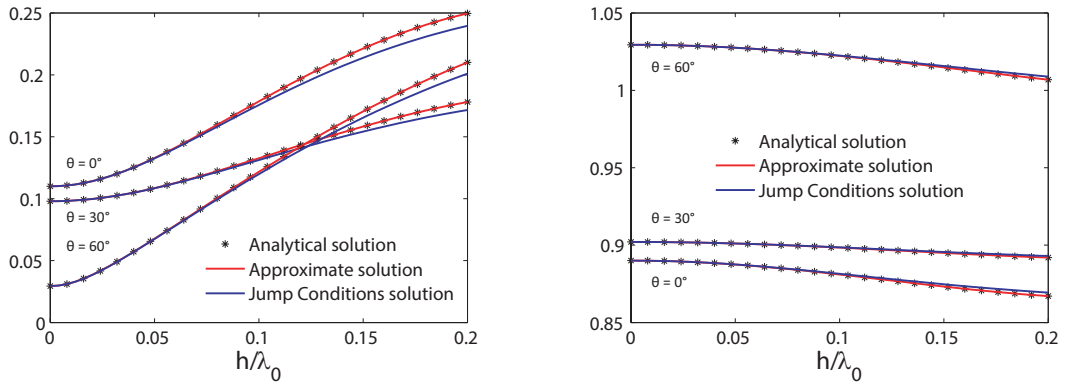

(a) Reflection coefficient $\mathcal{R}$ (b) Tresmission coefficient $\mathcal{T}$

Figure 5.3: *Setting the incident angle $\theta_1 = 0°$, $30°$ and $60°$, the reflection coefficient $\mathcal{R}$ and transmission coefficient $\mathcal{T}$ of the analytical solution (point), approximate solution (red line), and jump conditions solution (blue line) are shown in (a) and (b), respectively.*

result with less error. In other words, the influence of the incidence angle θ on the reflection coefficient and transmission coefficient becomes significant when h/λ_0 is greater than 0.1. In addition, the difference between the material's "hardness" (referred to as acoustic impedance) of the interphase layer and the materials on both sides affects these errors to a large extent.

We propose the amplitude errors to show the reflected and transmitted wave intensities in different cases. These errors are defined as

$$\mathcal{R}_{Err} = \frac{||\mathcal{R}(a,\theta) - \mathcal{R}_{ref}(a,\theta)||}{||\mathcal{R}_{ref}(a,\theta)||}, \quad \mathcal{T}_{Err} = \frac{||\mathcal{T}(a,\theta) - \mathcal{T}_{ref}(a,\theta)||}{||\mathcal{T}_{ref}(a,\theta)||},$$

where the reference case is an analytical solution described above. Obviously, the equivalent jump conditions display a lower error when the equivalent thickness $a = h$, that is the thickness does not change. Increasing or decreasing the equivalent thickness value will cause a larger error. As shown in Fig.(5.4), in this model, the reflection coefficient error reaches 40% when the incident angle $\theta = 0°$ and the equivalent thickness $a = 2h$. In contrast, the transmitted wave error does not change much.

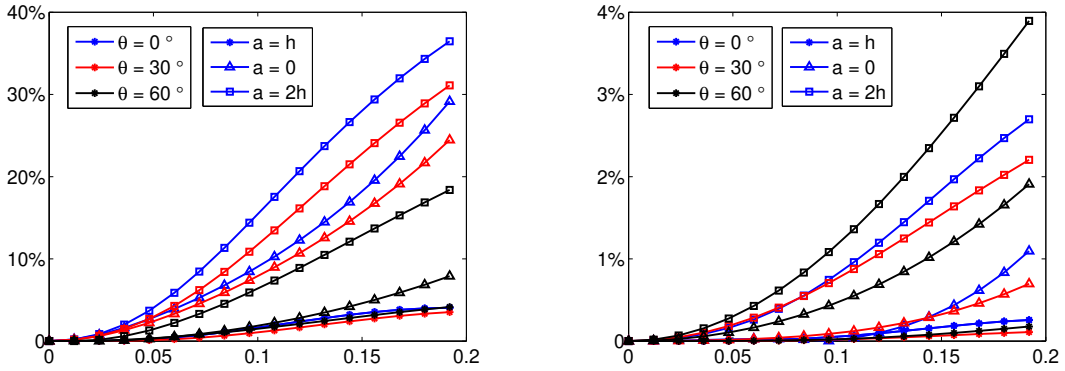

(a) Reflection coefficient errors $\mathcal{R}_{Err}$

(b) Tresmission coefficient errors $\mathcal{T}_{Err}$

Figure 5.4: *(a) Reflection coefficient $\mathcal{R}$ errors and (b) transmission coefficient $\mathcal{T}$ errors of different equivalent thicknesses a (with $a = h$-asterisk, $a = 0$-triangle and $a = 2h$-square symbol) and different incident angles θ (with $\theta = 0°$-blue , $\theta = 30°$-red and $\theta = 60°$-black line).*

5.4 Conclusion

In general, we consider the interface of the two closely bonded materials as the perfect interface, that is, the displacement field $\boldsymbol{u}$ and the traction vector $\boldsymbol{\tau} = \boldsymbol{\sigma} \cdot \boldsymbol{n}$ at the interface satisfy the continuity in the elastic problem. However, in many cases, the application conditions of the perfect interface cannot be satisfied. In order to solve the complexity of the thin interlayer in modeling, we provide two effective interface models: the first one is the equivalent jump conditions model, which ignores the modeling of the thin interphase and replace it with two jump conditions of $\boldsymbol{u}$ and $\boldsymbol{\tau}$; the second one is the equivalent imperfect interface model, which transforms the thin interphase to an imperfect interface with equivalent jump conditions of $\boldsymbol{u}$ and $\boldsymbol{\tau}$. The above two equivalent models are derived from the approximate expression of the Taylor series expansion of the physical field across the interface, so the applicable conditions of the model are only satisfied with the thin interphase layer with a small thickness h, which is recommended to be less than $0.1\lambda_0$.

From the comparison of the reflection coefficient $\mathcal{R}$ and transmission coefficient $\mathcal{T}$ for the two models and the original one, we find that the equivalent jump conditions model has a better matching result when the thickness of the thin interlayer h is less than 0.1 times the wavelength in interphase layer λ_0. Moreover, the error of the comparison is not related to the incident angle, which also means that the accuracy of the equivalent

model is only related to the thickness of the interphase layer. Obviously, in addition to the jump conditions model which can maintain a low error, the equivalent model with a thickness changed will greatly increase the error. Consequently, it is necessary to limit the application of the jump condition model to thin interphase composites with a large thickness. Moreover, finding more higher-order accuracy jump condition models is also a valuable subject.

Chapter 6

Numerical implementation of elastodynamic imperfect interface models

This chapter mainly describes a numerical method, which is the Explicit Simplified Interface Method (ESIM), for implementing the jump conditions of the physics fields on a smooth interface. This method was proposed to deal with the discontinuity of the physical field on an interface (Piraux & Lombard, 2001). In the current work, this method is applied to the second-order hyperbolic dynamic equation. At the same time, the jump conditions of the thin intermediate layer model and its equivalent thickness model are implemented by the Lax-Wendroff difference scheme.

6.1 Explicit Simplified Interface Method

Among many numerical methods for implementing interface jump conditions, the Explicit Simplified Interface Method (ESIM) is a simple and understandable finite difference method in the time domain. With the help of the Taylor approximation of virtual points near the interface, the ESIM can be applied to smooth interfaces of general shape. This makes the interface position independent of the selection of the difference grid, which is suitable for more general problems. The ESIM describes a numerical method for implementing the jump conditions of the physics fields across the smooth interface. This

method was proposed to deal with the discontinuity of the physical field across the perfect interface (Piraux & Lombard, 2001; Lombard & Piraux, 2004). Its advantage is that the position of the interface does not depend on the selection of the difference grid, which benefits from the Taylor approximation of the difference-point near the interface. In the subsequent development, it was applied to the numerical implementation of the equivalent jump conditions for the imperfect interface and the thin interphase composite.

6.1.1 Geometric construction of virtual points

As shown in Fig.(6.1), we take the virtual point P on the left interface as an example. The k-order Taylor series expansion of the displacement field u^* for the virtual point P can be expressed as

$$u^* = \sum_{n=0}^{k} \left(\sum_{m=0}^{n} \left(\frac{(x_1^*)^{n-m}(y_1^*)^m}{(n-m)!m!} \frac{\partial^n u^{(1)}}{\partial x^{n-m} \partial y^m} \right) \right) + \mathcal{O}\left((x_1^*)^{k+1}, (y_1^*)^{k+1} \right), \tag{6.1}$$

where $u^{(1)}$ is the displacement field at the point $P^{(1)}(x_1^*, y_1^*)$. To simplify the description, we define

$$E_n^{(1)} = \left[\frac{(x_1^*)^n}{n!}, ..., \frac{(x_1^*)^{n-m}(y_1^*)^m}{(n-m)!m!}, ..., \frac{(y_1^*)^n}{n!} \right], \quad \mathcal{E}_n^{(1)} = \left[\frac{\partial^n u^{(1)}}{\partial x^n}, ..., \frac{\partial^n u^{(1)}}{\partial x^{n-m} \partial y^m}, ..., \frac{\partial^n u^{(1)}}{\partial y^n} \right],$$

where $(m = 0, ..., n)$. Then, the expression (6.1) can be simplified to the format $u^* = \mathcal{P}^{(1)}\mathcal{U}^{(1)}$, where $\mathcal{P}^{(1)}$ and $\mathcal{U}^{(1)}$ have definitions

$$\mathcal{P}^{(1)} = \left[E_1^{(1)}, E_2^{(1)}, ..., E_k^{(1)} \right], \quad \mathcal{U}^{(1)} = \left[\mathcal{E}_n^{(1)}, \mathcal{E}_2^{(1)}, ..., \mathcal{E}_k^{(1)} \right]^T.$$

We note that the dimension of the matrix $\mathcal{P}^{(1)}$ is $(1 \times n_n)$ with $n_n = (k+1)(k+2)/2$.

On the other hand, we use the Taylor series to approximate the relationship between the points $P^{(1)}$, $P^{(2)}$ and their surrounding points. These correlation points are denoted as $P_a^{(1)}$ and $P_b^{(2)}$, and their numbers are n_a and n_b, respectively. All the displacements of the points $P_a^{(1)}$ and $P_b^{(2)}$ constitute the vectors $U_a^{(1)}$ and $U_b^{(2)}$. Therefore, we have n_a and

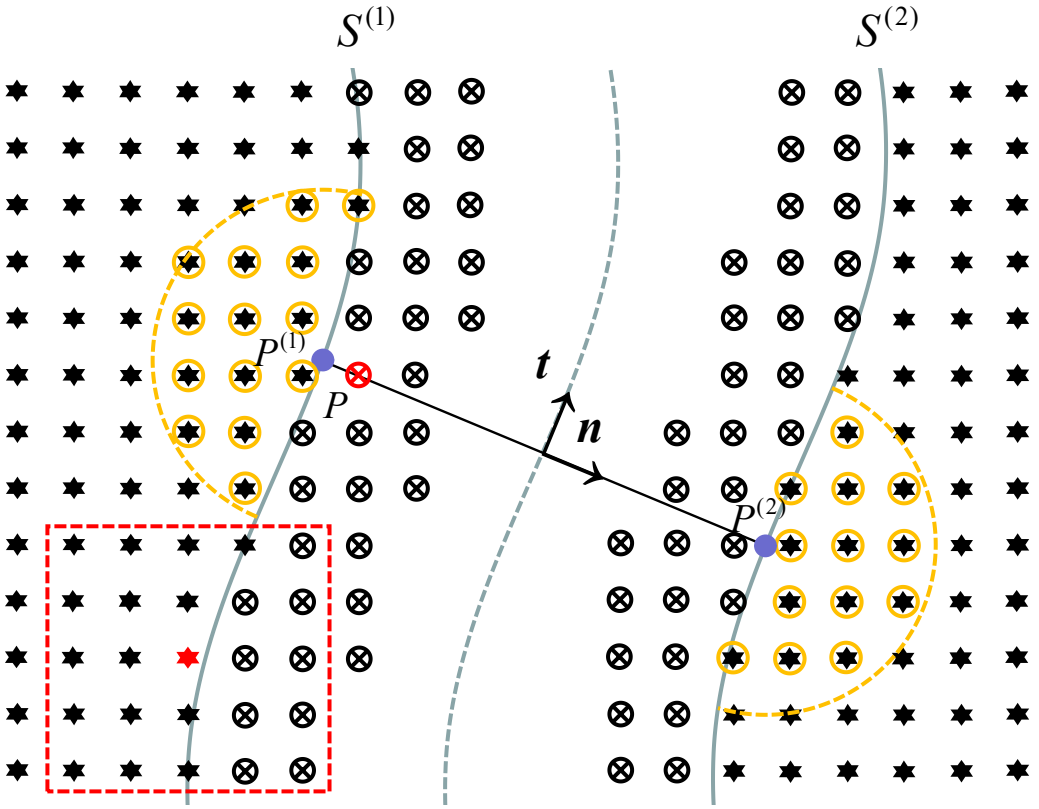

Figure 6.1: *A 2D jump conditions model with two parallel smooth interfaces $\mathcal{S}^{(1)}$ and $\mathcal{S}^{(2)}$. The symbol $*$ represents the real points in the media $\mathcal{O}^{(1)}$ and $\mathcal{O}^{(2)}$, and the symbol $\otimes$ represents the virtual points outside the interface. The red rectangular dotted domain indicates the spatial difference area of the red $*$ point. The yellow circular dashed domain indicates the Taylor approximation area of the points $P^{(1)}$ and $P^{(2)}$ at two interfaces corresponding to the red $\otimes$ point P, and these $\circledast$ points therein will be used instead of the virtual point P.*

n_b equations

$$U_a^{(1)} = \boldsymbol{\mathcal{P}}_a^{(1)} \mathcal{U}^{(1)}, \quad U_b^{(2)} = \boldsymbol{\mathcal{P}}_b^{(2)} \mathcal{U}^{(2)},$$

where $\mathcal{U}^{(2)}$ has a similar definition with $\mathcal{U}^{(1)}$, and $\boldsymbol{\mathcal{P}}_a^{(1)}$ and $\boldsymbol{\mathcal{P}}_b^{(2)}$ are two coefficient matrices with the dimension $(n_a \times n_n)$ and $(n_b \times n_n)$.

6.1.2 Implement of jump conditions

Remark. *As mentioned in the previous section, the displacement field* $[[u]]$ *and the traction vector* $[[\tau]]$ *show continuity on the perfect interface, i.e.*$[[u]] = 0$ *and* $[[\tau]] = 0$. *In addition, the tangential component of the displacement gradient field also exhibits continuity. Another manifestation of this property is Snell's law. In the current problem, with the definition of the normal vector* $\boldsymbol{n} = (cos(\varphi), sin(\varphi))$ *and the tangent vector* $\boldsymbol{t} = (-sin(\varphi), cos(\varphi))$, *the tangent part of the spatial derivative (the displacement gradient field) can be expressed as*

$$\boldsymbol{\nabla} u(x, y, t) \cdot \boldsymbol{t} = \left(-\frac{\partial}{\partial x} sin(\varphi) + \frac{\partial}{\partial y} cos(\varphi) \right) u(x, y, t). \tag{6.2}$$

On the other hand, the time derivative of the displacement field also shows continuity. The relationship between the multi-order time derivative and the space derivative can be given as (take index $2k$ *as an example)*

$$\frac{\partial^{2k} u(x, y, t)}{\partial t^{2k}} = c^{2k} \left(\frac{\partial^2}{\partial x^2} + \frac{\partial^2}{\partial y^2} \right)^k u(x, y, t). \tag{6.3}$$

The above expressions (6.2) and (6.3) introduce two higher-order relationships that are automatically satisfied by the jump conditions of the displacement field $[[u]]$ and the traction vector $[[t]]$, they can be used to construct multiple jump condition equations. Considering the limitation of the approximate order K (even number) of Taylor series, the jump conditions $[[u]]$ and $[[t]]$ can form up to n_u and n_τ equations, respectively. For example, for a perfect interface, the number of equations $n_u = (K+2)^2/4$ and $n_\tau = K(K+2)/4$, and the total number $n_{jc} = n_u + n_\tau = (K+1)(K+2)/2$. Similarly, for the jump conditions shown in Eqs.(5.18a) and (5.18b), the jump condition of the displacement field

$[[u]]$ is related to the first-order derivative of the displacement ∇u, and the jump condition of the traction vector $[[\tau]]$ is related to the second-order derivative of the displacement Δu. Then, the maximum number n_u and n_τ of jump equations satisfy $n_u = K(K+2)/4$ and $n_\tau = K^2/4$, and the total number of equations $n_{jc} = K(K+1)/2$. For example, when we set $K = 4$, we can construct the following jump conditions in this case :

$$[[u]], \quad [[u]]', \quad [[u]]'', \quad [[u]]''', \quad [[u]]_{tt}, \quad [[u]]'_{tt}, \quad [[\tau]], \quad [[\tau]]', \quad [[\tau]]'', \quad [[\tau]]_{tt},$$

where the superscript prime represents the time partial derivative, and the subscript $\boldsymbol{t}$ represents the tangential component of the gradient field. It is worth noting that $[[u]]_t$ and $[[\tau]]$ have the same physical meaning, so they are not listed repeatedly. Therefore, when we consider the highest partial derivative order of the jump condition is K, we can get $n_j = K(K+1)/2$ equations

$$\boldsymbol{\mathcal{Q}}^{(1)}\mathcal{U}^{(1)} = \boldsymbol{\mathcal{Q}}^{(2)}\mathcal{U}^{(2)},$$

where $\boldsymbol{\mathcal{Q}}^{(1)}$ and $\boldsymbol{\mathcal{Q}}^{(2)}$ are two coefficient matrices with the dimension $(n_j \times n_n)$.

6.1.3 Determination of the virtual displacement fields

Recalling the virtual point expression (6.1) constructed previously, the number of coefficient matrix $\mathcal{P}$ is n_n. This means that we need to construct n_n equations to solve $\mathcal{P}$. However, the total number of equations n_{jc} that can be constructed for the jump condition is less than n_n. Therefore, in order to make the above relationship solvable, we can define $\mathcal{U}^{(2)} = \left(\boldsymbol{\mathcal{Q}}^{(2)}\right)^{-1} \boldsymbol{\mathcal{Q}}^{(1)}\mathcal{U}^{(1)}$, where $\left(\boldsymbol{\mathcal{Q}}^{(2)}\right)^{-1}$ is the least-square pseudo-inverse of $\boldsymbol{\mathcal{Q}}^{(2)}$. Finally, the virtual point $P^{(1)}$ has the displacement field

$$u^* = \boldsymbol{\mathcal{P}}^{(1)} \begin{bmatrix} \boldsymbol{\mathcal{P}}_a^{(1)} \\ \boldsymbol{\mathcal{P}}_b^{(2)} \left(\boldsymbol{\mathcal{Q}}^{(2)}\right)^{-1} \boldsymbol{\mathcal{Q}}^{(1)} \end{bmatrix}^{-1} \begin{bmatrix} U_a^{(1)} \\ U_b^{(2)} \end{bmatrix},$$

where $(\cdot)^{-1}$ stands for the least-square pseudo-inverse operator. Returning to Eq.(6.1), all virtual points in $\boldsymbol{U}$ can be represented by the above expression.

It is worth noting that if the jump conditions are not null, the number of equations

is less than the required number, that is $n_{jc} < n_n$. Of course, using the least-squares pseudo-inverse matrix will inevitably make the result inaccurate. We note that for general jump conditions, the ratio of $n_{jc}/n_n = K/(K+2)$ will be close to 1 with the increase of K. This means that a larger k can increase the accuracy of the inverse matrix in this regard. However, according to expression (6.1), when the value of K increases, the calculation amount of the spatial difference terms increases. Lombard et al. (2017) also discussed this phenomenon in the acoustic propagation.

6.2 2D anti-plan shear wave propagation

The effect of errors in reflected and incident waves at different incident angles and different thicknesses of the interphase layer are shown in previous chapter. In this subsection, we consider the case of 2D shear wave propagation in a three-phase composite containing a thin interphace layer. The model is defined as: the shear modulus $G_1 = 2.6 \times 10^9(Pa)$, $G_2 = 3.0 \times 10^9(Pa)$ and $G_0 = 2.0 \times 10^9(Pa)$; the mass density $\rho_1 = 1400(Kg/m^3)$, $\rho_2 = 1500(Kg/m^3)$ and $\rho_0 = 1000(Kg/m^3)$; the wave frequency $f = 1000(Hz)$. In order to ensure the accuracy and visibility of the numerical results, we set the thickness of the interphase layer h to $0.1\lambda_0$ (λ_0 represents the wavelength of the interphase layer).

6.2.1 Normal incidence

We consider a simple normal single-period incident wave propagating across a thin interphase layer. Fig.(6.2) shows the state of the propagation time $t = 0.40(s)$. The four blocks from left to right in the figure are the numerical solution, the jump conditions solution ($a = h$), the equivalent imperfect interface solution ($a = 0$), and the double thickness jump conditions solution ($a = 2h$).

As shown in the curves of Fig.(6.3), in the jump conditions solution, the reflected wave is nearly perfectly matched, but the transmitted wave has a slight phase error. Conversely, in the equivalent imperfect interface solution, the transmitted wave has an ideal result, but the reflected wave does not match well. In the double equivalent thickness results, both reflected and transmitted waves have large errors. It is not difficult to find that the errors of the reflected and transmitted waves in these four models are mainly reflected in

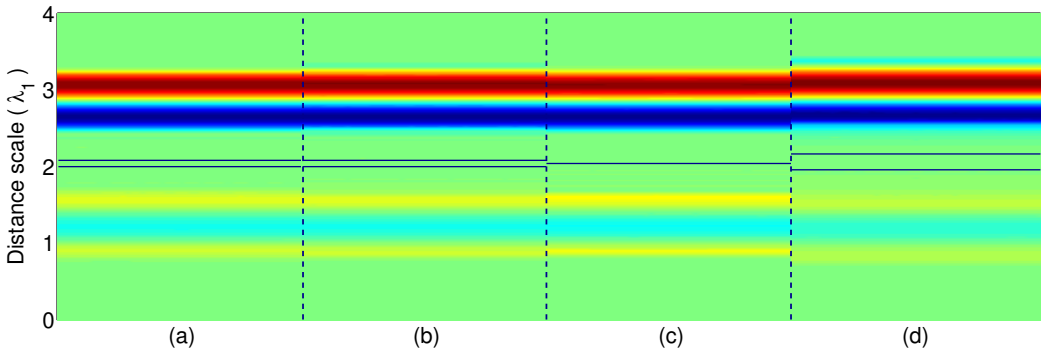

Figure 6.2: *A single-cycle shear wave propagate from the bottom to the top with incident angle* $\theta_1 = 0$. *The four blocks from left to right in the figure are the simulation results at time* $t = 0.40(s)$ *of the numerical solution (a), the jump conditions solution (b), the equivalent imperfect interface solution (c), and the double thickness jump conditions solution (d).*

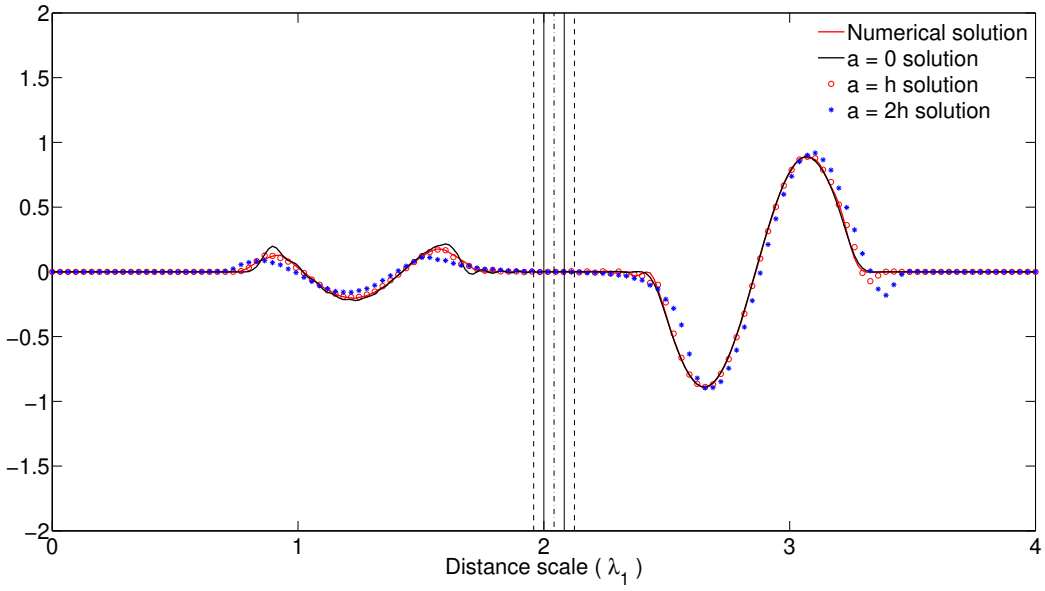

Figure 6.3: *Amplitude curves of normal incident wave: the numerical solution (red line), the jump conditions solution (red circle), the equivalent imperfect solution (black line), and the double thickness jump conditions solution (blue asterisk).*

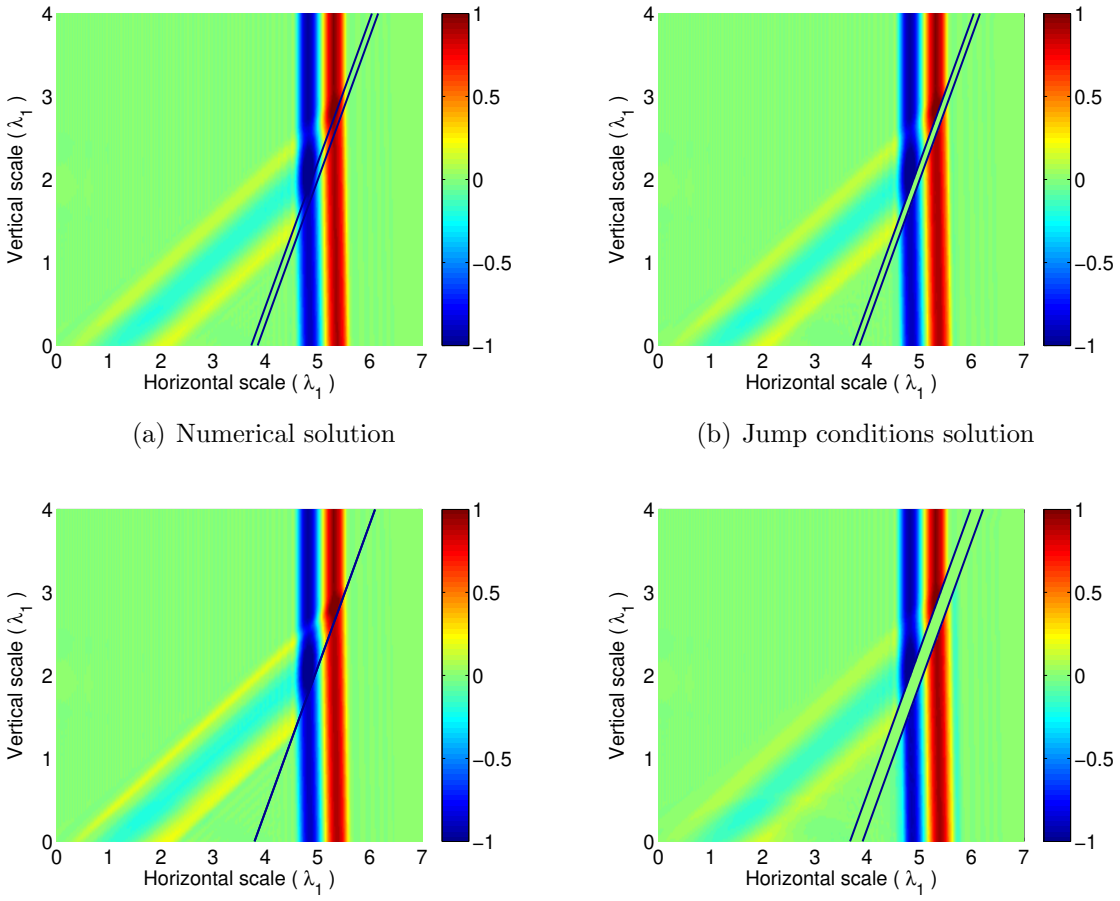

(a) Numerical solution

(b) Jump conditions solution

(c) Equivalent imperfect interface solution

(d) Double thickness jump conditions solution

Figure 6.4: *Consider a single-period shear wave propagating from the left to the right with the incident angle $\theta_1 = 30°$. The four blocks in the figure are the simulation results at time $t = 0.55(s)$ of the numerical solution (a), the jump conditions solution (b), the equivalent imperfect interface solution (c), and the double thickness jump conditions solution (d).*

the wave propagation phase rather than the amplitude.

6.2.2 Oblique incidence

Next, we set the incident angle of the wave to $\theta_1 = 30°$, and also consider the propagation of a single-period wave. As shown in Fig.(6.4), the numerical simulation results are consistent with the normal incidence case. The reflection wave of the jump conditions solution and the transmission wave of the equivalent imperfect interface solution have good matching results, but the double thickness jump conditions solution is not ideal in both aspects.

Subsequently, we capture the propagation state of the wave at vertical scale $0.5\lambda_1$ as

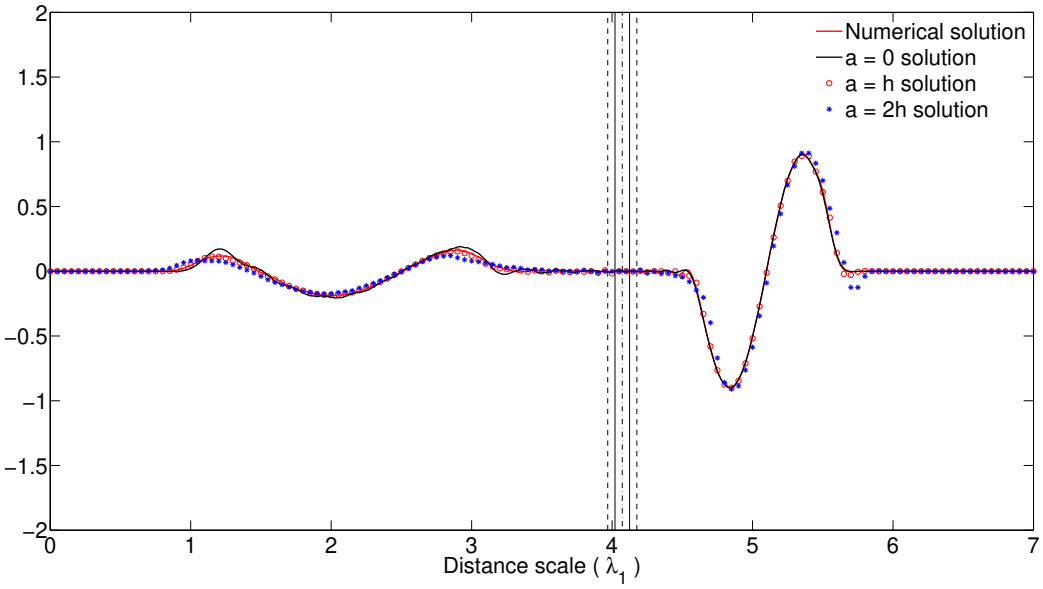

Figure 6.5: *Amplitude curves of oblique incident wave: the numerical solution (red line), the jump conditions solution (red circle), the equivalent imperfect solution (black line), and the double thickness jump conditions solution (blue asterisk).*

shown in Fig.(6.5). In addition, the propagation state of the wave in the vertical scale of $2.2\lambda_1$ is shown in Fig.(6.6). Fig.(6.6) shows some details at the interface in Fig.(6.5). The jump relationship of the displacement field for each model is clearly displayed.

6.2.3 Point wave source incidence

Finally, we consider a single-period wave source at the central point. The propagation at the time $t = 0.25(s)$ is shown in Fig.(6.8). The difference between the various models shown in the figure does not seem to be obvious. The main error is still the difference in the phase between the reflected wave and the transmitted wave.

Fig.(6.9) and (6.10) show the propagation state of the waves at vertical scales $3.5\lambda_1$ and $2.0\lambda_1$, respectively.

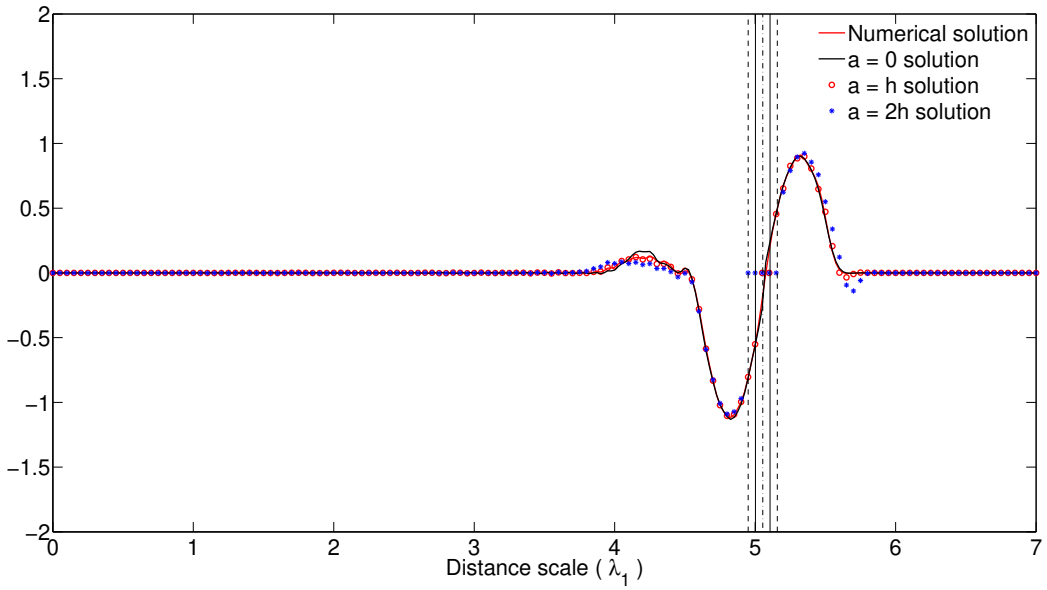

Figure 6.6: *Amplitude curves of oblique incident wave: the numerical solution (red line), the jump conditions solution (red circle), the equivalent imperfect solution (black line), and the double thickness jump conditions solution (blue asterisk).*

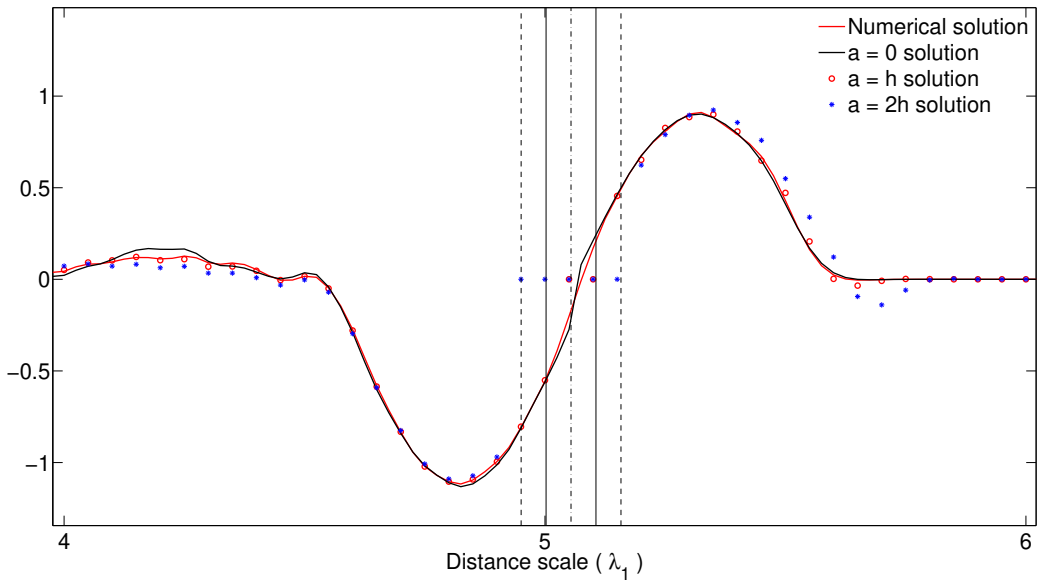

Figure 6.7: *Amplitude curves of oblique incident wave: the numerical solution (red line), the jump conditions solution (red circle), the equivalent imperfect solution (black line), and the double thickness jump conditions solution (blue asterisk).*

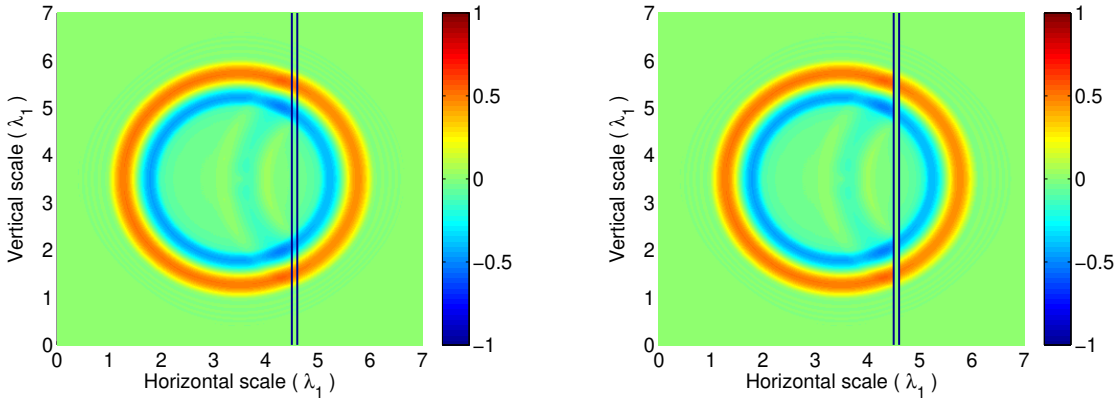

(a) Numerical solution

(b) Jump conditions solution

(c) Equivalent imperfect interface solution

(d) Double thickness jump conditions solution

Figure 6.8: *Consider a single-period shear wave that spreads from the center. The four blocks in the figure are the simulation results at time* $t = 0.25(s)$ *of the numerical solution (a), the jump conditions solution (b), the equivalent imperfect interface solution (c), and the double thickness jump conditions solution (d).*

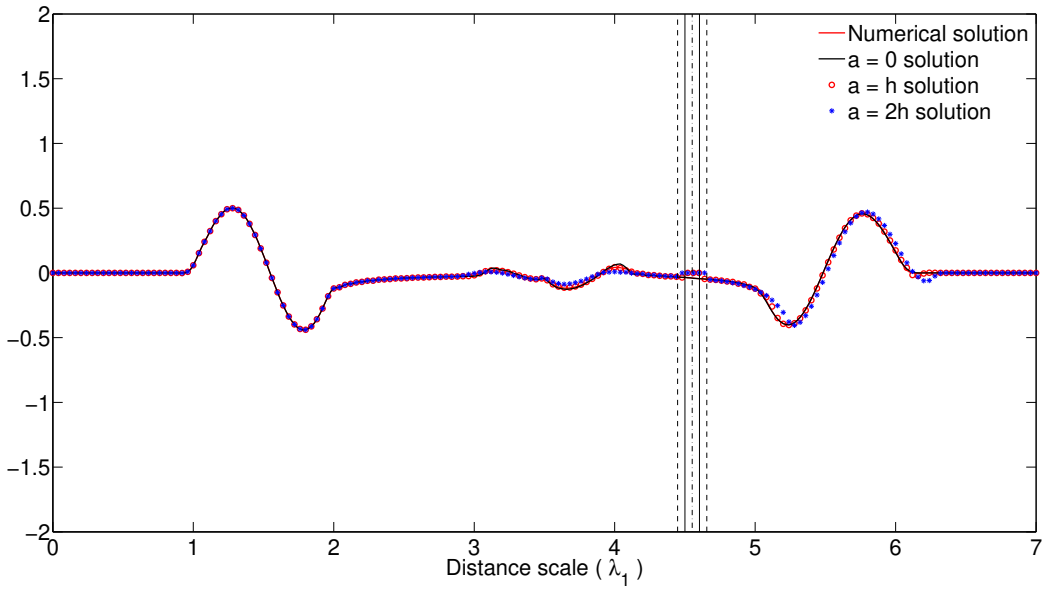

Figure 6.9: *Amplitude curves of source incident wave: the numerical solution (red line), the jump conditions solution (red circle), the equivalent imperfect solution (black line), and the double thickness jump conditions solution (blue asterisk).*

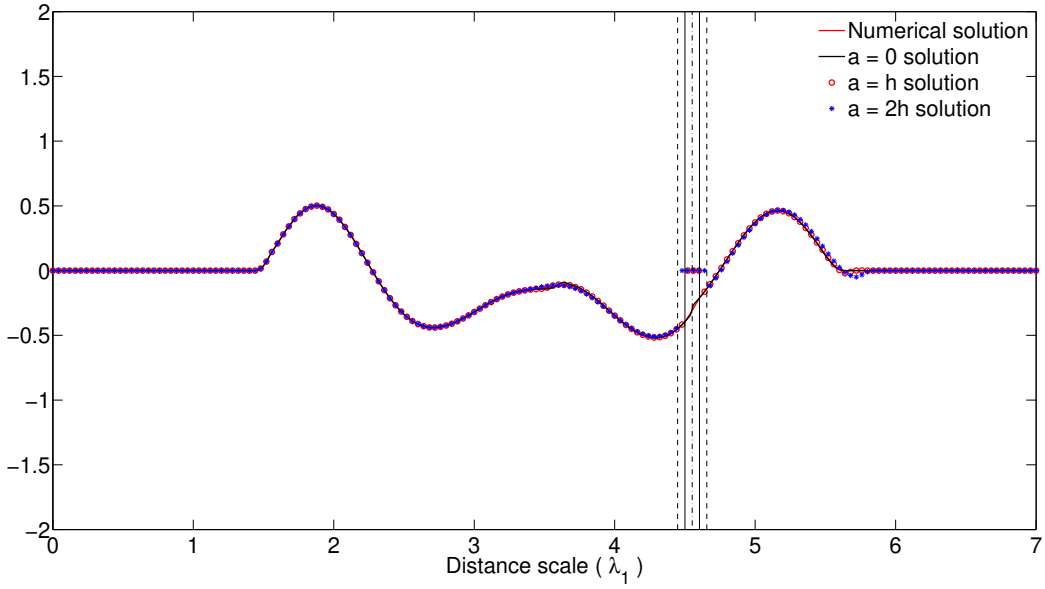

Figure 6.10: *Amplitude curves of source incident wave: the numerical solution (red line), the jump conditions solution (red circle), the equivalent imperfect solution (black line), and the double thickness jump conditions solution (blue asterisk).*

6.3 Conclusion

The finite-difference time-domain (FDTD) method presented in this chapter is implemented with the help of the ESIM numerical scheme. Thanks to the application characteristics of ESIM, which allows the interface to be independent of the grid of difference-point, we can arbitrarily choose the thickness of h of the intermediate layer. On the other hand, in order to improve the accuracy of the numerical method, we provide five points or more finite-difference expressions, which are determined according to the number of forwarding and backward difference-point. Considering the accuracy of the equivalent models, we recommend locking the thickness of the intermediate layer within $0.1\lambda_0$.

After the comparison, we can get the following conclusions: (1) The reflected wave of the equivalent jump conditions model and the transmitted wave of the equivalent imperfect interface model have good matching results, the simulation results of the double-thickness jump condition model are not ideal; (2) The amplitude curves show that the error of the jump conditions model with different thickness compared with the original model is mainly reflected in the phase of the wave.

Conclusions

The content of this thesis mainly shows the research on two dynamic homogenization methods of periodic composites (Part I) and the equivalent models of thin interphase layer composites (Part II). After the following summaries, we put forward the expectations of related work and possible research directions in the future.

Dynamic homogenization methods for periodic composites

The first part of this thesis is devoted to advancing the development of two elastodynamic homogenization methods: Willis elastodynamic homogenization theory and the two-scale homogenization method. Among them, Willis' theory has been greatly developed since it was applied to dynamic elasticity problems. The current work does not fully understand and explain the physical meaning of Willis' theory, but only uses Willis' theory to deal with the homogenization process of periodic layered materials in dynamic cases. At the first, we formulate the effective constitutive law with the help of the virtual work principle and prove the Hermitian symmetry of the effective modulus in the effective constitutive law. Secondly, an iterative method for obtaining the dynamic homogenization equation of periodic layered composites is proposed. This method allows the exact solution to be obtained through iterative calculations of arbitrary initial dispersion relations. In addition, the two-scale homogenization method a classic asymptotic method to deal with the homogenization of composites. The work on the two-scale homogenization method is mainly to propose a local displacement hypothesis related to effective displacement, which simplifies the solution of high-order homogenization equation by combining hierar-

chical equations. And based on the local displacement hypothesis, a high-order general expression of effective elastic tensor and effective density is derived.

The research on dynamic homogenization of periodic composites is a broad development domain, but the current research is only applied to some simple dynamic cases. For example, the Two-scale method mentioned in this thesis is based on the 1D layered model and a simple 2D model, so for more general 2D models, the application of the Two-scale method will likely become a good research subject. In addition, the exploration of more homogenization methods and asymptotic methods is also a possible research direction.

Equivalent models of thin interphase layer composites

The second part of this thesis is mainly to complete the derivation of the jump conditions of the thin interphase layer in the dynamic case, the establishment of its equivalent imperfect interface model, and their numerical implementations. Firstly, we extend the static case in the work of Gu & He (2011) to obtain the jump conditions of the displacement and traction vector of the dynamic equation across the thin homogeneous layer and determine the jump conditions of the equivalent imperfect interface. Then, several equivalent models are proposed for comparison to find a suitable equivalent model. After comparison, we find that the equivalent jump condition model has the smallest error. Finally, in the numerical case chapter, the multi-point central difference expression of the second-order hyperbolic wave equation is derived from the time-domain central difference scheme, and the aforementioned equivalent models are implemented through the Explicit Simplified Interface Method (ESIM). The numerical results show that the reflection wave of the equivalent jump conditions model and the transmission wave of the equivalent imperfect interface model have good matching results with the real solution.

The second part of the thesis is mainly devoted to the equivalent treatment of a homogeneous thin intermeddle layer, but there is a lack of discussion on non-homogeneous interphase. In recent years, there have been studies on the equivalent jump conditions of the periodically arranged thin intermeddle layer model by using the Two-scale description, such as Marigo et al. (2017), Marigo & Maurel (2017) and so on. Therefore, using the perfect interface to derive the jump conditions of the non-homogeneous thin intermeddle

layer model will also be a subject worth studying.

Annexes

Appendix A: Dispersion relation for Multi-phase layered periodic composites

In the body of my thesis, we discussed that the dispersion relationship of multilayer periodic composites satisfies Eq.(1.10). However, for the multi-phase composite, the analytical solution seems extremely complicated. Here I will prove this analytical solution expression of the dispersion relation for multilayer periodic composites. For example, we consider a m-phase layered composite with thickness ratio of α_n for $(n = 1, ..., m)$. We can construct the periodic condition matrix (size with $2m \times 2m$) of the m-layer composite as the form:

$$
\begin{bmatrix}
\times & \times & & & & & & & & & \times & \times \\
\times & \times & & & & & & & & & \times & \times \\
\times & \times & \boxed{\times} & \boxed{\times} & & & & & & & & \\
\times & \times & \boxed{\times} & \boxed{\times} & & & & & & & & \\
 & & \boxed{\times} & \boxed{\times} & \times & \times & & & & & & \\
 & & \boxed{\times} & \boxed{\times} & \times & \times & & & & & & \\
 & & & & & & \ldots & \ldots & & & & \\
 & & & & & & \ldots & \ldots & & & & \\
 & & & & & & & & \times & \times & \times & \times \\
 & & & & & & & & \times & \times & \times & \times \\
 & & & & & & & & & & \times & \times \\
 & & & & & & & & & & \times & \times
\end{bmatrix},
$$

where the cross symbol represents a non-zero value. We try to adjust the last two columns of the coefficient matrix and move it to the bottom end. Then the following format is satisfied for the components of $(2n-1)$ and $(2n)$ columns (the framed components) in the matrix (we call a cell):

$$\begin{bmatrix} -e^{z_n l\sum\alpha_{n-1}} & -e^{z_n^* l\sum\alpha_{n-1}} \\ -iw\eta_n e^{z_n l\sum\alpha_{n-1}} & iw\eta_n e^{z_n^* l\sum\alpha_{n-1}} \\ e^{z_n l\sum\alpha_n} & e^{z_n^* l\sum\alpha_n} \\ iw\eta_n e^{z_n l\sum\alpha_n} & -iw\eta_n e^{z_n^* l\sum\alpha_n} \end{bmatrix},$$

where $\alpha_0 = 0$, and the coefficient $z_n, z_n^* = -ik \pm iw/c_n$. Therefore, it is easy to determine that the different combinations of the above-mentioned matrices are as follows:

$$\begin{aligned}
&(1,2) : A = -2iw\eta_n e^{-2ikl\sum\alpha_{n-1}}, \\
&(1,3) : B_1 = 2ie^{-ikl(\sum\alpha_n+\sum\alpha_{n-1})} sin\left(wl\frac{\alpha_n}{c_n}\right), \\
&(1,4) : B_2 = 2iw\eta_n e^{-ikl(\sum\alpha_n+\sum\alpha_{n-1})} cos\left(wl\frac{\alpha_n}{c_n}\right), \\
&(2,3) : C_1 = -2iw\eta_n e^{-ikl(\sum\alpha_n+\sum\alpha_{n-1})} cos\left(wl\frac{\alpha_n}{c_n}\right), \\
&(2,4) : C_2 = 2iw^2\eta_n^2 e^{-ikl(\sum\alpha_n+\sum\alpha_{n-1})} sin\left(wl\frac{\alpha_n}{c_n}\right), \\
&(3,4) : D = -2iw\eta_n e^{-2ikl\sum\alpha_n},
\end{aligned}$$

where 6 combinations are the different cases of the product for the m-th cell. For a m-phase layered model, the components of the matrix determinant composed of the above different combinations have $N = 2+2^m$ items in total. When solving the zero-determinant relationship of the coefficient matrix, different combinations of m cells can be simplified according to Euler's formula:

$$e^{ik} = cos(k) + i\ sin(k).$$

For the convenience of explanation, we take $m = 3$ as an example to write the combi-

nation of all the component items of the coefficient matrix:

$$
\begin{aligned}
&A^{(1)} * A^{(2)} * A^{(3)} = \mathcal{K}\mathcal{M}e^{ikl},\\
&B_1^{(1)} * C_1^{(2)} * C_2^{(2)} = \mathcal{K}\mathcal{M}\frac{\eta_3}{\eta_1} sin\left(wl\frac{\alpha_1}{c_1}\right) cos\left(wl\frac{\alpha_2}{c_2}\right) sin\left(wl\frac{\alpha_3}{c_3}\right),\\
&B_1^{(1)} * C_2^{(2)} * B_2^{(3)} = -\mathcal{K}\mathcal{M}\frac{\eta_2}{\eta_1} sin\left(wl\frac{\alpha_1}{c_1}\right) sin\left(wl\frac{\alpha_2}{c_2}\right) cos\left(wl\frac{\alpha_3}{c_3}\right),\\
&B_2^{(1)} * B_1^{(2)} * C_2^{(3)} = -\mathcal{K}\mathcal{M}\frac{\eta_3}{\eta_2} cos\left(wl\frac{\alpha_1}{c_1}\right) sin\left(wl\frac{\alpha_2}{c_2}\right) sin\left(wl\frac{\alpha_3}{c_3}\right),\\
&B_2^{(1)} * B_2^{(2)} * B_2^{(3)} = -\mathcal{K}\mathcal{M} cos\left(wl\frac{\alpha_1}{c_1}\right) cos\left(wl\frac{\alpha_2}{c_2}\right) cos\left(wl\frac{\alpha_3}{c_3}\right),\\
&C_1^{(1)} * C_1^{(2)} * C_1^{(3)} = \mathcal{K}\mathcal{M} cos\left(wl\frac{\alpha_1}{c_1}\right) cos\left(wl\frac{\alpha_2}{c_2}\right) cos\left(wl\frac{\alpha_3}{c_3}\right),\\
&C_1^{(1)} * C_2^{(2)} * B_1^{(3)} = \mathcal{K}\mathcal{M}\frac{\eta_2}{\eta_3} cos\left(wl\frac{\alpha_1}{c_1}\right) sin\left(wl\frac{\alpha_2}{c_2}\right) sin\left(wl\frac{\alpha_3}{c_3}\right),\\
&C_2^{(1)} * B_1^{(2)} * C_1^{(3)} = \mathcal{K}\mathcal{M}\frac{\eta_1}{\eta_2} sin\left(wl\frac{\alpha_1}{c_1}\right) sin\left(wl\frac{\alpha_2}{c_2}\right) cos\left(wl\frac{\alpha_3}{c_3}\right),\\
&C_2^{(1)} * B_2^{(2)} * B_1^{(3)} = -\mathcal{K}\mathcal{M}\frac{\eta_1}{\eta_3} sin\left(wl\frac{\alpha_1}{c_1}\right) cos\left(wl\frac{\alpha_2}{c_2}\right) sin\left(wl\frac{\alpha_3}{c_3}\right),\\
&D^{(1)} * D^{(2)} * D^{(3)} = \mathcal{K}\mathcal{M}e^{-ikl},
\end{aligned}
$$

where the superscript (n) indicates the combination of the $(2n-1)$-th and $2n$-th columns, and the coefficients $\mathcal{K}$ and $\mathcal{M}$ are

$$
\begin{aligned}
&\mathcal{K} = (-iw)^m e^{-2ikl\gamma_0}, \quad \gamma_0 = \sum \alpha_1 + ... + \sum \alpha_{m-1} + \frac{1}{2},\\
&\sum \alpha_m = 1, \quad \mathcal{M} = 2^m \left(\prod_{n=1}^{m} \eta_n\right).
\end{aligned}
$$

The sign of plus or minus for the combination items depends on the order of the combination. After confirmation, for all combinations, the coefficients C_1 and C_2 are negative and the rest is positive.

Remark: *The definition of "the sign of plus or minus depends on the combination order" comes from the property of the determinant that causes the sign to change when the row or column is changed (the* ***elementary transformation*** *of the matrix). Therefore,*

for the different combinations of $(1,2,3,4)$*, the different combination results are:*

$$(1,2):A\Rightarrow+,\quad (1,3):B_1\Rightarrow-,\quad (1,4):B_2\Rightarrow-,$$
$$(2,3):C_1\Rightarrow+,\quad (2,4):C_2\Rightarrow+,\quad (3,4):D\Rightarrow+.$$

So far, we can determine all the component terms of the determinant of the coefficient matrix. It is also worth mentioning that since we have adjusted the last two columns of the coefficient matrix, we need to perform negative operations on combinations that do not contain A and D. Then, the zero-determinant expression of the coefficient matrix can be expressed as

$$\begin{aligned}
&A^{(1)}*A^{(2)}*A^{(3)}+D^{(1)}*D^{(2)}*D^{(3)}\\
&+B_1^{(1)}*C_1^{(2)}*C_2^{(2)}-B_1^{(1)}*C_2^{(2)}*B_2^{(3)}\\
&-B_2^{(1)}*B_1^{(2)}*C_2^{(3)}+B_2^{(1)}*B_2^{(2)}*B_2^{(3)}\\
&-C_1^{(1)}*C_1^{(2)}*C_1^{(3)}+C_1^{(1)}*C_2^{(2)}*B_1^{(3)}\\
&+C_2^{(1)}*B_1^{(2)}*C_1^{(3)}-C_2^{(1)}*B_2^{(2)}*B_1^{(3)}=0.
\end{aligned}$$

Try to simplify the above expression, we have

$$\begin{aligned}
&2\eta_1\eta_2\eta_3cos(kl)-2\eta_1\eta_2\eta_3cos(wl\frac{\alpha_1}{c_1})cos(wl\frac{\alpha_2}{c_2})cos(wl\frac{\alpha_2}{c_2})\\
&\quad+(\eta_1^2\eta_3+\eta_2^2\eta_3)sin(wl\frac{\alpha_1}{c_1})sin(wl\frac{\alpha_2}{c_2})cos(wl\frac{\alpha_2}{c_2})\\
&\quad+(\eta_1^2\eta_2+\eta_3^2\eta_2)sin(wl\frac{\alpha_1}{c_1})cos(wl\frac{\alpha_2}{c_2})sin(wl\frac{\alpha_2}{c_2})\\
&\quad+(\eta_2^2\eta_1+\eta_3^2\eta_1)cos(wl\frac{\alpha_1}{c_1})sin(wl\frac{\alpha_2}{c_2})sin(wl\frac{\alpha_2}{c_2})=0.
\end{aligned}$$

Finally, we get the analytical solution of the dispersion relation for three-phase layered composites. Furthermore, for any multilayer composite material with $m\geqslant 2$, this method can be used to obtain an analytical solution.

Appendix B: Properties of the tensor $\mathcal{X}_n$

Based on the new effective displacement field hypothesis proposed in chapter 3, according to the two-scale description, we can obtain the effective constitutive relationship expression. However, this will inevitably bring about a problem: the definition and solution of tensor $\mathcal{X}$. Regarding the definition of tensor $\mathcal{X}$, we take $\mathcal{X}_1$ as an example to give the definition. We know that the introduction of $\mathcal{X}_1$ is to give the expression of $\tilde{\boldsymbol{u}}_1$:

$$\tilde{\boldsymbol{u}}_1 = \tilde{U}_1 + \mathcal{X}_1 : i\boldsymbol{k} \otimes^s \tilde{U}_0,$$

where $\mathcal{X}_1$ is introduced as a third-order tensor, and it satisfies an zero-average on the REV. Apart from that, the tensor $\mathcal{X}_1$ should also satisfy minor symmetry $(\mathcal{X}_1)_{ikl} = (\mathcal{X}_1)_{ilk}$, which gives

$$(\boldsymbol{\nabla}_{\boldsymbol{y}} \otimes^s \mathcal{X}_1)_{ijkl} = \frac{1}{2}[(\boldsymbol{\nabla}_{\boldsymbol{y}}\mathcal{X}_1)_{ijkl} + (\boldsymbol{\nabla}_{\boldsymbol{y}}\mathcal{X}_1)_{jikl}].$$

Then, we have

$$\begin{aligned}
\mathbb{C} : (i\boldsymbol{k} \otimes^s \tilde{U}_1) &= \mathbb{C} \cdot i\boldsymbol{k} \cdot \tilde{U}_1 \ , \\
\mathbb{C} : [\boldsymbol{\nabla}_{\boldsymbol{y}} \otimes^s (\mathcal{X}_1 : i\boldsymbol{k} \otimes^s \tilde{U}_0)] &= \mathbb{C} : \boldsymbol{\nabla}_{\boldsymbol{y}} \otimes^s \mathcal{X}_1 : (i\boldsymbol{k} \otimes^s \tilde{U}_0) \\
&= \mathbb{C} : \boldsymbol{\nabla}_{\boldsymbol{y}}\mathcal{X}_1 \cdot i\boldsymbol{k} \cdot \tilde{U}_0 \ .
\end{aligned}$$

According to the above $\tilde{\boldsymbol{u}}_1$ expression, the lowest-order homogenized local dynamic equation is given as

$$i\boldsymbol{k} \cdot \langle \mathbb{C} : (\boldsymbol{I} \otimes \boldsymbol{I} + \boldsymbol{\nabla}_{\boldsymbol{y}}\mathcal{X}_1) \rangle : i\boldsymbol{k} \otimes^s \langle \tilde{\boldsymbol{u}} \rangle = -w^2 \langle \boldsymbol{\rho} \rangle \langle \tilde{\boldsymbol{u}} \rangle,$$

where $\langle \tilde{\boldsymbol{u}} \rangle = U_0 + O(\epsilon^1)$. Therefore, the effective impedance can be expressed as:

$$\mathcal{Z}_0 = iw\langle \boldsymbol{\rho} \rangle iw - i\boldsymbol{k} \cdot \langle \mathbb{C} : (\boldsymbol{I} \otimes \boldsymbol{I} + \boldsymbol{\nabla}_{\boldsymbol{y}}\mathcal{X}_1) \rangle \cdot i\boldsymbol{k}.$$

Generally, the definition of $\mathcal{X}_n$ also satisfies minor symmetry symmetry, e.g. the fourth-

order tensor $(\mathcal{X}_2)_{ijkl} = (\mathcal{X}_2)_{ikjl}$, and

$$\begin{aligned}
\mathbb{C} : \{i\boldsymbol{k} \otimes^s [\mathcal{X}_1 : i\boldsymbol{k} \otimes^s \tilde{U}_1]\} &= \mathbb{C} : (i\boldsymbol{k} \otimes^s \mathcal{X}_1) : (i\boldsymbol{k} \otimes^s \tilde{U}_1) \\
&= \mathbb{C} : (i\boldsymbol{k} \otimes \mathcal{X}_1) \cdot i\boldsymbol{k} \cdot \tilde{U}_1 \ , \\
\mathbb{C} : \{\boldsymbol{\nabla}_{\boldsymbol{y}} \otimes^s [(\mathcal{X}_2 : i\boldsymbol{k}) : i\boldsymbol{k} \otimes^s \tilde{U}_0]\} &= \mathbb{C} : \boldsymbol{\nabla}_{\boldsymbol{y}} \otimes^s (\mathcal{X}_2 \cdot i\boldsymbol{k}) : (i\boldsymbol{k} \otimes^s \tilde{U}_0) \\
&= \mathbb{C} : \boldsymbol{\nabla}_{\boldsymbol{y}} (\mathcal{X}_2 \cdot i\boldsymbol{k}) \cdot i\boldsymbol{k} \cdot \tilde{U}_0 \ .
\end{aligned}$$

Similarly, for the n-th tensor $\mathcal{X}_n$, we have

$$\begin{aligned}
\mathbb{C} : \{i\boldsymbol{k} \otimes^s [\left(\mathcal{X}_{n-1} \odot^{n-2} (i\boldsymbol{k})^{n-2}\right) : i\boldsymbol{k} \otimes^s \tilde{U}_1]\} &= \mathbb{C} : \{i\boldsymbol{k} \otimes^s \left(\mathcal{X}_{n-1} \odot^{n-2} (i\boldsymbol{k})^{n-2}\right)\} : (i\boldsymbol{k} \otimes^s \tilde{U}_1) \\
&= \mathbb{C} : \{i\boldsymbol{k} \otimes \left(\mathcal{X}_{n-1} \odot^{n-2} (i\boldsymbol{k})^{n-2}\right)\} \cdot i\boldsymbol{k} \cdot \tilde{U}_1 \ , \\
\mathbb{C} : \{\boldsymbol{\nabla}_{\boldsymbol{y}} \otimes^s [\left(\mathcal{X}_n \odot^{n-1} (i\boldsymbol{k})^{n-1}\right) : i\boldsymbol{k} \otimes^s \tilde{U}_0]\} &= \mathbb{C} : \{\boldsymbol{\nabla}_{\boldsymbol{y}} \otimes^s \left(\mathcal{X}_n \odot^{n-1} (i\boldsymbol{k})^{n-1}\right)\} : (i\boldsymbol{k} \otimes^s \tilde{U}_0) \\
&= \mathbb{C} : \{\boldsymbol{\nabla}_{\boldsymbol{y}} \left(\mathcal{X}_n \odot^{n-1} (i\boldsymbol{k})^{n-1}\right)\} \cdot i\boldsymbol{k} \cdot \tilde{U}_0 \ .
\end{aligned}$$

Appendix C: Polynomial approximation of the tensor $\mathcal{X}_n$ in layered composite

In the 1D case, we proposed that the tensors $\mathcal{X}_n$ are expressed by polynomial functions related to the micro variable $\boldsymbol{y}$:

$$\mathcal{X}_n = \boldsymbol{a}_n^n \boldsymbol{y}^n + ... + \boldsymbol{a}_n^1 \boldsymbol{y} + \boldsymbol{a}_n^0,$$

where $\boldsymbol{a}$ are the coefficient vectors whose size is related to the number of material layers. At the same time, the function $\mathcal{X}_n$ needs to meet the continuity conditions and periodicity conditions of interfaces, and the zero-average condition (for $n \geqslant 1$).

Analysis of coefficient vectors $\boldsymbol{a}$ in polynomial function $\mathcal{X}_n$

We assume that the representative cell is an m-phase layered model, witch has the thickness ratio $(\alpha_1, ..., \alpha_m)$ with $\sum_{i=1}^m \alpha_i = 1$ and the cell size l. The layered material properties are given as Young's modulus E and mass density ρ, and the corresponding values of different layers are indicated by subscripts. To simplify the expression, we denote the two extremes of the n-th layer as $\alpha_n^{(-)} l$ and $\alpha_n^{(+)} l$, respectively. They meet the definitions:

$$\alpha_n^{(-)} = \alpha_1 + \alpha_2 + ... + \alpha_{n-1}, \quad \alpha_n^{(+)} = \alpha_1 + \alpha_2 + ... + \alpha_n.$$

Solution of $\mathcal{X}_1$

According to the above continuity and periodicity conditions, we can determine the coefficient vectors $\boldsymbol{a}_1^1$:

$$\boldsymbol{a}_1^1(n) = \frac{1}{PE_n} - 1, \quad P = \sum_{i=1}^m \frac{\alpha_i}{E_i}, \quad n = 1, 2, ..., m.$$

And the coefficient vectors $\boldsymbol{a}_1^0$ satisfy:

$$\boldsymbol{a}_1^0(n) = \frac{l}{P} \left(\sum_{i=n}^{m-1} \alpha_i^{(+)} \left(\frac{1}{E_{i+1}} - \frac{1}{E_i} \right) \right) + Q, \quad n = 1, 2, ..., m-1, \quad \boldsymbol{a}_1^0(m) = Q,$$

where the intermediate coefficient Q can be determined by

$$Q = \frac{l}{P}\sum_{i=1}^{m}\left(\frac{(\alpha_i^{(+)})^2-(\alpha_i^{(-)})^2}{2E_i}(PE_i-1)-\alpha_i\sum_{j=i}^{m-1}\alpha_j^{(+)}\left(\frac{1}{E_{j+1}}-\frac{1}{E_j}\right)\right).$$

It is confirmed that only when $m = 2$, which is the two-phase layered model, the $\mathcal{X}_1$ function satisfies the integral of each layer is zero, we take the n-th layer as an example:

$$\int_{\alpha_n^{(-)}l}^{\alpha_n^{(+)}l} \boldsymbol{a}_1^1(n)\boldsymbol{y}+\boldsymbol{a}_1^0(n)\ d_{\boldsymbol{y}}=0, \quad n=1,2. \tag{6.4}$$

In this case, the effective density $\langle\boldsymbol{\rho}_1\rangle$ always satisfies

$$\langle\boldsymbol{\rho}_1\rangle = ik\langle\rho\mathcal{X}_1\rangle = 0. \tag{6.5}$$

However, for the case of $m \geqslant 3$, the results can be expressed in the following general expression

$$\int_{\alpha_n^{(-)}l}^{\alpha_n^{(+)}l} \boldsymbol{a}_1^1(n)\boldsymbol{y}+\boldsymbol{a}_1^0(n)d_{\boldsymbol{y}}=\sum_{(p,q)}\epsilon_{npq}\frac{\alpha_n\alpha_p\alpha_q}{4P}(-\frac{1}{E_p}+\frac{1}{E_q}), \quad n=1,2,...,m, \tag{6.6}$$

where p and q can represent all combinations of different numbers between 1 and m except n. In addition, ϵ_{npq} represents the Levi-Civita symbol of the number n, p and q, that is, when npq is in order, it is 1, otherwise it is -1. For example, when we set $m = 3$ and $n = 2$, we have $\epsilon_{231} = 1$ and $\epsilon_{213} = -1$. Then, the effective density $\langle\boldsymbol{\rho}_1\rangle$ of a three-phase layered model can be expressed as

$$\langle\boldsymbol{\rho}_1\rangle = ik\langle\rho\mathcal{X}_1\rangle = ik\frac{\alpha_1\alpha_2\alpha_3}{2P}\left[\rho_1\left(-\frac{1}{E_2}+\frac{1}{E_3}\right)+\rho_2\left(-\frac{1}{E_3}+\frac{1}{E_1}\right)+\rho_3\left(-\frac{1}{E_1}+\frac{1}{E_2}\right)\right],$$

where ρ_n represents the density value of the n-th layer medium. Obviously, in general, the right side of the above expression is not always equal to 0. This means that in general (except for the two-layer model), we cannot ignore all odd terms (or imaginary parts) in Eq.(3.15).

Solution of $\mathcal{X}_n$

For the solution of the higher-order function $\mathcal{X}_n$, we need to use the general relationship shown in Eq.(3.18), which gives the necessary relation of all higher-order terms between $\mathcal{X}_n$ and $\mathcal{X}_{n-1}$. Taking $\mathcal{X}_2$ as an example, the coefficient $\boldsymbol{a}_2^2$ can be determined by Eq.(3.9). In addition, the coefficients $\boldsymbol{a}_2^1$ and $\boldsymbol{a}_2^0$ can be solved by the continuity and periodicity conditions of the displacement field and the traction vector, and the zero-average condition of $\mathcal{X}_2$. After determining the function $\mathcal{X}_2$, we verified that $\nabla\mathcal{X}_2$ has similar properties to $\mathcal{X}_1$: when $m = 2$ (two-layer composite), we have

$$\int_{\alpha_n^{(-)}}^{\alpha_n^{(+)}} 2\boldsymbol{a}_2^2(n)\boldsymbol{y} + \boldsymbol{a}_2^1(n)\ d_{\boldsymbol{y}} = 0, \quad n = 1, 2,$$

that gives the effective stiffness $\langle\mathbb{C}_1\rangle = ik\langle E(\mathcal{X}_1 + \nabla\mathcal{X}_2)\rangle = 0$; however, for the case of $m \geqslant 3$, the result of $\langle\nabla\mathcal{X}_2\rangle$ is not always equal to zero. Therefore, we can conclude that for the two-layer composites, there are always $\langle\mathbb{C}_1\rangle = 0$ and $\langle\boldsymbol{\rho}_1\rangle = 0$, but for the multilayer case, this conclusion is generally not true (the conclusion depends on the properties of each layer).

The same method can be used to determine higher-order expressions of $\mathcal{X}$. In addition, we found that for all odd numbers n, the functions $\mathcal{X}_n$ and $\nabla\mathcal{X}_{n+1}$ have the same properties with $\mathcal{X}_1$ and $\nabla\mathcal{X}_2$. This means that for the two-layer composite, all odd-numbered terms of $\mathbb{C}_n^{hom}$ and $\boldsymbol{\rho}_n^{hom}$ in Eq.(3.15) are zero; but for the multilayer case, these imaginary terms are generally not zero. Numerical simulation confirms that these Imaginary terms are much smaller than the corresponding real terms, which makes these imaginary terms still negligible.

Bibliography

Amirkhizi, A. V., & Nemat-Nasser, S. (2008). Microstructurally-based homogenization of electromagnetic properties of periodic media. *Comptes Rendus Mecanique*, *336*, 24–33.

Andrianov, I. V., Bolshakov, V. I., Danishevs' kyy, V. V., & Weichert, D. (2008). Higher order asymptotic homogenization and wave propagation in periodic composite materials. *Proceedings of the Royal Society A: Mathematical, Physical and Engineering Sciences*, *464*, 1181–1201.

Andrianov, I. V., Danishevs' kyy, V. V., Topol, H., & Weichert, D. (2011). Homogenization of a 1d nonlinear dynamical problem for periodic composites. *ZAMM-Journal of Applied Mathematics and Mechanics/Zeitschrift für Angewandte Mathematik und Mechanik*, *91*, 523–534.

Andrianov, I. V., Danishevs'kyy, V. V., Ryzhkov, O. I., & Weichert, D. (2013). Dynamic homogenization and wave propagation in a nonlinear 1d composite material. *Wave Motion*, *50*, 271–281.

Auriault, J., & Bonnet, G. (1985). Dynamique des composites élastiques périodiques. *Arch. Mech*, *37*, 269–284.

Bensoussan, A., Lions, J.-L., & Papanicolaou, G. (2011). *Asymptotic analysis for periodic structures* volume 374. American Mathematical Soc.

Benveniste, Y. (2006). A general interface model for a three-dimensional curved thin anisotropic interphase between two anisotropic media. *Journal of the Mechanics and Physics of Solids*, *54*, 708–734.

Benveniste, Y. (2006). An o (h n) interface model of a three-dimensional curved interphase in conduction phenomena. *Proceedings of the Royal Society A: Mathematical, Physical and Engineering Sciences*, *462*, 1593–1617.

Boutin, C. (1996). Microstructural effects in elastic composites. *International Journal of Solids and Structures*, *33*, 1023–1051.

Boutin, C., & Auriault, J. (1993). Rayleigh scattering in elastic composite materials. *International Journal of Engineering Science*, *31*, 1669–1689.

Chen, H., & Chan, C. T. (2010). Acoustic cloaking and transformation acoustics. *Journal of Physics D: Applied Physics*, *43*, 113001.

Chiavassa, G., & Lombard, B. (2011). Time domain numerical modeling of wave propagation in 2d heterogeneous porous media. *Journal of Computational Physics*, *230*, 5288–5309.

David, M., Marigo, J.-J., & Pideri, C. (2012). Homogenized interface model describing inhomogeneities located on a surface. *Journal of Elasticity*, *109*, 153–187.

Fang, N., Xi, D., Xu, J., Ambati, M., Srituravanich, W., Sun, C., & Zhang, X. (2006). Ultrasonic metamaterials with negative modulus. *Nature materials*, *5*, 452–456.

Fish, J., Chen, W., & Nagai, G. (2002a). Non-local dispersive model for wave propagation in heterogeneous media: one-dimensional case. *International Journal for Numerical Methods in Engineering*, *54*, 331–346.

Fish, J., Chen, W., & Nagai, G. (2002b). Non-local dispersive model for wave propagation in heterogeneous media: multi-dimensional case. *International Journal for Numerical Methods in Engineering*, *54*, 347–363.

Gu, S., & He, Q.-C. (2011). Interfacial discontinuity relations for coupled multifield phenomena and their application to the modeling of thin interphases as imperfect interfaces. *Journal of the Mechanics and Physics of Solids*, *59*, 1413–1426.

Gu, S.-T., Liu, J.-T., & He, Q.-C. (2014). Size-dependent effective elastic moduli of particulate composites with interfacial displacement and traction discontinuities. *International Journal of Solids and Structures*, *51*, 2283–2296.

Gu, S.-T., Wang, A.-L., Xu, Y., & He, Q.-C. (2015). Closed-form estimates for the effective conductivity of isotropic composites with spherical particles and general imperfect interfaces. *International Journal of Heat and Mass Transfer*, *83*, 317–326.

Hadamard, J. (1903). *Leçons sur la propagation des ondes et les équations de l'hydrodynamique*. A. Hermann.

Hill, R. (1961). Discontinuity relations in mechanics of solids. *Progress in solid mechanics*, *2*, 245–276.

Hill, R. (1972). An invariant treatment of interfacial discontinuities in elastic composites. *Continuum mechanics and related problems of analysis.(A 73-32076 15-32) Moscow, Izdatel'stvo Nauka, 1972,*, (pp. 597–604).

Hill, R. (1983). Interfacial operators in the mechanics of composite media. *Journal of the Mechanics and Physics of Solids*, *31*, 347–357.

Hu, R., & Oskay, C. (2017). Nonlocal homogenization model for wave dispersion and attenuation in elastic and viscoelastic periodic layered media. *Journal of Applied Mechanics*, *84*.

Hu, R., & Oskay, C. (2018). Spatial–temporal nonlocal homogenization model for transient anti-plane shear wave propagation in periodic viscoelastic composites. *Computer Methods in Applied Mechanics and Engineering*, *342*, 1–31.

Hu, R., & Oskay, C. (2019). Multiscale nonlocal effective medium model for in-plane elastic wave dispersion and attenuation in periodic composites. *Journal of the Mechanics and Physics of Solids*, *124*, 220–243.

Kalamkarov, A. L., Andrianov, I. V., & Danishevs'kyy, V. V. (2009). Asymptotic homogenization of composite materials and structures. *Applied Mechanics Reviews*, *62*.

Keller, J. B. (1960). *Wave propagation in random media* volume 60. Institute of Mathematical Sciences, New York University.

Keller, J. B. (1977). Effective behavior of heterogeneous media. In *Statistical mechanics and statistical methods in theory and application* (pp. 631–644). Springer.

Laws, N. (1975). On interfacial discontinuities in elastic composites. *Journal of Elasticity*, *5*, 227–235.

Liu, Z., Chan, C. T., & Sheng, P. (2005). Analytic model of phononic crystals with local resonances. *Physical Review B*, *71*, 014103.

Liu, Z., Zhang, X., Mao, Y., Zhu, Y., Yang, Z., Chan, C. T., & Sheng, P. (2000). Locally resonant sonic materials. *Science*, *289*, 1734–1736.

Lombard, B., Maurel, A., & Marigo, J.-J. (2017). Numerical modeling of the acoustic wave propagation across a homogenized rigid microstructure in the time domain. *Journal of Computational Physics*, *335*, 558–577.

Lombard, B., & Piraux, J. (2004). Numerical treatment of two-dimensional interfaces for acoustic and elastic waves. *Journal of Computational Physics*, *195*, 90–116.

Lombard, B., & Piraux, J. (2006). Numerical modeling of elastic waves across imperfect contacts. *SIAM journal on scientific computing*, *28*, 172–205.

Lörcher, F., & Munz, C.-D. (2007). Lax–wendroff-type schemes of arbitrary order in several space dimensions. *IMA journal of numerical analysis*, *27*, 593–615.

Marigo, J.-J., & Maurel, A. (2016). Homogenization models for thin rigid structured surfaces and films. *The Journal of the Acoustical Society of America*, *140*, 260–273.

Marigo, J.-J., & Maurel, A. (2017). Second order homogenization of subwavelength stratified media including finite size effect. *SIAM Journal on Applied Mathematics*, *77*, 721–743.

Marigo, J.-J., Maurel, A., Pham, K., & Sbitti, A. (2017). Effective dynamic properties of a row of elastic inclusions: the case of scalar shear waves. *Journal of elasticity*, *128*, 265–289.

Meng, S., & Guzina, B. B. (2018). On the dynamic homogenization of periodic media: Willis' approach versus two-scale paradigm. *Proceedings of the Royal Society A: Mathematical, Physical and Engineering Sciences*, *474*, 20170638.

Milton, G. W., & Willis, J. R. (2007). On modifications of newton's second law and linear continuum elastodynamics. *Proceedings of the Royal Society A: Mathematical, Physical and Engineering Sciences*, *463*, 855–880.

Nassar, H., He, Q.-C., & Auffray, N. (2015). Willis elastodynamic homogenization theory revisited for periodic media. *Journal of the Mechanics and Physics of Solids*, *77*, 158–178.

Nassar, H., He, Q.-C., & Auffray, N. (2016). On asymptotic elastodynamic homogenization approaches for periodic media. *Journal of the Mechanics and Physics of Solids*, *88*, 274–290.

Nemat-Nasser, S., & Srivastava, A. (2011). Overall dynamic constitutive relations of layered elastic composites. *Journal of the Mechanics and Physics of Solids*, *59*, 1953–1965.

Nemat-Nasser, S., & Srivastava, A. (2013). Bounds on effective dynamic properties of elastic composites. *Journal of the Mechanics and Physics of Solids*, *61*, 254–264.

Nemat-Nasser, S., Willis, J. R., Srivastava, A., & Amirkhizi, A. V. (2011). Homogenization of periodic elastic composites and locally resonant sonic materials. *Physical Review B*, *83*, 104103.

Norris, A. N., Shuvalov, A., & Kutsenko, A. (2012). Analytical formulation of three-dimensional dynamic homogenization for periodic elastic systems. *Proceedings of the Royal Society A: Mathematical, Physical and Engineering Sciences*, *468*, 1629–1651.

Pendry, J. B. (2000). Negative refraction makes a perfect lens. *Physical review letters*, *85*, 3966.

Pham, K., Maurel, A., & Marigo, J.-J. (2017). Two scale homogenization of a row of locally resonant inclusions-the case of anti-plane shear waves. *Journal of the Mechanics and Physics of Solids*, *106*, 80–94.

Piraux, J., & Lombard, B. (2001). A new interface method for hyperbolic problems with discontinuous coefficients: one-dimensional acoustic example. *Journal of Computational Physics*, *168*, 227–248.

Schwartzkopff, T., Dumbser, M., & Munz, C.-D. (2004). Fast high order ader schemes for linear hyperbolic equations. *Journal of Computational Physics*, *197*, 532–539.

Schwartzkopff, T., Munz, C.-D., & Toro, E. F. (2002). Ader: A high-order approach for linear hyperbolic systems in 2d. *Journal of Scientific Computing*, *17*, 231–240.

Shuvalov, A., Kutsenko, A., Norris, A., & Poncelet, O. (2011). Effective willis constitutive equations for periodically stratified anisotropic elastic media. *Proceedings of the Royal Society A: Mathematical, Physical and Engineering Sciences*, *467*, 1749–1769.

Smith, D. R., Padilla, W. J., Vier, D., Nemat-Nasser, S. C., & Schultz, S. (2000). Composite medium with simultaneously negative permeability and permittivity. *Physical review letters*, *84*, 4184.

Smyshlyaev, V. P., & Cherednichenko, K. D. (2000). On rigorous derivation of strain gradient effects in the overall behaviour of periodic heterogeneous media. *Journal of the Mechanics and Physics of Solids*, *48*, 1325–1357.

Walpole, L. (1981). Elastic behavior of composite materials: theoretical foundations. In *Advances in applied mechanics* (pp. 169–242). Elsevier volume 21.

Wautier, A., & Guzina, B. B. (2015). On the second-order homogenization of wave motion in periodic media and the sound of a chessboard. *Journal of the Mechanics and Physics of Solids*, *78*, 382–414.

Willis, J. R. (1980a). Polarization approach to the scattering of elastic waves—i. scattering by a single inclusion. *Journal of the Mechanics and Physics of Solids*, *28*, 287–305.

Willis, J. R. (1980b). A polarization approach to the scattering of elastic waves—ii. multiple scattering from inclusions. *Journal of the Mechanics and Physics of Solids*, *28*, 307–327.

Willis, J. R. (1985). The nonlocal influence of density variations in a composite. *International Journal of Solids and Structures*, *21*, 805–817.

Willis, J. R. (1997). Dynamics of composites. In *Continuum micromechanics* (pp. 265–290). Springer.

Willis, J. R. (2009). Exact effective relations for dynamics of a laminated body. *Mechanics of Materials*, *41*, 385–393.

Willis, J. R. (2011). Effective constitutive relations for waves in composites and metamaterials. *Proceedings of the Royal Society A: Mathematical, Physical and Engineering Sciences*, *467*, 1865–1879.

Willis, J. R. (2012). The construction of effective relations for waves in a composite. *Comptes Rendus Mécanique*, *340*, 181–192.